Various Correspondences Between Simple Driven and Equilibrium Statistical Hard Core Models

Wipsar Sunu Brams Dwandaru

H. H. Wills Physics Laboratory
University of Bristol

A thesis submitted to the University of Bristol in accordance with the requirements of the degree of Ph.D. in the Faculty of Science

December 2010

Abstract

A research project concerning the relationship between equilibrium and non-equilibrium systems has been conducted. The main objective of this project is to explore various connections between hard core lattice fluids on one hand, and hopping models such as the totally asymmetric exclusion process (TASEP) on the other. The goal is that the properties of the TASEP may be determined via calculations done for the equilibrium hard core model.

The master equation is applied as the main equation to describe the probabilities of the physical systems under consideration in this thesis. The master equation is employed to solve the special case of a TASEP consisting of a single site with time-dependent input and output rates. Hence, the full probabilities of the empty and occupied site are attained thus giving the time-dependent one-body and current densities.

Various mean-field results from variants of the TASEP are presented. First, we study some examples of the TASEP in 1D with time-dependent input and output rates consisting of a cosine function term which is a function of time. The parameters being varied are the strength of oscillations, period of oscillation, and the initial value of the input and output rates. We let the system evolve for considerably long (discrete) times, i.e. 10^5 to 10^6 time steps. Two types of dynamics are considered here, i.e. sequential and parallel updating. The one-body and current densities are obtained for each case from simulation and theoretical calculations.

Next, the correspondence between the TASEP and the hard core lattice fluid mixture in 2D is exploited in order to obtain the one-body and current densities of the TASEP in 2D with constant input and output hopping rates. Here, the particles of the TASEP and their possible movements correspond to the particles of the equilibrium hard core model. Hence, the one-body and current densities of the TASEP are associated to the one-body densities of the equilibrium model. Further modification of the TASEP in 2D is carried out such that a TASEP with a junction is constructed.

An alternative correspondence between the TASEP and the continuous hard rod fluid in 1D is proposed. Here, the particle trajectories of the TASEP are associated to the (microscopic) configurations of the hard rod fluid. Thus the quantities of the TASEP may be associated with the appropriate quantities in the continuous hard rod fluid, viz.: i) the lifetime of a particle occupying a site is associated to the diameter of the rod; ii) the number of ejections per unit time of particle occupying the site (the output hopping rate) is related to the number of particles per volume occupied by the particles, and iii) the input hopping rate corresponds to the total pressure of the hard rod model. From this correspondence it turns out that the one-body density of the TASEP corresponds to the total packing fraction of the hard rods, while the current density corresponds to the total density of the continuous hard rod model.

Finally, functionals of the current densities are constructed for the TASEP. As in classical density functional theory (DFT), the current density functional consists of ideal and excess parts

in its 'free energy' functional term. The functional derivatives with respect to the current densities give the Euler-Lagrange equations such that the equation of motions of the TASEP may be obtained. These equation of motions are supported by the appropriate continuity equations. Furthermore, a formal argument is proposed for the existence of the current density functional above. This argument is based upon the constraint search method which is originally formulated in [1] for electronic (quantum) DFT.

Keywords: totally asymmetric exclusion process (TASEP), hard core lattice fluid, the master equation, continuous hard rod model, current density functional, classical density functional theory (DFT).

Dedication

I dedicate this thesis to my beloved family

To my mother who fought a long and difficult battle with her illness. I will always remember and carry on her courage, strength, and wisdom. She never stop caring for me from the day I was born. That is why I dedicate this thesis to her.

To my father for supporting me so that I can pursue my PhD study. The earliest memory that I can remember was in pre-school when he bought me a Science book. From that moment on I knew that understanding the beauty of nature through physics is what I would like to do in life. I was fascinated by physics back then as I am now.

To Ningsih, my wife, who always stood by my side throughout my research. I would never produce this work without her. I love you.

Acknowledgements

First, and foremost, I would like to articulate my sincere gratitude to my supervisor, Prof. Matthias Schmidt, for all his support, encouragement, and patience, and also his wisdom throughout this project. I really appreciate the trust he has given me (as one of his PhD students) and carrying out one of his research project. I really enjoyed the research project given to me every step of the way without any regrets. His kindness to me and my family will always be remembered.

I would also like to thank my second supervisor, Prof. Bob Evans, for following the progress of my research project in the annual interviews and also looking after my non-academic needs. I was delighted in typing his lecture notes concerning the density functional theory. Finally, I would like to thank all his support on behalf of my family.

I would like to thank Dr. Paul Hopkins for many interesting discussions that we had. It has been an exciting experience to discuss physics with him. I am looking forward to further interesting discussions in the future. I would also like to thank my colleagues and friends in the Theory group: Thomas Smith for helping me to get started with my simulations, Gavin Leithall, Morgan Cameron, and Jon Phillips for all their support and helpful physics discussions. I am really fond of the scientific atmosphere we were creating and I hope the best for them.

I would like to thank the University of Bristol for funding my PhD project through the Overseas Research Student (ORS) Scholarship. I would also like to thank the staff of the Physics department: Tracie Anderson, Vicki Johnson, Audrey Michael, and Yvonne Walker for all the advice and administrative support.

Authors Declaration

I declare that the work in this thesis was carried out in accordance with the regulations of the University of Bristol. The work is original except where indicated by special reference in the text and no part of the thesis has been submitted for any other degree. Any views expressed in the thesis are those of the author and in no way represent those of the University of Bristol. The thesis has not been presented to any other University for examination either in the United Kingdom or overseas.

(Wipsar Sunu Brams Dwandaru)

Indeed, in the creation of the heavens and the earth and the alternation of the night and the day are signs for those of understanding-who remember Allah while standing or sitting or [lying] on their sides and **give thought to the creation of the heavens and the earth**, [saying], 'Our Lord, You did not create this aimlessly; exalted are You [above such thing]; then protect us from the punishment of the Fire'.

(Al-Imran: 190-191)

It is the facts that matter, not the proofs. Physics can progress without the proofs, but we can't go on without the facts...if the facts are right, then the proofs are a matter of playing around with algebra correctly.

(Richard P. Feynman)

Contents

Chapter 1

Introduction

This thesis is motivated by the growing research interest in understanding physical aspects of out-of-equilibrium systems through the lens of statistical mechanics. 'Out-of-equilibrium' systems are characterized by the existence of external driving forces that produce currents that flow through the system. The equilibrium regime, in contrast, is defined by the absence of such currents. As long as non-zero currents are maintained the system remains far from equilibrium.

Non-equilibrium systems provide appealing physical models that can be used to investigate in detail various far-from-equilibrium physical phenomena. In fact an abundant variety of physical phenomena that manifest themselves in everyday life are of non-equilibrium nature. In physics, a wide variety of out-of-equilibrium behaviour can be observed ranging from high energy physics [2–4], nano-scale phenomena [5, 6], quantum optics (laser and maser) [2, 7], radioactive decay [8], chemical reactions [9], soft materials, e.g. sedimentation of colloids [10, 11] and liquid crystals [12, 13], up to astrophysics and cosmology [14]. Everyday life phenomena, such as transport processes in biological systems [15–17], out-of-equilibrium pattern formation [18, 19], turbulence [20, 21], weather forecast [22–24], the behaviour of a group of insects [15, 25], birth and death processes [26], the evolution of the stock market [27], and less frequent phenomena, e.g. earthquakes [28, 29], are of non-equilibrium nature. There is an interesting underlying principle of such diverse physical phenomena which is worthwhile to be studied. This is their stochastic behaviour driven by external forces. Such behaviour cannot simply be investigated within known equilibrium methods.

An example of a physical process which is relevant to this thesis is the traffic flow

of vehicles [30, 31]. The traffic flow is given as an example because this process may be discussed using the physical model studied throughout the thesis. An illustration is given in the following, which involves a one-way lane. Consider a traffic flow of vehicles between two traffic lights, denoted by A and B, in a straight one-way street. The vehicles are assumed to be similar in size. The vehicles enter the street if traffic light A shows the green light and travel along the street between A and B and then exit the street when traffic light B shows the green light. As many of these vehicles are moving along the street with some average speed ν, and an average current J, the average number of vehicles passing through the street, ρ, may be determined by $\rho = J/\nu$. In order to investigate the (thermodynamic) properties of this system, a physical model may be constructed whereby an idealization of the system is considered. First, the continuous space is discretized into lattice sites with equal lattice spacing. Then, the vehicles may be considered as hard core particles. Thus, vehicles traveling on a one-way street are modeled by particles hopping along lattice sites.

The idealized model above is an example of driven diffusive systems [32–34]. In particular the so-called totally asymmetric exclusion process (TASEP) in one dimension (1D) is a popular particle hopping model which has become a reference model for studying non-equilibrium driven systems. The TASEP is a mathematical model by which particles occupying 1D lattice sites may jump to their (nearest) neighbour site as long as the neighbour site is not occupied by any other particle. The jump occurs towards one direction only, e.g. to the right, which produces a totally asymmetric movement of particles. Various types of dynamics which produce sustainable currents can be imposed on the TASEP. Furthermore, different types of boundary conditions may be imposed on the TASEP, i.e. open or periodic boundaries. These boundaries have pronounced effects on the behaviour of the system. With the open boundary conditions where particles may enter or exit the lattice sites, much interesting physics may be realized, e.g. in the steady state rich phases are exhibited in its phase diagram [15, 34–36]. This is one reason why the TASEP is being intensively studied. On the other hand, periodic boundary conditions impose a ring topology (loop) on the lattice sites such that the total number of particles is conserved. Hence, one obtains an equilibrium case of particles hopping (randomly) along the sites with equal probability [34, 37]. However, if the hopping rates of the particles are inhomogeneous even in the bulk, a phase transition between low and high densities occurs [38]. This model was originally constructed to study

the biopolymerization kinetics on nucleic acid templates [39, 40]. In its development the TASEP has been studied extensively as a fundamental model for one-dimensional transport, with applications to intracellular transport [41, 42], and traffic and transport in porous media. This model is also being considered for studying the performance of wireless line networks [43]. One should note that some exact results for steady state are known [36, 44, 45].

Despite the importance of non-equilibrium systems, their statistical mechanics is still poorly understood, even their theoretical foundation. This is contrary to the well-developed equilibrium statistical mechanics, where Gibbs ensembles play a fundamental role [46, 47]. Once the ensemble is known, one may in principle calculate the partition functions and then derive the thermodynamic quantities relevant for the system. In non-equilibrium statistical mechanics, there is no widely accepted definition of an ensemble as a general framework [32, 48]. Thus, one relies on different kinetic theories in order to approach physical problems on a case-by-case basis.

One possible method to study non-equilibrium (and equilibrium) systems within statistical mechanics is utilizing the master equation. This is a set of first-order-partial differential equations which govern the time evolution of the probabilities of a system. In fact, the term master equation is attributed to any equation that regulates the flow of probabilities (in stochastic or deterministic processes) and the evolution of averaged quantities [8]. This differential equation may be expressed as a gain-loss (or a matrix) equation in terms of transition rates. The main objective is to solve the partial differential equation in order to obtain a set of time-dependent probabilities. Then one may further calculate a hierarchy of correlation functions from the set of probabilities, starting from one-body quantities, two-body quantities and so on. There are many methods to solve the master equation depending upon the model under consideration, see e.g. [33, 36, 49–51]. In this thesis we propose and argue for an approach that is based upon a variational principle. We take the master equation of the TASEP as a concrete example for our study. An advantage of using the master equation is that it gives a radical simplification in the time evolution treatment of a system as it bounds to the Markov process where memory effects are neglected [4].

One important aspect of this thesis is related to the interatomic interactions between particles. In our model purely-hard core interactions are employed. The form of this interaction is an infinite repulsive potential when the distance between centres of parti-

cles is σ or smaller. There is no interaction for distances larger than σ. The purely-hard core interaction is arguably the simplest interatomic form [46, 47]. This interaction is used in the description of the TASEP above, where hard core particles are hopping along lattice sites. In equilibrium statistical mechanics, fluid models based upon purely-hard core potentials received serious attention around the mid of 20th century due to the availability of computers [52–54]. Computer simulations of hard sphere particles were initially conducted to investigate the equation-of-state of the model, and in order to resolve the existence of the solid-liquid phase transition [55–57]. An additional attractive potential may be incorporated into the model in order to study hard spheres with surface adhesion [58]. Other applications of the hard core model include the analysis of sedimentation of DNA molecules [59] and investigation in the melting of simple fluids [60]. In fact, the growing interest in colloidal suspension substances [61] leads to the use of hard sphere particles as a model for colloids in glassy phases and jamming [62] as well as sedimentation [10, 11].

Hard core lattice fluids are the lattice analogue of hard core continuous models, specialized to the case of discrete space of lattice sites. Many studies have been carried out upon this model especially for lattice models, e.g. in [63, 64] where hard sphere fluids are considered as hard cubes (or hard discs in two dimensions) and their centers constrained to lie on lattice sites. Low and high densities series expansions were derived exactly for the plain-triangular lattice gas, and in three dimensions, for the simple cubic and body-centered cubic lattice gases with next nearest neighbour exclusion [65]. In [66, 67] the lattice model is applied to surface adsorption. In addition, this model is also employed in biological science to study the gradual evolution of species [68].

A powerful framework to describe static properties of equilibrium systems, including models with hard core interactions, is classical density functional theory (DFT) [69–72]. This theory is utilized in classical statistical physics for describing phenomena in inhomogeneous fluids including adsorption [71, 73], freezing [74], surface and interface behaviour [75], and colloid-polymer mixtures [76]. In general, the main objective of DFT is to construct an approximate functional for the intrinsic free energy $\mathcal{F}$ of a classical system. In order to achieve this, the theory uses the concept that $\mathcal{F}$ can be written as a functional of the one-body density $\rho(\mathbf{r})$, viz. $\mathcal{F}[\rho(\mathbf{r})]$, where $\mathbf{r}$ is the position coordinate. Moreover, $\mathcal{F}[\rho(\mathbf{r})]$ may be obtained via the Legendre transform of the grand potential functional $\Omega[\rho]$, which is also a functional of ρ. A functional derivative of $\mathcal{F}[\rho]$ with

respect to ρ gives the one-body direct correlation function, i.e. $c^{(1)}[\rho;\mathbf{r}]$. An important step in any DFT is the variational principle, in which $\Omega[\rho]$ is minimized, i.e. the functional derivative of $\Omega[\rho]$ with respect to $\rho(\mathbf{r})$ vanishes at the correct equilibrium density $\rho_0(\mathbf{r})$. Once $\rho_0(\mathbf{r})$ is attained, one may then derive other thermodynamic quantities of the system.

The success of classical DFT in describing various properties of equilibrium systems leads to a natural desire to use it in attempts to treat non-equilibrium systems [70, 77–83]. There is an appealing advantage of using DFT for dynamical systems, i.e. it provides insights into the dynamics of the systems on the microscopic level via statistical mechanics. Recently there has been a vast number of results coming out of DFT that are devoted to dealing with off-equilibrium, near equilibrium or relaxation to equilibrium systems. The extension of classical DFT to dynamical systems is known as dynamical DFT (DDFT) [79, 81, 84], or time-dependent DFT (TDDFT) [82, 85]. To our knowledge, the idea of using DFT to study dynamical equilibrium and non-equilibrium systems following the success of (equilibrium) classical DFT was initially introduced around 1979, in [70], to analyze the kinetics of spinodal decomposition at the level of a varying time-dependent one-body density. In this early development of the DDFT, it is postulated [70, 78], without rigorous derivation, that the current density of a system is thermodynamically driven by the gradient of the (equilibrium) chemical potential, the latter being obtained as the functional derivative of the (equilibrium) free energy functional $\mathcal{F}[\rho]$. In [78], a time-dependent one-body density, which has a structure of a generalized Smoluchowski equation, is derived using the aforementioned assumption combined with the continuity equation and the functional $\mathcal{F}[\rho]$. Formal derivations of the DDFT or TDDFT then follow in numerous articles [77, 79, 81–83] using various assumptions and kinetic equations as starting points, e.g. Brownian motion [81], the Langevin stochastic equation [79], hydrodynamic equations [77], and Newton's equations of motion [83]. Interestingly, the equation for the time evolution of the one-body density that are gained from these derivations has a rather similar form [86]. In addition, the definition of one-body density used for a system effects the nature of its time evolution, i.e. whether it is stochastic or deterministic [86]. DDFT (or TDDFT) has been employed to study the dynamics of soft matter, including the glass transition of dense colloidal suspension [87], solvation in simple mixtures [85], ultrasoft particles under time-varying potentials [88], relaxation of model fluids of platelike colloidal parti-

cles [89], and sedimentation of hard-sphere-like colloidal particles confined in horizontal capillaries [10].

There are certainly other compelling theories tackling non-equilibrium systems. The mode coupling theory (CMT) is used to study close to equilibrium systems, e.g. to discuss the glass transition in simple liquids [90]. A non-linear diffusion equation (NLDE) is applied to study supercooled simple liquids which gives a good description of the hydrodynamic properties, e.g. see [91]. In order to calculate the density distribution of a dynamical system the Langevin equation has been used, e.g. in [92]. There are also theories based upon the trajectory space of the systems, e.g. in [93] where the ensembles of trajectories corresponding to the large deviations of time-integrated quantities of the Glauber-Ising chain model are considered, and in [94] where kinetically constrained glass models are investigated by analyzing the trajectories of the dynamics.

In view of the fact that the development of dynamical DFT is still ongoing research, in this thesis we would like to put forward an alternative approach. The concept of DDFT relies, as an input, on $\mathcal{F}[\rho]$, which is a functional of the one-body density. The current density, i.e. the average number of particles going through a given volume per unit time, is obtained as an output from the theory. However, based on the idea that a non-zero current is maintained in the system, here we construct a functional of the current density rather than of the one-body density. The one-body density is then determined using the continuity equation. The master equation is the starting point. The so-called microscopic current is introduced into the formal solution of the master equation. Then a variational principle is postulated for the functional of the current density similar to the procedure of classical DFT. Finally, a fundamental argument is proposed for the existence of the current density functional.

We take the TASEP and several of its variants in steady state and in non-steady state regimes as our case studies. Hence, one objective in this project is to construct an (approximate) theory similar to that of DFT [1, 69–71, 95] utilizing the master equation, but based on the microscopic current. An attempt to incorporate DFT in order to study the physical properties of the TASEP was given in [45], in which a correspondence between the hard core lattice model of a monomer-dimer mixture and the TASEP was proposed. From this correspondence one may obtain the mean field one-body and current density profiles of the TASEP (through the DFT of the monomer-dimer mixture). Another attempt at relating equilibrium and non-equilibrium systems is given in [96].

Here, the simple symmetric exclusion process (SSEP) at the (fluctuating) hydrodynamic limit may be mapped into an isolated system satisfying the detailed balance condition where the probability distribution is provided by the Gibbs-Boltzmann measure.

This thesis is organized as follows. In Chapter 2 brief descriptions are provided for: the master equation, the TASEP, classical DFT, the hard core lattice fluid model, and DDFT. Various results from the TASEP and its variants are presented in Chapter 3, including i) the analytical solution of the TASEP with only one site, ii) mean-field one-body and current densities of the TASEP with time-dependent input and output rates (employing sequential and parallel dynamics), iii) mean-field one-body and current densities for the TASEP with open boundaries in 2D, and iv) mean-field one-body and current densities of the TASEP with a junction. In Chapter 4 an alternative correspondence between the TASEP and the 1D continuous hard rod fluid is proposed. In Chapter 5 the current density functionals of the 1D TASEP are constructed, for: i) the TASEP with a single site and ii) the TASEP with N sites, within the mean-field approximation. A formal arguments for the existence of these current density functionals are given in Chapter 6. Chapter 7 contains a general discussion of the results obtained from Chapter 3 to 6. Finally, conclusions and outlook are given in Chapter 8.

Chapter 2

Background of Study

2.1 The Master Equation

A phenomenological first-order-partial differential equation that gives the time evolution of the probabilities of a system is usually referred to as a master equation. As with any differential equation, the master equation needs to be (at least formally) solved in order to obtain the time-dependent probabilities of the system. This equation is commonly used to describe Markovian processes where memory effects are neglected. An early attempt to derive the master equation was made, by Pauli for the quantum case [7, 97]. See ref. [97] for a brief history of the master equation. Throughout this thesis, the existence of an (abstract) master equation is assumed and we will not dwell in its derivation from more fundamental dynamics. However, those readers who are interested may consult e.g. ref. [98], where the master equation is derived from the Chapman-Kolmogorov equation, and refs. [2, 7] where the quantum master equation is derived.

The systems which we consider possess discrete microscopic states, labelled by n, n'. These microscopic states form a state space $\mathcal{S}$, i.e. $n', n \in \mathcal{S}$. They can be quite general depending on the degrees of freedom of the physical system under consideration. We assign a probability $P_n(t)$ to each microscopic state n, which gives the likelihood of the system to be in state n at time t. The probability satisfies the normalization condition, i.e.: $\sum_n P_n(t) = 1$. The system starts to evolve at time $t = 0$ with initial condition $P_n(0)$. A transition from state n to state n' may occur at time t with rate $w_{n'n}(t)$. The

time evolution of $P_n(t)$ is governed by the master equation expressed as [2, 7, 97, 99]:

$$\frac{\partial P_n(t)}{\partial t} = \sum_{n'} \left[w_{nn'}(t) P_{n'}(t) - w_{n'n}(t) P_n(t) \right], \tag{2.1.1}$$

or alternatively in a matrix form,

$$\frac{\partial P_n(t)}{\partial t} = \sum_{n'} \mathcal{W}_{nn'}(t) P_{n'}(t), \tag{2.1.2}$$

where $P_{n'}(t)$ is the probability of the system to be in state n' at time t and $w_{nn'}(t)$ is the transition rate from state n' to state n at time t. $\mathcal{W}_{nn'}(t)$ is a matrix defined by

$$\mathcal{W}_{nn'}(t) = (1 - \delta_{nn'})\, w_{nn'}(t) - \delta_{nn'} \sum_{k} w_{kn'}(t), \tag{2.1.3}$$

with $\delta_{nn'}$ being the Kronecker delta. The matrix (2.1.3) satisfies $\sum_n \mathcal{W}_{nn'}(t) = 0$ which shows that the total probability is conserved. One interesting feature of (2.1.1) is that the physics lies entirely in the transition rates $w_{n'n}(t)$ [100]. In other words, the transition rates define the physical model under consideration. Therefore, once the $w_{n'n}(t)$ are specified, an attempt to solve for $P_n(t)$ may be executed.

A special case in many non-equilibrium systems is the steady state condition. This condition is usually designated as non-equilibrium stationary state (NESS). By definition, the steady state condition is obtained if the probability is stationary, i.e.: $P_n(t) = P_n$, and hence $\partial P_n(t)/\partial t = 0$. Here we consider a simple case where the transition rate from state n' to n is constant in time (stationary), i.e. $w_{nn'}(t) = w_{nn'} = \text{const}$. At the limit $t \to \infty$, the system is expected to reach steady state. Thus, in steady state, equation (2.1.1) simplifies to

$$\sum_{n'} w_{nn'} P_{n'} = \sum_{n'} w_{n'n} P_n. \tag{2.1.4}$$

Hence, the product between the transition rates, $w_{nn'}$, and their corresponding probabilities, $P_{n'}$, going out from state n' is equal to the sum of the product between $w_{n'n}$ and P_n going into state n'. As a consequence transitions between microscopic states may occur which produces a constant current along the system. Moreover, it is precisely this non-zero (constant) current that maintains the system at steady state far-from-equilibrium.

Stronger constraint may be imposed on equation (2.1.4). In equilibrium, the current throughout the system must be zero (there is no net effect of transitions between microscopic states). This is achieved if the product between the transition rate and its

corresponding probability going out of state n' is equal to the same product going into state n', i.e.:

$$w_{nn'}P_{n'} = w_{n'n}P_n. \tag{2.1.5}$$

This is known as the detailed balance condition. It is clear that there is no current in the system since any pair of transitions going into and going out of state n' cancel each other. Furthermore, equation (2.1.5) certainly implies equation (2.1.4) but not vice versa.

2.2 The Totally Asymmetric Exclusion Process

In this Section, a brief overview of the TASEP is presented. We constrain this discussion to the case of the TASEP on a 1D lattice $\mathcal{L}$.

2.2.1 Description of the Model

Consider a lattice system in 1D, $\mathcal{L}$, with sites $i = 0, 1, 2, \ldots, N \in \mathcal{L}$, where N is the total number of lattice sites, and $i = 0$ is the zeroth site of $\mathcal{L}$. We decorate $\mathcal{L}$ by placing particles with hard core interactions at sites $1 \leq i \leq N$. If a particle occupies site i the particle excludes any other particle from occupying this site (site exclusion). If $\tau_{i,n}$ is the occupation number of site i of microscopic state n, then this quantity is defined by,

$$\tau_{i,n} = \begin{cases} 1, & \text{if site } i \text{ of state } n \text{ is occupied,} \\ 0, & \text{otherwise.} \end{cases} \tag{2.2.1}$$

At any given time t one may specify the microscopic (configurational) state, n, of the system as $\{\tau_{i,n}\} = \{\tau_{1,n}, \tau_{2,n}, \tau_{3,n}, \ldots, \tau_{N-1,n}, \tau_{N,n}\}$. Thus, n is specified by a sequence of occupation numbers at each site. In order to illustrate this, an example is given in Figure 2.1. The microscopic configuration of Fig. 2.1 can be written as $n = \{1001 \ldots 111 \ldots 110\}$, where the ellipses indicate the sequence of occupation numbers not written explicitly for convenience. The probability of state $n = \{1001 \ldots 111 \ldots 110\}$ at time t is then given by $P_n(t)$.

2.2.2 The Dynamics

The dynamics of the particles in $\mathcal{L}$ is specified by systematic iterative instructions to update a given microscopic configuration at each time step. This gives the (average)

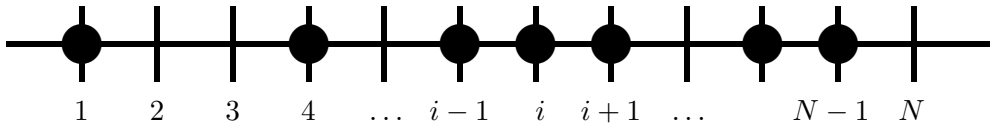

Figure 2.1: An example of a configurational state of the TASEP in 1D with N sites. The 1D lattice consists of a set of sites (vertical tick marks) with equal distances (lattice spacing). The sites are labelled by $i \in \mathcal{L}$, which starts from $i = 1$ (left-most site) to $i = N$ (right-most site). Particles (filled circles) may occupy the lattice sites. However, due to site exclusion only one particle may sit on any given site. In the example above, sites $i = 1$, $i = 4$, $i - 1$, i, $i + 1$, $N - 2$, and $N - 1$ are occupied by one particle.

motion of particles along $\mathcal{L}$. There are various types of dynamics that may be given to particles or to the sites. Here we employ two of those types, namely random sequential and parallel updating. Note that time, t, is considered to be a discrete parameter in this discussion. Hence, one time step may be denoted by $t \to t + 1$ where the shortest time interval is 1 time step.

Sequential updating

Sequential updating requires that at each (discrete) time step, a site is chosen randomly with probability $1/(N + 1)$ where we also consider the zeroth site, i.e. $i = 0$ [hence there are $(N + 1)$ total number of sites]. If site $1 \leq i \leq N - 1$ is chosen and there is a particle occupying the site, the particle can hop with rate $k_{i(i+1)}(t)$ to the right-nearest neighbour so long as no other particle is at site $i + 1$. $k_{i(i+1)}(t)$ is the hopping rate of a particle from site i to site $i + 1$ at time t. A visual example of the sequential updating process is depicted in Fig. 2.2. Thus, if at some time t the system is arranged in the microscopic state $n = \{\tau_{1,n}, \tau_{2,n}, \ldots, \tau_{N-1,n}, \tau_{N,n}\}$, then at the next time step, $t + 1$, the state may stay at state n (if no jump occurs) or updated to another *possible* state, $n' = \{\tau_{1,n'}, \tau_{2,n'}, \ldots, \tau_{N-1,n'}, \tau_{N,n'}\}$, via satisfying

$$\tau_{i,n'} = \begin{cases} \tau_{i,n}\tau_{i+1,n}, & \text{with probability } \frac{k_{i(i+1)}(t)}{N+1}, \\ \tau_{i,n} + [1 - \tau_{i,n}]\,\tau_{i-1,n}, & \text{with probability } \frac{k_{(i-1)i}(t)}{N+1}, \\ \tau_{i,n}, & \text{with probability } 1 - \frac{1}{N+1}\left(k_{i(i+1)}(t) + k_{(i-1)i}(t)\right). \end{cases} \tag{2.2.2}$$

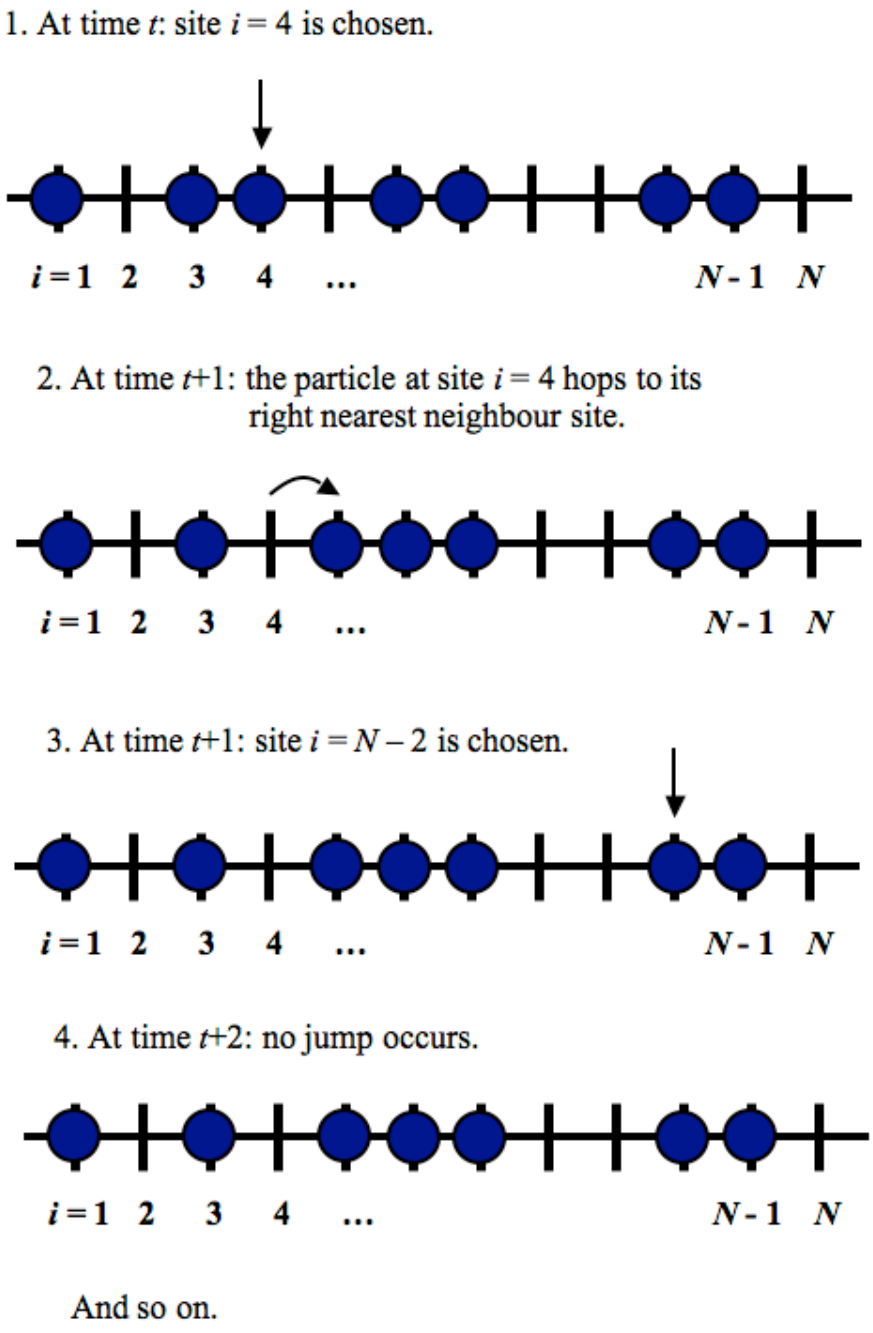

Figure 2.2: A sketch of the dynamical process of the TASEP with open boundaries where the positions of the particles are sequentially updated. The lattice sites are depicted by vertical lines labelled by $i = 0, 1, \ldots, N-1, N$. The filled (blue) circles occupying the sites are hard core particles. The dark arrow (drawn horizontally) gives the direction in which the particle jumps. The straight arrows (drawn vertically) indicate the chosen site.

The first case above applies if site i is updated. The second case is given if site $i-1$ is the updated site, and finally all other sites will not be updated according to the third possibility. A special case of interest in the TASEP with sequential updating is setting the hopping rate constant throughout the bulk, that is $k_{i(i+1)}(t) = 1$ for $1 \leq i \leq N-1$.

Furthermore, the sequential dynamics produces a transition from one state, n, to another state, n', at each (discrete) time step. Consider the state n from Figure 2.1 as an example, but now with a complete configuration with a total of 12 lattice sites, i.e. $n = \{100101110110\}$. Let there be another state, $n' = \{010101110110\}$. According to the above updating process, if site $i = 1$ is chosen at time t, a transition from state n to n', $n \to n'$, i.e. $\{\mathbf{10}0101110110\} \to \{\mathbf{01}0101110110\}$ occurs with transition rate $w_{n'n}(t) = k_{12}(t)$. By definition of the sequential updating process, there are also prohibited transitions from one state to other states. Transitions such as $n = \{10\mathbf{01}01110110\} \to n'' = \{10\mathbf{10}01110110\}$ are not allowed, such that in this case $w_{n''n}(t) = 0$.

Parallel updating

A different situation occurs for parallel updating dynamics. Here, all particles that have an empty neighbouring site jump to their respective right-nearest neighbour site with hopping rate of $k_{i(i+1)}(t)$. Fig. 2.3 shows an example of this. As time evolves a number of particles hopping at the same time produce parallel motion of particles rather than sequential (one by one) at each time step. Therefore, if at time t a microscopic state is given by $n = \{\tau_{i,n}\}$, then a transition from state n to state $n' = \{\tau_{i,n'}\}$ at time $t+1$ is given by,

$$\tau_{i,n'} = \begin{cases} \tau_{i,n}\tau_{i+1,n} & \text{with probability } k_{i(i+1)}(t) \\ \tau_{i-1,n}\,(1-\tau_{i,n}) & \text{with probability } k_{(i-1)i}(t) \\ \tau_{i,n} & \text{with probability } 1-k_{i(i+1)}(t), \end{cases} \tag{2.2.3}$$

where the first and second possibilities are used if the updated sites are i and $i-1$, whereas the third is used for sites consisting of particles that do not jump.

As in sequential dynamics, a case of interest in this updating process is choosing constant hopping rates throughout the bulk, i.e.: $k_{i(i+1)}(t) = 1$ for $1 \leq i \leq N-1$. This indicates that particles (each occupying a site) with empty neighbouring sites jump to their respective right nearest neighbour site at each time step, $t \to t+1$, with certainty (probability 1). As an example, take again Figure 2.1 where the full configurational

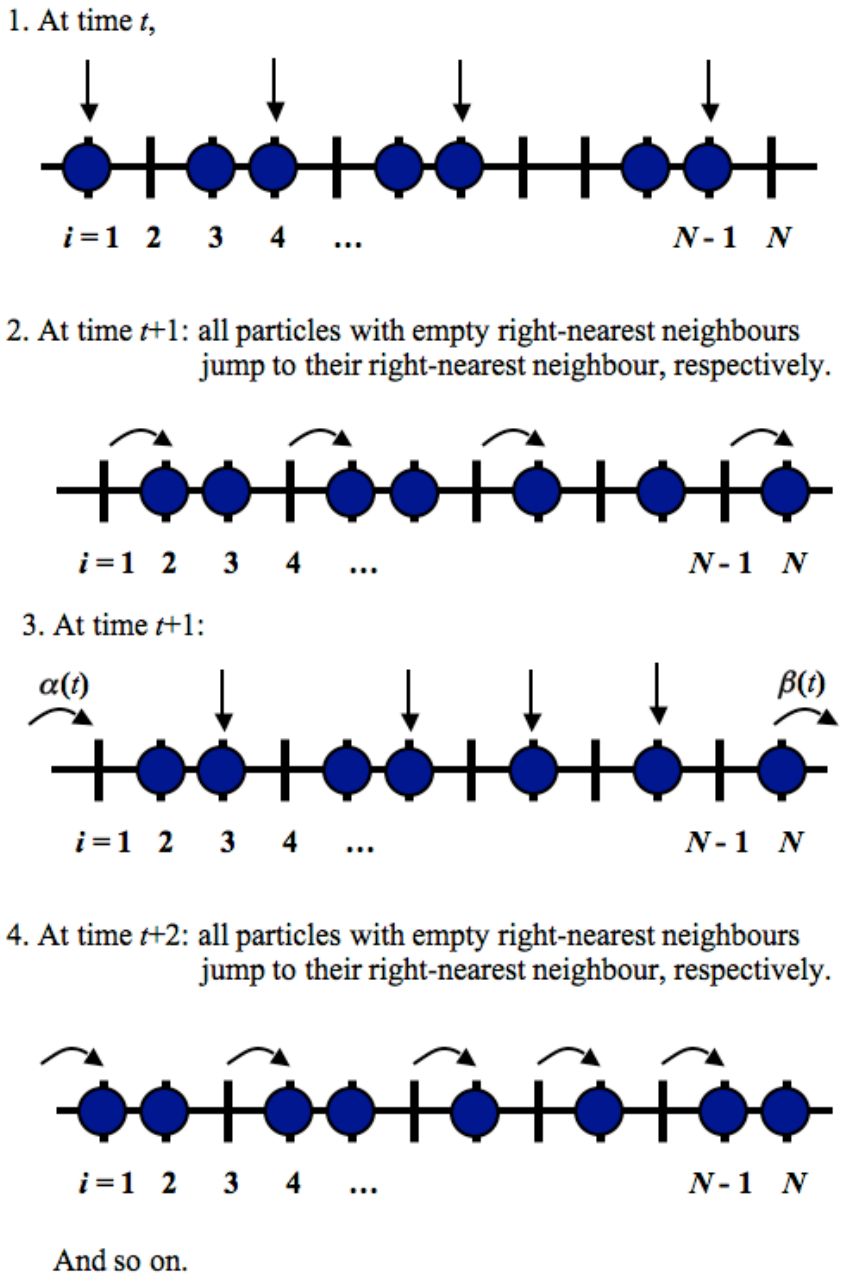

Figure 2.3: A sketch of parallel updating of the TASEP. The lattice sites are depicted by vertical lines, labelled by $i = 1, 2, \ldots, N-1, N$. The filled (blue) circles occupying the sites are hard core particles. The dark arrows give the direction in which the particles jump. All particles with empty neighbouring site may jump to their respective right nearest neighbours.

state is $n = \{\mathbf{10}0\mathbf{10}1\mathbf{11}1\mathbf{0}\mathbf{11}\mathbf{0}\}$, where we have boldface the pairs of occupation numbers which undergo a parallel updating. If $n' = \{010011101101\}$ is another microscopic state, then according to the parallel updating process, a transition from state n to state n' is possible with rate $w_{n'n} = 1$.

2.2.3 Boundary Conditions

Two types of boundary conditions are commonly utilized in the TASEP, viz.: open and periodic boundaries. For open boundaries, a particle may enter the lattice, $\mathcal{L}$, with an input hopping rate of $\alpha(t)$ to the left-most site, i.e. site $i = 1$ if there is no particle at site $i = 1$. Furthermore, if there is a particle at site $i = N$, then the particle may exit $\mathcal{L}$ with a hopping rate of $\beta(t)$.

For periodic boundaries, the left-most and right-most sites are joined such that a closed loop of lattice sites is formed. The necessary conditions for this case are

$$\tau_1 = \tau_{N+1}, \qquad \text{and} \qquad \tau_N = \tau_0. \tag{2.2.4}$$

2.2.4 One-Body and Current Densities

Two different types of densities are considered in this thesis: the one-body and current densities. These may vary in time (t) and position (i). For the TASEP these quantities are denoted by $\rho_i(t)$ and $J_{i(i+1)}(t)$, viz.: the one-particle density of site i at time t and the current density from site i to site $i+1$ at time t, respectively. Generally, the one-body and the current densities are related phenomenologically via

$$\mathbf{J}_i(t) = \rho_i(t)\mathbf{v}_i(t), \tag{2.2.5}$$

where $\mathbf{J}_i(t)$ and $\mathbf{v}_i(t)$ are the current and average velocity densities of the particle flow at site i at time t. For a model (such as the TASEP) where the particle number is locally conserved, the continuity equation,

$$\nabla \cdot \mathbf{J}_i(t) = -\frac{\partial \rho_i(t)}{\partial t}, \tag{2.2.6}$$

is also satisfied. For the discrete system of the TASEP one may define $\nabla \cdot \mathbf{J}_i(t) \to J_{i(i+1)}(t) - J_{(i-1)(i)}(t)$, such that the continuity equation (2.2.6) reads

$$\frac{\partial \rho_i(t)}{\partial t} = J_{(i-1)i}(t) - J_{i(i+1)}(t), \tag{2.2.7}$$

where the time parameter, t, may be continuous or discrete, $J_{(i-1)i}(t)$ is the current density linking site $i-1$ to site i at time t. Hence, $\rho_i(t)$ may be determined from the knowledge of the current densities $J_{(i-1)i}(t)$ and $J_{i(i+1)}(t)$ by integrating equation (2.2.7)-for continuous time, yielding

$$\rho_i(t) = \rho_i(0) + \int_0^t \mathrm{d}t' \left[J_{(i-1)i}(t') - J_{i(i+1)}(t')\right], \tag{2.2.8}$$

where $\rho_i(0)$ is the initial one-body density of site i at an initial time of $t = 0$.

Alternatively, $\rho_i(t)$, may be determined by summing the time-dependent probabilities, $P_n(t)$, over all microscopic states, n, at site i and time t, that is

$$\rho_i(t) = \sum_n \tau_{i,n} P_n(t), \tag{2.2.9}$$

where the time dependency of the one-body density lies on $P_n(t)$.

By considering that n' is a microscopic state obtained after updating state n (using the discrete time step), equation (2.2.2) may be averaged to obtain the one-particle density of site i at time $t+1$ for the sequential updating of the TASEP as

$$\begin{aligned}\sum_{n'} \tau_{i,n'} P_{n'}(t+1) &= \frac{k_{i(i+1)}(t)}{N+1} \sum_n \left[\tau_{i,n}\tau_{i+1,n} P_n(t)\right] \\ &+ \frac{k_{(i-1)i}(t)}{N+1} \sum_n \left[\tau_{i,n} + (1-\tau_{i,n})\,\tau_{i-1,n}\right] P_n(t) \\ &+ \left(1 - \frac{\left[k_{i(i+1)}(t) + k_{(i-1)i}(t)\right]}{N+1}\right) \sum_n \tau_{i,n} P_n(t). \end{aligned} \tag{2.2.10}$$

Using the definition of the one-body density (2.2.9) in (2.2.10) gives

$$\begin{aligned}\rho_i(t+1) &= \frac{k_{i(i+1)}(t)}{N+1}\rho_{i(i+1)}(t) + \frac{k_{(i-1)i}(t)}{N+1}\left[\rho_i(t) + \rho_{i-1}(t) - \rho_{(i-1)i}(t)\right] + \rho_i(t) \\ &\quad - \frac{\left[k_{i(i+1)}(t) + k_{(i-1)i}(t)\right]}{N+1}\rho_i(t) \\ &= \rho_i(t) + \frac{k_{(i-1)i}(t)}{N+1}\left[\rho_{i-1}(t) - \rho_{(i-1)i}(t)\right] - \frac{k_{i(i+1)}(t)}{N+1}\left[\rho_i(t) - \rho_{i(i+1)}(t)\right], \end{aligned}$$

or

$$\rho_i(t+1) - \rho_i(t) = -\frac{1}{N+1}\left[k_{i(i+1)}(t)\left(\rho_i(t) - \rho_{i(i+1)}(t)\right) - k_{(i-1)i}(t)\left(\rho_{i-1}(t) - \rho_{(i-1)i}(t)\right)\right], \tag{2.2.11}$$

where $2 \leq i \leq N-1$, and $\rho_{i(i+1)}(t)$ is the density-density correlation function (sometimes known as the two-body density). This quantity determines the average probability of

particles occupying site i when there is another particle occupying the right-nearest neighbour site, $i+1$, at time t. Because the discrete time steps are adopted, the LHS of equation (2.2.11) may be defined as a discrete derivative of the density with respect to time, i.e.:

$$\frac{\partial \rho_i(t)}{\partial t} \equiv \rho_i(t+1) - \rho_i(t). \tag{2.2.12}$$

Now inserting definition (2.2.12) into equation (2.2.11) and comparing the latter to equation (2.2.7), we find that equation (2.2.11) is a continuity equation where the current density is given by

$$J_{i(i+1)}(t) = k_{i(i+1)}(t)\left[\rho_i(t) - \rho_{i(i+1)}(t)\right]. \tag{2.2.13}$$

For parallel updating, equation (2.2.3) may be averaged to get the one-particle density of site i at time $t+1$, viz.:

$$\begin{aligned}\sum_{n'} \tau_{i,n'} P_{n'}(t+1) &= (1 - k_{i(i+1)}(t)) \left(\sum_n \tau_{i,n} P_n(t)\right) + k_{i(i+1)}(t) \left(\sum_n \left[\tau_{i,n}\tau_{i+1,n}\right] P_n(t)\right) \\ &\quad + k_{(i-1)i}(t) \left(\sum_n \left[\tau_{i-1,n} - \tau_{i-1,n}\tau_{i,n}\right] P_n(t)\right).\end{aligned} \tag{2.2.14}$$

Using again (2.2.9) in (2.2.14) yields

$$\rho_i(t+1) = \rho_i(t) + \left[k_{(i-1)i}(t)\left(\rho_{i-1}(t) - \rho_{(i-1)i}(t)\right) - k_{i(i+1)}(t)\left(\rho_i(t) - \rho_{i(i+1)}(t)\right)\right], \tag{2.2.15}$$

or, applying again (2.2.12) and (2.2.13) upon (2.2.15) gives back equation (2.2.7), that is

$$\rho_i(t+1) - \rho_i(t) = \frac{\partial \rho_i(t)}{\partial t} = -\left[J_{i(i+1)}(t) - J_{(i-1)i}(t)\right].$$

Equations (2.2.11) and (2.2.15) are central equations in subsequent Chapters.

2.2.5 The Steady State Solution

As mentioned above, an important condition investigated in the field of driven systems is the non-equilibrium steady state (NESS). Consider constant input and output rates, i.e.: $\alpha(t) = \alpha$ and $\beta(t) = \beta$, and constant hopping rates throughout the bulk, viz: $k_{(i-1)i}(t) = k_{(i-1)i}$ and $k_{i(i+1)}(t) = k_{i(i+1)}$. In steady state, the system is maintained in non-equilibrium via a non-vanishing current, but the average density is stationary (does not vary with time). This condition may be achieve when the system has evolved over a sufficiently long time, such that

$$\frac{\partial \rho_i(t)}{\partial t} = 0,$$

hence $\rho_i(t) = \rho_i$. As a consequence, equations (2.2.11) and (2.2.15) become

$$k_{i(i+1)} \left(\rho_i - \rho_{i(i+1)}\right) = k_{(i-1)i} \left(\rho_{(i-1)} - \rho_{(i-1)i}\right). \tag{2.2.16}$$

Furthermore, according to equation (2.2.7) the current density becomes

$$J_{i(i+1)} = J_{(i-1)i}, \tag{2.2.17}$$

which is satisfied by (2.2.16). This indicates that at stationary state, the current density still exists, but it is the same at all lattice sites, at any time t. This is in fact a feature that differentiates the NESS and the equilibrium condition. For open boundaries additional equations are added at the boundaries. These are,

$$\alpha \left[1 - \rho_1\right] = \rho_1 - \rho_{12}, \tag{2.2.18}$$

by setting $k_{01} = \alpha$ in (2.2.16), and

$$\rho_{N-1} - \rho_{(N-1)N} = \beta \rho_N, \tag{2.2.19}$$

by inserting $k_{N(N+1)} = \beta$.

2.2.6 Exact Results via a Recursion Formula

Exact results are known for the TASEP in steady state. A recursion formula [36] and a matrix technique [34] are constructed for calculating the one-body density of the TASEP with constant input and output rates. Another exact result is obtained by solving the master equation for the parallel and ordered sequential updating asymmetric exclusion process for an infinite one dimensional lattice [33]. In this thesis only the recursion formula is considered as this method is relevant to this present project. This formula is applied in Chapter 3 as a comparison to the analytical solution of the TASEP with a single site. Those who are interested in the matrix method may refer ref. [34].

In the following the results (without rigorous proof) of [36] is described. This is ultimately the one-body density of the TASEP in 1D with sequential dynamics at steady state. Beforehand, the readers are reminded that some mathematical expressions in this section might look complicated. Hence one may need some thoughts in order to understand them. So, consider first $P_{n,N}$ as the time-independent probability of state $n = \{\tau_1, \tau_2, \ldots, \tau_N\}$ with N number of sites in steady state. Using the dynamics given

in equation (2.2.2) and considering constant rates, $k_{(i-1)i}(t) = k_{i(i+1)}(t) = 1$, $P_{n,N}$ may be written in the form of,

$$\begin{aligned} P_{n,N} &= \frac{1}{N+1}\left((1-\alpha)P_{n,N} + \alpha\tau_1\left[P_{n(\tau_1=0),N} + P_{n(\tau_1=1),N}\right]\right) \\ &+\frac{1}{N+1}\left[P_{n,N} + (\tau_2-\tau_1)P_{n(\tau_1=1,\tau_2=0),N}\right] \\ &+\ldots \\ &+\frac{1}{N+1}\left[P_{n,N} + (\tau_N-\tau_{N-1})P_{n(\tau_{N-1}=1,\tau_N=0),N}\right] \\ &+\frac{1}{N+1}\left((1-\beta)P_{n,N} + \beta(1-\tau_N)\left[P_{n(\tau_N=0),N} + P_{n(\tau_N=1),N}\right]\right), \end{aligned} \tag{2.2.20}$$

where $n(\tau_1 = 0) = \{0, \tau_2, \ldots, \tau_N\}$, $n(\tau_1 = 1) = \{1, \tau_2, \ldots, \tau_N\}$, $n(\tau_1 = 1, \tau_2 = 0) = \{1, 0, \tau_3, \ldots, \tau_N\}$ and so forth, are extended notations of the configurational states n. The equation (2.2.20) may be stated as

$$\begin{aligned} &\alpha(2\tau_1 - 1)P_{n(\tau_1=0),N} + (\tau_2-\tau_1)P_{n(\tau_1=1,\tau_2=0),N} + \ldots \\ &+(\tau_N-\tau_{N-1})P_{n(\tau_{N-1}=1,\tau_N=0),N} + (1-2\tau_N)P_{n(\tau_N=1),N} = 0. \end{aligned} \tag{2.2.21}$$

Equation (2.2.21) represents a set of 2^N coupled linear equations which have to be solved simultaneously. In [36] it is proved that the probability $P_{n,N+1}$ may be obtained from $P_{n,N}$ via a recursion method. However instead of using $P_{n,N}$ directly, it is convenient to write down the probability in terms of a weight function, $f_{n,N}$, which is proportional to $P_{n,N}$, i.e.:

$$P_{n,N} = \frac{f_{n,N}}{Z_N}, \tag{2.2.22}$$

where

$$Z_N = \sum_n f_{n,N}. \tag{2.2.23}$$

A recursion formula is provided in [36] to determine the set of $f_{n,N}$, that is:

$$\begin{aligned} f_{n,N} &= \alpha\tau_N f_{n,N-1} + \alpha\beta(1-\tau_N)\tau_{N-1}\left[f_{n(\tau_{N-1}=1),N-1} + f_{n(\tau_{N-1}=0),N-1}\right] \\ &+\ldots \\ &+\alpha\beta(1-\tau_N)(1-\tau_{N-1})\ldots(1-\tau_2)\tau_1\left[f_{n(\tau_1=1),N-1} + f_{n(\tau_1=0),N-1}\right] \\ &+\beta(1-\tau_N)(1-\tau_{N-1})\ldots(1-\tau_1)f_{n,N-1}. \end{aligned} \tag{2.2.24}$$

For the trivial example $N = 1$ (single site), the recursion above gives,

$$f_{n=2,N=1} = \beta, \qquad \text{and} \qquad f_{n=1,N=1} = \alpha, \tag{2.2.25}$$

where $n = 2 = \{\tau_1 = 0\}$ and $n = 1 = \{\tau_1 = 1\}$. For $N = 2$ one obtains,

$$f_{1,2} = \beta^2, \qquad f_{2,2} = \alpha\beta(\alpha + \beta), \qquad f_{3,2} = \alpha\beta, \qquad \text{and} \qquad f_{4,2} = \alpha^2, \tag{2.2.26}$$

where $n = 1 = \{0, 0\}$, $n = 2 = \{1, 0\}$, $n = 3 = \{0, 1\}$, and $n = 4 = \{1, 1\}$. Thus, using (2.2.24), (2.2.25), and (2.2.26) it is possible, in principle, to get $f_{n,N}$ for any N. Then the average occupancy of site i with N lattice sites, $\rho_{i,N}$, may be determined as

$$\rho_{i,N} = \frac{T_{i,N}}{Z_N}, \tag{2.2.27}$$

where

$$T_{i,N} = \sum_n \tau_{i,n} f_{n,N}. \tag{2.2.28}$$

According to [36] the difficulty of computing $T_{i,N}$ and Z_N from equation (2.2.24) is that there are no closed recursions for the latter quantities. In order to tackle this difficulty, other quantities, i.e. $Y_{K,N}$ and $X_{g,K,N}$, are defined, that is

$$Y_{K,N} = \sum_n (1 - \tau_N)(1 - \tau_{N-1}) \dots (1 - \tau_K) f_{n,N}, \tag{2.2.29}$$

and

$$X_{g,K,N} = \sum_n (1 - \tau_N) \dots (1 - \tau_K) \tau_g f_{n,N}. \tag{2.2.30}$$

Now, these new quantities are related to those above by

$$Z_N = Y_{N+1,N}, \tag{2.2.31}$$

and

$$T_{g,N} = X_{g,N+1,N}. \tag{2.2.32}$$

Finally, in order to compute equations (2.2.31) and (2.2.32) closed recursion formulas can be obtained. For $1 \leq K \leq N + 1$, one gets for Y_N:

$$\begin{aligned} &Y_{1,N} = \beta Y_{1,N-1}, \\ &Y_{K,N} = Y_{K-1,N} + \alpha\beta Y_{K,N-1} \qquad \text{for} \qquad 2 \leq K \leq N, \\ &Y_{N+1,N} = Y_{N,N} + \alpha Y_{N,N-1}. \end{aligned} \tag{2.2.33}$$

Hence, together with the initial conditions,

$$Y_{1,1} = \beta \qquad \text{and} \qquad Y_{2,1} = \alpha + \beta, \tag{2.2.34}$$

all $Y_{K,N}$ are determined from equation (2.2.33)

For $g+1 \leq K \leq N+1$ one obtains for X_N,

$$\begin{aligned} X_{g,g+1,N} &= \alpha\beta Y_{g+1,N-1} \quad \text{for} \quad 1 \leq g \leq N-1, \\ X_{g,K,N} &= X_{g,K-1,N} + \alpha\beta X_{g,K,N-1} \quad \text{for} \quad g+2 \leq K \leq N, \\ X_{g,N+1,N} &= X_{g,N,N} + \alpha X_{g,N,N-1} \quad \text{for} \quad 1 \leq g \leq N-1, \\ X_{N,N+1,N} &= \alpha Y_{N,N-1}. \end{aligned} \tag{2.2.35}$$

Hence, all the $X_{g,K,N}$ may be determined using the recursion formulas (2.2.33) with initial conditions (2.2.34), and (2.2.35) with an initial condition

$$X_{1,2,1} = \alpha. \tag{2.2.36}$$

2.2.7 The Mean-Field Approach

The above exact solution of the TASEP is restricted to the case of constant input and output hopping rates. The recursion formula or the matrix method have not been, to the best of our knowledge, applied if the rates are time-dependent. There is, however, another approach to investigate at least qualitative features of the TASEP. This is the mean-field method, which is based on an approximation that the particles only 'feel' the average effect of neighbouring particles. Based on this approximation, the two-body correlation function appearing in equation (2.2.13) is written as $\rho_{i(i+1)}(t) \approx \rho_i(t)\rho_{i+1}(t)$, that is the effect of particles at site $i+1$ on particles at site i at time t is simplified by the average of each site separately. So, equation (2.2.13) can be factorized as

$$J_{i(i+1)}(t) = k_{i(i+1)}(t)\left[\rho_i(t) - \rho_i(t)\rho_{i+1}(t)\right] = k_{i(i+1)}(t)\rho_i(t)[1-\rho_{i+1}(t)]. \tag{2.2.37}$$

Hence, inserting back equation (2.2.37) into equations (2.2.11), yields

$$\frac{\partial\rho_i(t)}{\partial t} = \frac{1}{N+1}\left(k_{(i-1)i}(t)\rho_{i-1}(t)[1-\rho_i(t)] - k_{i(i+1)}(t)\rho_i(t)[1-\rho_{i+1}(t)]\right), \tag{2.2.38}$$

for sequential updating, and without the factor $1/(N+1)$ on the RHS of (2.2.38) for parallel updating. In steady state, the mean-field approximation becomes

$$J_{i(i+1)} = \rho_i\left[1-\rho_{i+1}\right] = \rho_{i-1}\left[1-\rho_i\right] = J_{(i-1)i}, \tag{2.2.39}$$

$$\alpha\left[1-\rho_1\right] = \rho_1\left[1-\rho_2\right], \tag{2.2.40}$$

and

$$\rho_{(N-1)} - \rho_{(N-1)}\rho_N = \beta\rho_N. \tag{2.2.41}$$

The simple form of the dynamic equations (2.2.37)-(2.2.41) in the mean-field approximation comes at the price of losing some information about the physical features of the system. One significant consequence of this approximation is the neglect of correlations between any two sites. This might be valid for systems with low fluctuations. For particle hopping models, in particular for the TASEP, at each time step $t \to t+1$, a particle may jump from site i to site $i+1$. As time progresses, the trajectory of each particle constitutes the memory of the system. For a full treatment of the system, the trajectories of two particles at neighbouring sites cannot overlap. However, in the mean-field approximation, each site is considered independent from its neighbouring sites. This may result in overlap of trajectories, hence the loss of some memory features of the system.

One way to test the validity of the mean-field approximation is through numerical comparison to simulation results. This is done in the next Section, where we compare mean-field and simulation results for the one-body and current densities for given constant input and output rates of the TASEP with open boundaries. The mean-field approximation is applied in many subsequent parts of the thesis, including Chapters 3, 4, and 5.

2.2.8 Phase Diagram and Density Profiles for Sequential Dynamics

In the following several physical features of the model are described, that is, the phase diagram and the corresponding density profiles. The model being considered is the TASEP with sequential updating and open boundaries at steady state.

The phase diagrams of the sequential and parallel [101] updating are quite similar, and is illustrated in Figure 2.4. It is drawn in terms of the input and output rates, α and β, respectively. The horizontal and vertical-axes indicate the values of α and β, respectively. These rates take numerical values from 0 to 1. There are four phases exhibited in the phase diagrams, viz.: low density, high density, coexistence, and maximal current phases. The low density phase is the region on the upper-left part of the phase diagram. The high density phase is shown in the lower part of the phase diagram. The coexistence phase is obtained at the boundary (half diagonal) between the low and high density phases. The maximal current is the region on the top-right of the phase diagram.

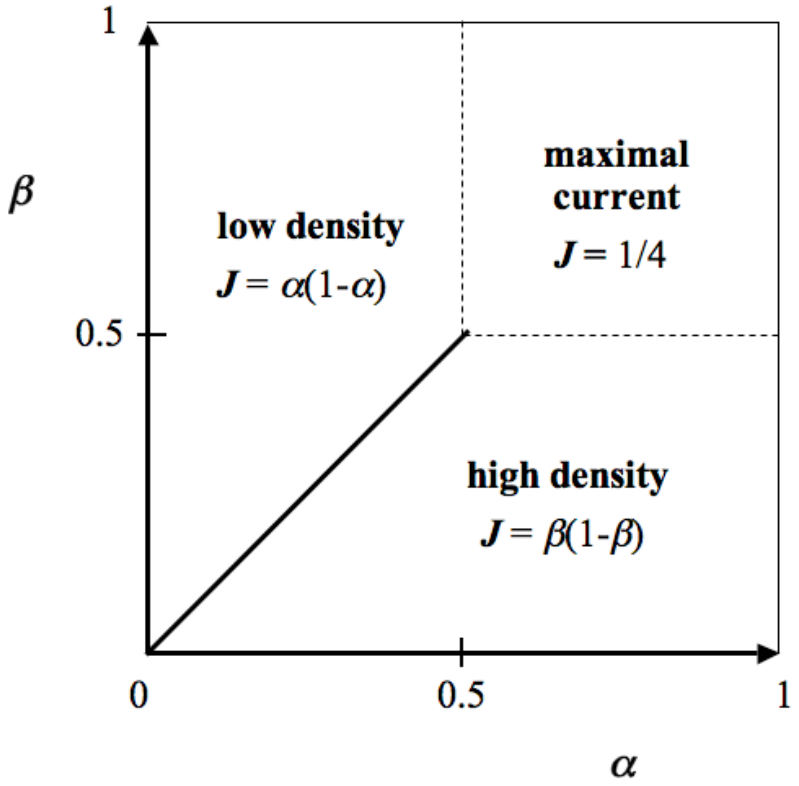

Figure 2.4: Phase diagram of the TASEP with open boundaries at steady state. The phase diagram is attained in terms of the input and output hopping rates where the horizontal and vertical axes are α and β, respectively. The equations inside the phase diagram are values of the constant current density for each phase. The low density regime is obtained for $\alpha < \beta$ and $\alpha < 0.5$. The high density phase is obtained for $\alpha > \beta$ and $\beta < 0.5$. The coexistence phase (full line) between high and low densities is obtained for $\alpha = \beta$ and $\alpha, \beta < 0.5$. Finally, the maximal current phase produces the maximum value of the current density, i.e.: $J = 0.25$. This phase is obtained if $\alpha, \beta > 0.5$.

These density profiles are discussed in more detail in the following.

For $\alpha < \beta$ and $\alpha < 0.5$, the low density phase is obtained. Typical one-body and current density profiles in the low density phase are given in Fig. 2.5. In this phase, it is more probable for particles (at the boundaries) to exit the lattice $\mathcal{L}$ rather than enter it. Therefore, the average one-body density throughout the system should be low, i.e. less than 0.5 or $\rho_i < 0.5$. From Figure 2.5, it may be observed that the one-body density, ρ_i, both from the mean-field theory (blue dotted line) and simulation (red crosses), is mostly flat with $\rho_i = 0.3$, starting from the left boundary and throughout the bulk, except near the exit of $\mathcal{L}$ where ρ_i increases. The flat density profile is controlled by the input rate, α, whereas the behavior of ρ at the end of the sites depends upon the output rate, β. If β is large (but < 1.0) then the density at the end of the sites increases (as shown in Fig. 2.5), otherwise it decreases. Notice also that the one-body density resulting from the theoretical (mean-field) result agrees very well with the simulation.

The high density phase is produced whenever $\alpha > \beta$ and $\beta < 0.5$. Hence, many particles occupy $\mathcal{L}$ such that the average density of the particle is larger than 0.5. Jamming of particles may also appear along the lattice sites. Typical one-body and current densities in the high density phase is given in Figure 2.6. The one-body density is given by the (blue) dotted line (from mean-field theory) and (red) crosses (from simulation). The mean-field and simulation results agree very well. The profile of the one-body density is nearly flat throughout the lattice sites, except near the entrance of $\mathcal{L}$. The flat profile dominates over the whole bulk and it is controlled by β, while near the entrance of $\mathcal{L}$ the profile may increase or decrease depending upon α. In this case, for $\alpha = 0.9$ and $\beta = 0.3$ the profile near the entrance of $\mathcal{L}$ increases as it approaches the entrance, and the flat profile has a value of 0.7. The current densities are depicted by the (pink) dotted line [mean-field], and the (green) crosses [simulation]. The two results clearly agree with each other. The current density is entirely flat from the entrance until the end of $\mathcal{L}$ with a value of 0.21.

Another interesting feature of the TASEP is the coexistence phase. According to the phase diagram, the coexistence phase is reached when $\alpha = \beta$ and $\alpha, \beta < 0.5$. This is a phase where the low and high (one-body) densities coexist. Typical density profiles of the coexistence phase are given in Figure 2.7 with $\alpha = \beta = 0.2$ chosen as hopping rates. The one-body density profile is shown by the (blue) dotted line, mean-field theory, and (red) crosses, the simulation. Consider the mean-field profile of the one-body density.

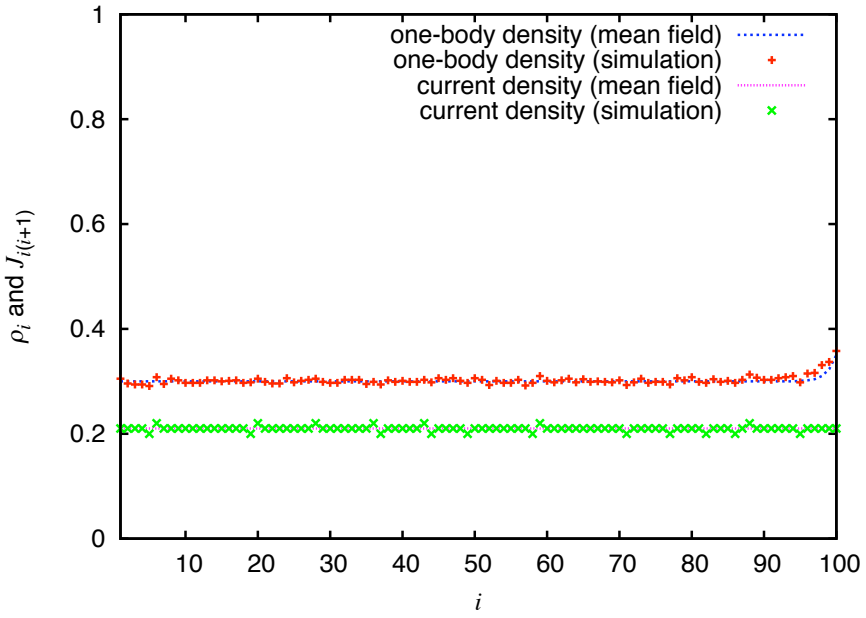

Figure 2.5: An example of the low density profile of the TASEP with sequential updating and constant input and output hopping rates in steady state. Here the case of $\alpha = 0.3$ and $\beta = 0.6$ is considered. The horizontal axis labels the lattice sites (i) with $N = 100$ the total number of lattice sites. The vertical axis labels the (one-body and current) density profiles. The one-body density may be observed from the (blue) dotted line and (red) crosses, which resulted from the theoretical (mean-field) calculation and simulation, respectively. The current density is exhibited from the (pink) dotted line (mean-field theory) and (green) crosses (simulation). The one-body density profile is mainly flat throughout the bulk and deviates (increases) as it approaches the end of the sites. The current density is flat throughout $\mathcal{L}$.

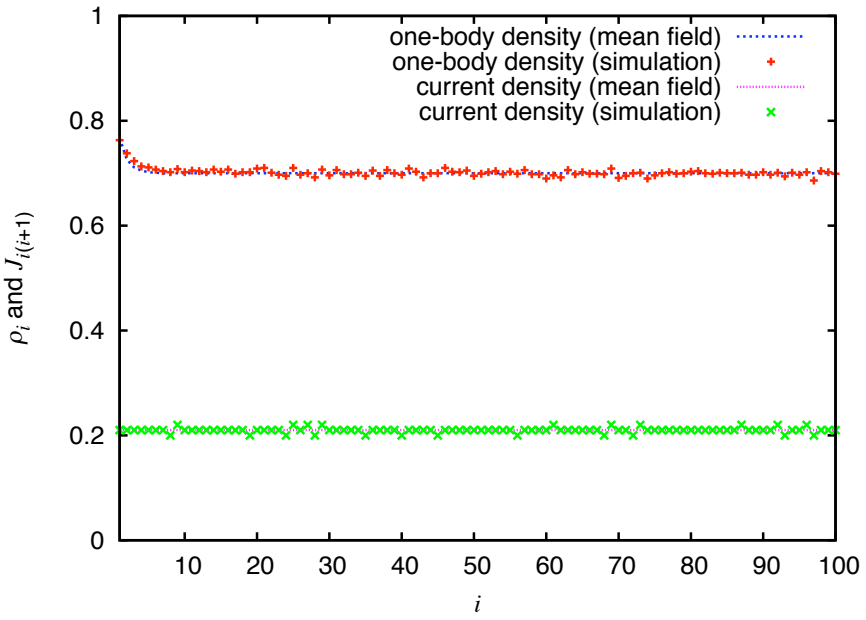

Figure 2.6: An example of the high density profiles for the TASEP with sequential updating and open boundaries in steady state. The horizontal axis labels the lattice sites, i, with $N = 100$, and the vertical axis labels the (one-body and current) densities. The one-body density is depicted by the (blue) dotted line [mean-field] and (red) crosses [simulation]. The current density is given by the (pink) dotted line [mean-field] and (green) crosses [simulation]. The one-body density profile is mainly flat throughout the bulk to the end of the sites, but deviates (increases) at the entrance of the sites. The current density is flat throughout the sites with a value of 0.21.

The profile starts from a flat low density of 0.2 at the entrance of $\mathcal{L}$. The value of the flat low density profile is governed by the input hopping rate, which is in this case 0.2. Away from the entrance of the lattice sites, at some point, a sudden change from the low density to a high density with a value of 0.8 occurs. This sudden change from the low to the high densities is known as a shock. Away from the shock one ends up in a flat high density region until the remaining sites. However, the simulation result shows a straight line (with no shock). This is due to the fact that the true location of the shock changes at each time step at steady state, i.e. the shock location is stochastic. It is clearly observed that no motion of the shock location occurs in the mean-field profile. The current density of the coexistence phase is given in Figure 2.7 by the flat profiles from mean-field theory ([pink] dotted line) and simulation ([green] crosses). It is clear that the two results are in a good agreement with each other.

The final phase of the sequential updating TASEP is obtained for $0.5 < \alpha, \beta \leq 1.0$, and is designated as the maximal current phase. In this phase, the lattice sites are being entered and exited by a large number of particles because of the high probability of particles coming into and coming out of $\mathcal{L}$. Thus particles diffuse along the lattice sites and the bulk of the profile takes a value close to 0.5. Typical density profiles of the maximal current phase are depicted in Figure 2.8 for $\alpha = 0.6$ and $\beta = 0.8$. The mean-field one-body density is given by the dotted (blue) line, whereas the simulation result is given by the (red) crosses. The two results agree well, except close to the exit sites of $\mathcal{L}$. However, there is still overall qualitative agreement between the results. Starting from the entrance of $\mathcal{L}$ the value of the one-body density is just below 0.6 and continues to decrease reaching the value of 0.5 as the density profile approaches the center of $\mathcal{L}$. Going away from the center, the one-body density decreases further until the end of $\mathcal{L}$ with a value falling below 0.4. Around the entrance sites the one-body density is higher than 0.5 while close to the exit sites the density is lower than 0.5. The two profiles intersect at 0.5 at the center of $\mathcal{L}$. When the size of the lattice sites is infinite, the density will be 0.5 at every site apart from the end points, i.e. as $N \to \infty$, then $\rho_{\text{bulk}} \to 0.5$. The mean-field current density is given by the dotted (pink) line (mean-field), whereas the simulation result is given by the (green) crosses. The two results are consistent whereby a flat profile is obtained. The value of the current density is constant at 0.25, and this is the maximum value for the TASEP with sequential dynamics.

To summarize, the mean-field and simulation results for the one-body density agree

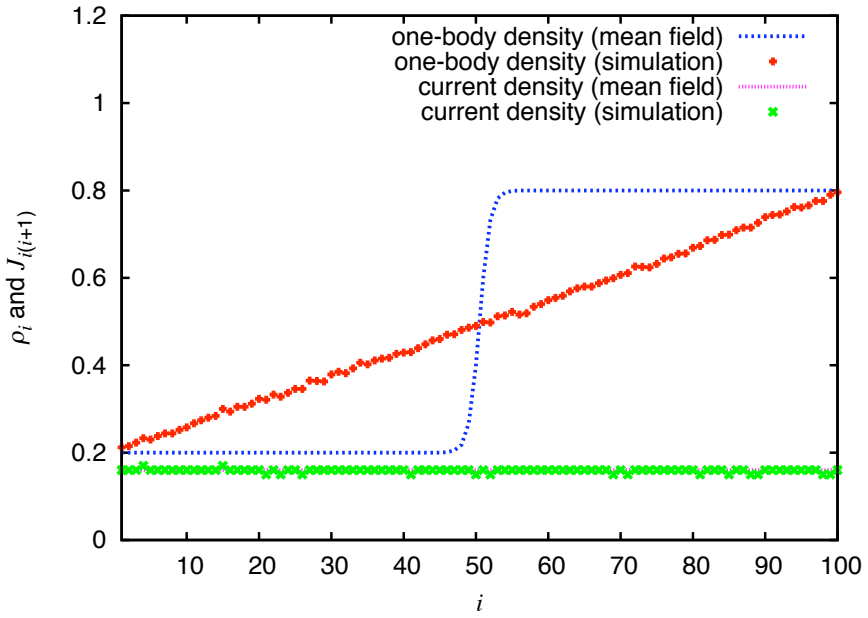

Figure 2.7: An example of the coexistence phase densities of the TASEP with $\alpha = \beta = 0.2$ in steady state. The horizontal axis labels the lattice sites, i, with $N = 100$ sites. The vertical axis labels the (one-body and current) density profiles. The mean-field one-body density profile is shown in (blue) dotted line, whereas the simulation result is given by the (red) crosses. According to the mean-field theory the profile of the one-body density starting from the entrance site is flat with value 0.2, which is a low density (< 0.5). A sudden jump or shock happens at site $i = 50$. The density then remains flat at a high density of 0.8 until the remaining sites. However, according to the simulation the one-body density profile is a straight line. For the current density profile, there is a good agreement between the theory [(pink) line] and simulation [(green) crosses] results. The current density is flat everywhere indicating a constant value throughout the lattice sites at any time.

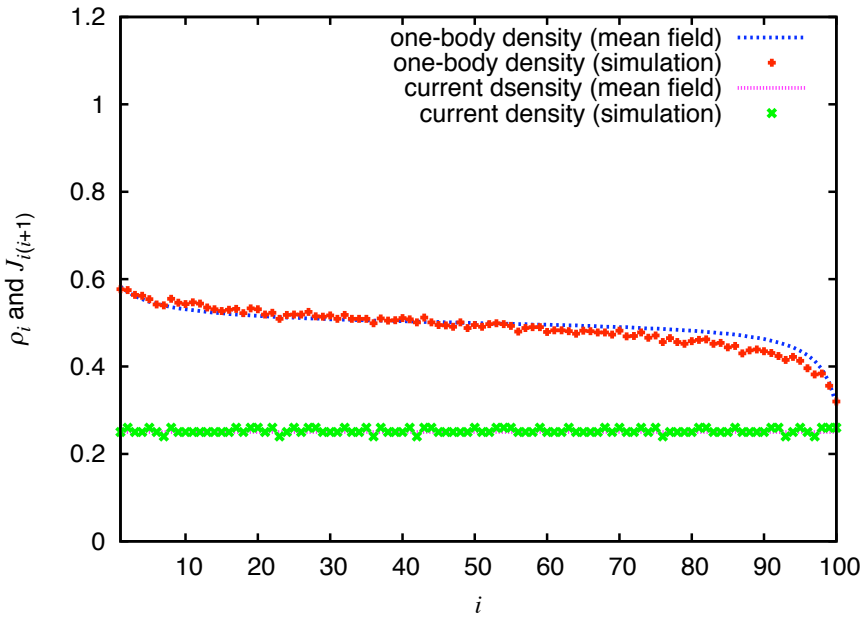

Figure 2.8: The one-body and current densities of the maximal current phase of the TASEP with sequential updating, where $\alpha = 0.6$ and $\beta = 0.8$ for $N = 100$. The horizontal axis labels the lattice sites (i) and the vertical axis labels the (one-body and current) densities. The one-body density profile is shown by the (blue) dotted line from the mean-field theory, whereas the (red) crosses are the simulation result. The current density is given by the (pink) dotted line and the (green) crosses, which are obtained from the mean-field calculation and simulation, respectively. Qualitatively, the profile of the one-body density starts from a high density value of less than 0.6, then it decreases to 0.5 at the center, and finally it decreases further at the exit sites. The theory and simulation agree nicely in the first 50 sites but they deviate over the last 30 or so sites. On the other hand, the current densities from the mean-field theory [(pink) dotted line] and simulation [(green) crosses] agree nicely. The current density is flat with value of 0.25.

very well for low and high density phases, thus justifying the mean-field approximation discussed in the previous Section. However, when the current reaches its maximum value of 0.25, the mean-field profile of the one-body density deviates from the simulation result near the ends of the lattice. This shows that the correlations between (neighbouring) sites may not be simply neglected. The mean-field result also fails to detect the stochastic behaviour of the shock at coexistence between low and high densities. Nevertheless, the mean-field profile is still capable of capturing some qualitative behaviour of the one-body density in the coexistence and maximal current phases. Furthermore, for all phases, the mean-field and simulation results for the current density profiles agree very well.

2.3 Classical Density Functional Theory

2.3.1 Theoretical Foundations

Classical density functional theory (DFT) is a powerful framework that is based on a variational principle and that can be applied to tackle various problems in the (equilibrium) statistical physics of fluids. The aforementioned variational principle was originally proposed in [102], known as the Hohenberg-Kohn theorem [103, 104], especially developed for quantum systems. An extension of the theorem for finite (non-zero) temperature was done in [105], and fully realized for classical DFT in [69–71]. In the development of the theory, another proof for the variational principle of DFT, namely the constrained search method, was given in [1] and further adopted in [104]. In the following several aspects of the proof in [69] are presented. Alternatively, the constrained search method is also provided, which to the best of our knowledge has not been done before for classical DFT. The latter proof is used later on, especially in Chapter 6.

We consider the grand canonical ensemble of a system of classical particles, where the probability density, f_0, for M particles at temperature $\mathcal{T}$ is given by,

$$f_0 = \Xi^{-1} \exp\left(-\mathcal{B}\left(H_M - \mu M\right)\right), \tag{2.3.1}$$

where H_M is the Hamiltonian of M particles, μ is the chemical potential, and $\mathcal{B} = 1/(k_B\mathcal{T})$ with k_B is the Boltzmann constant. Ξ is the grand canonical partition sum, i.e.:

$$\Xi = \mathrm{Tr}_{\mathrm{cl}} \exp\left(-\mathcal{B}\left(H_M - \mu M\right)\right), \tag{2.3.2}$$

with $\mathrm{Tr}_{\mathrm{cl}}$ is the sum over all particles and integral over all degrees of freedom (in continuous space), viz.:

$$\mathrm{Tr}_{\mathrm{cl}} = \sum_{M=0}^{\infty} \frac{1}{h^{3M} M!} \int \mathrm{d}\mathbf{r}_1 \ldots \mathrm{d}\mathbf{r}_M \int \mathrm{d}\mathbf{p}_1 \ldots \mathrm{d}\mathbf{p}_M, \tag{2.3.3}$$

where $\mathbf{r}_1, \ldots, \mathbf{r}_M$ are the position coordinates of particles $1, \ldots, M$, and $\mathbf{p}_1, \ldots, \mathbf{p}_M$ are the momentum coordinates of particles $1, \ldots, M$.

Next, a functional is introduced, which is defined as follows

$$\Omega[f] = \mathrm{Tr}_{\mathrm{cl}} f \left(H_M - \mu M + \mathcal{B}^{-1} \ln f \right), \tag{2.3.4}$$

where f is any trial probability density that satisfies $\mathrm{Tr}_{\mathrm{cl}} f = 1$. For the equilibrium probability density, i.e. $f = f_0$, the functional (2.3.4) yields

$$\begin{aligned} \Omega[f_0] &= \mathrm{Tr}_{\mathrm{cl}} f_0 \left(H_M - \mu M + \mathcal{B}^{-1} \ln f_0 \right) \\ &= \mathrm{Tr}_{\mathrm{cl}} f_0 \left(H_M - \mu M + \mathcal{B}^{-1} \left[- \ln \Xi - \mathcal{B}(H_M - \mu M) \right] \right) \\ &= -\mathcal{B}^{-1} \ln \Xi \equiv \Omega_0, \end{aligned} \tag{2.3.5}$$

where Ω_0 is the (equilibrium) grand potential. An important property of the functional (2.3.4) is that it reaches a minimum when $f = f_0$, viz.:

$$\Omega[f] > \Omega[f_0] \; ; \qquad f \neq f_0. \tag{2.3.6}$$

The above inequality may be proven using the Gibbs inequality [70], which is given as follows. First, from equations (2.3.1) and (2.3.5), $\Omega[f]$ of equation (2.3.4) can be written as

$$\Omega[f] = \Omega[f_0] + \mathcal{B}^{-1} \mathrm{Tr}_{\mathrm{cl}} f \ln \left(\frac{f}{f_0} \right). \tag{2.3.7}$$

Moreover, the Gibbs inequality gives

$$f \ln \left(\frac{f_0}{f} \right) < f \left(\frac{f_0}{f} - 1 \right) \quad \Rightarrow \quad \mathrm{Tr}_{\mathrm{cl}} f \ln \left(\frac{f}{f_0} \right) > \mathrm{Tr}_{\mathrm{cl}} (f_0 - f).$$

But the probability density must satisfy $\mathrm{Tr}_{\mathrm{cl}} f_0 = \mathrm{Tr}_{\mathrm{cl}} f = 1$. Therefore, the RHS of the inequality above gives 0, or

$$\mathcal{B}^{-1} \mathrm{Tr}_{\mathrm{cl}} f \ln \left(\frac{f}{f_0} \right) > 0. \tag{2.3.8}$$

Thus, in accordance with (2.3.8), the second term on the RHS of equation (2.3.7) is positive (> 0), hence the inequality (2.3.6).

In classical systems, the Hamiltonian may be restricted to a form:

$$H_M = \sum_{m=1}^{M} \frac{p_m^2}{2\Gamma} + U(\mathbf{r}_1, \ldots, \mathbf{r}_M) + \sum_{m=1}^{M} V_{\text{ext}}(\mathbf{r}_m), \tag{2.3.9}$$

where the first term is the sum over the kinetic energy of all particles, U is the interatomic potential between the particles, $V_{\text{ext}}(\mathbf{r})$ is the (arbitrary) external potential, and Γ is the particle mass. If the system is enclosed in a volume $\mathcal{V}$, the equilibrium one-body density is defined as

$$\rho_0(\mathbf{r}) = \langle \hat{\rho}(\mathbf{r}) \rangle = \text{Tr}_{\text{cl}} \left[f_0 \hat{\rho}(\mathbf{r}) \right], \tag{2.3.10}$$

where $\langle \ldots \rangle$ denotes the configurational average and the density operator, $\hat{\rho}(\mathbf{r})$, is

$$\hat{\rho}(\mathbf{r}) = \sum_{m=1}^{M} \delta(\mathbf{r} - \mathbf{r}_m). \tag{2.3.11}$$

We now provide a result for the existence of a density functional based upon the v-representability of the one-body density, $\rho_0(\mathbf{r})$. It is clear that f_0 is a function of V_{ext} through equation (2.3.1), and that therefore $\rho_0(\mathbf{r})$ is a functional of V_{ext}. Another valuable result can also be deduced, that is f_0 is a functional of $\rho_0(\mathbf{r})$. The proof begins via reductio ad absurdum where for a given interaction potential U, $V_{\text{ext}}(\mathbf{r})$ is uniquely determined by $\rho_0(\mathbf{r})$. The resultant V_{ext} then determines f_0. Hence, f_0 is a functional of $\rho_0(\mathbf{r})$.

An important consequence of the above result is that for a given interaction potential U,

$$\mathcal{F}[\rho] = \text{Tr}_{\text{cl}} f_0 \left(\sum_{m=1}^{M} \frac{p_m^2}{2\Gamma} + U + \mathcal{B}^{-1} \ln f_0 \right), \tag{2.3.12}$$

is a unique functional of the (trial) one-body density, $\rho(\mathbf{r})$. Furthermore, using a Legendre transform the grand potential functional is obtained for a given external potential as,

$$\Omega_V[\rho] = \mathcal{F}[\rho] + \int \mathrm{d}\mathbf{r} \rho(\mathbf{r}) V_{\text{ext}}(\mathbf{r}) - \mu \int \mathrm{d}\mathbf{r} \rho(\mathbf{r}). \tag{2.3.13}$$

The functional $\Omega_V[\rho]$ returns its minimum value if $\rho = \rho_0$, i.e. if the trial density is the correct equilibrium one-body density. The value is the grand potential Ω_0. The existence of the minimum value of $\Omega[\rho]$ may be proven by considering another equilibrium density ρ' associated with a probability density f' of unit trace, such that

$$\begin{aligned} \Omega[f'] &= \text{Tr}_{\text{cl}} f' \left(H_M - \mu M + \mathcal{B}^{-1} \ln f' \right) \\ &= \int \mathrm{d}\rho'(\mathbf{r}) V_{\text{ext}}(\mathbf{r}) + \mathcal{F}[\rho'] - \mu \int \mathrm{d}\mathbf{r} \rho'(\mathbf{r}) \\ &= \Omega[\rho'], \end{aligned} \tag{2.3.14}$$

where

$$\mathcal{F}[\rho'] = \mathrm{Tr}_{\mathrm{cl}} f' \left(\sum_{m=1}^{M} \frac{p_m^2}{2\Gamma} + U + \mathcal{B}^{-1} \ln f' \right). \tag{2.3.15}$$

However, it is known from equation (2.3.6) that $\Omega[f'] > \Omega[f_0]$, for $f' \neq f_0$, thus it follows that

$$\Omega_V[\rho'] > \Omega_V[\rho_0]. \tag{2.3.16}$$

In other words, the correct equilibrium one-body density, $\rho_0(\mathbf{r})$, minimizes $\Omega_V[\rho]$ over all density functions that can be associated with the potential $V_{\mathrm{ext}}(\mathbf{r})$.

This important result may be stated as a functional derivative, viz.:

$$\left. \frac{\delta \Omega_V[\rho]}{\delta \rho(\mathbf{r})} \right|_{\rho_0} = 0, \tag{2.3.17}$$

and

$$\Omega_V[\rho_0] = \Omega_0. \tag{2.3.18}$$

The above derivation of the foundation of classical DFT is based on the v-representability of the one-body density. A v-representable ρ is one which is associated with a probability density, f, of some Hamiltonian H_M with external potential V_{ext} [1, 104]. However, one may also derive the existence of a functional $Q[\rho]$ that is based on a weaker condition than the v-representability, i.e. that ρ may not always be associated to some external potential. This relaxed condition is called the M-representability of the one-body density. The functional $Q[\rho]$ is an analogue of $\mathcal{F}[\rho]$. The proof of the existence of $Q[\rho]$ is originally derived for quantum systems [1, 95], i.e. interacting electrons in atoms, molecules, and solids under the term 'constrained search method'. Here we put forward a similar argument for interacting classical particles. First one defines a functional $Q[\rho]$ which represents a functional of all one-body density that are M-representable for the sum of kinetic and interaction potential, i.e.:

$$Q[\rho] = \min_{f} \left[\mathrm{Tr}_{\mathrm{cl}} f \left(\sum_{m=1}^{M} \frac{p_m^2}{2\Gamma} + U + \mathcal{B}^{-1} \ln f \right) \right]. \tag{2.3.19}$$

It is important to understand the definition of $Q[\rho]$. $Q[\rho]$ is a functional that searches all probability densities, f, satisfying $\mathrm{Tr}_{\mathrm{cl}} f = 1$, which yield a fixed trial ρ where ρ need not be v-representable, and

$$\rho(\mathbf{r}) = \mathrm{Tr}_{\mathrm{cl}} \left[f \hat{\rho}(\mathbf{r}) \right]. \tag{2.3.20}$$

$Q[\rho]$ then returns a minimum value. In order that $Q[\rho]$ yields a valid functional, it is necessary to prove two theorems for any one-body density that satisfies the M-representability condition. These are

$$\int \mathrm{d}\mathbf{r}\,(V_{\mathrm{ext}}(\mathbf{r})-\mu)\,\rho(\mathbf{r})+Q[\rho]\geq\Omega_0, \tag{2.3.21}$$

and

$$\int \mathrm{d}\mathbf{r}\,(V_{\mathrm{ext}}(\mathbf{r})-\mu)\,\rho_0(\mathbf{r})+Q[\rho_0]=\Omega_0. \tag{2.3.22}$$

For convenience, additional notations are defined to facilitate the proofs. f^{ρ}_{min} is designated as the probability density that satisfies the RHS of equation (2.3.19). Then it follows that

$$Q[\rho]=\mathrm{Tr}_{\mathrm{cl}}f^{\rho}_{\mathrm{min}}\left(\sum_{m=1}^{M}\frac{p_m^2}{2\Gamma}+U+\mathcal{B}^{-1}\ln f^{\rho}_{\mathrm{min}}\right), \tag{2.3.23}$$

and

$$Q[\rho_0]=\mathrm{Tr}_{\mathrm{cl}}f^{\rho_0}_{\mathrm{min}}\left(\sum_{m=1}^{M}\frac{p_m^2}{2\Gamma}+U+\mathcal{B}^{-1}\ln f^{\rho_0}_{\mathrm{min}}\right). \tag{2.3.24}$$

First we proof equation (2.3.21). By its very definition, the LHS of (2.3.21) may be rearranged into

$$\begin{aligned}
&\int \mathrm{d}\mathbf{r}\,(V_{\mathrm{ext}}(\mathbf{r})-\mu)\,\rho(\mathbf{r})+Q[\rho]\\
=\;&\int \mathrm{d}\mathbf{r}\,(V_{\mathrm{ext}}(\mathbf{r})-\mu)\,\rho(\mathbf{r})+\mathrm{Tr}_{\mathrm{cl}}f^{\rho}_{\mathrm{min}}\left(\sum_{m=1}^{M}\frac{p_m^2}{2\Gamma}+U+\mathcal{B}^{-1}\ln f^{\rho}_{\mathrm{min}}\right)\\
=\;&\mathrm{Tr}_{\mathrm{cl}}f^{\rho}_{\mathrm{min}}\left(H_M-\mu M+\mathcal{B}^{-1}\ln f^{\rho}_{min}\right).
\end{aligned} \tag{2.3.25}$$

But according to equation (2.3.6),

$$\mathrm{Tr}_{\mathrm{cl}}f^{\rho}_{\mathrm{min}}\left(H_M-\mu M+\mathcal{B}^{-1}\ln f^{\rho}_{\mathrm{min}}\right)\geq\Omega_0. \tag{2.3.26}$$

Thus, combining equations (2.3.25) and (2.3.26), equation (2.3.21) is recovered. In order to prove (2.3.22), equation (2.3.6) is invoked once again,

$$\mathrm{Tr}_{\mathrm{cl}}f^{\rho_0}_{\mathrm{min}}\left(H_M-\mu M+\mathcal{B}^{-1}\ln f^{\rho_0}_{\mathrm{min}}\right)\geq\Omega_0, \tag{2.3.27}$$

or

$$\mathrm{Tr}_{\mathrm{cl}}f^{\rho_0}_{\mathrm{min}}\left(H_M-\mu M+\mathcal{B}^{-1}\ln f^{\rho_0}_{\mathrm{min}}\right)\geq\mathrm{Tr}_{\mathrm{cl}}f_0\left(H_M-\mu M+\mathcal{B}^{-1}\ln f_0\right). \tag{2.3.28}$$

But $f_{\min}^{\rho_0}$ and f_0 generate the same one-body density ρ_0, yielding,

$$\int \mathrm{d}\mathbf{r}\,(V_{\mathrm{ext}}(\mathbf{r})-\mu)\,\rho_0(\mathbf{r}) \quad + \quad \mathrm{Tr}_{\mathrm{cl}} f_{\min}^{\rho_0}\left(\sum_{m=1}^{M}\frac{p_m^2}{2\Gamma}+U+\mathcal{B}^{-1}\ln f_{\min}^{\rho_0}\right) \geq \int \mathrm{d}\mathbf{r}\,(V_{\mathrm{ext}}(\mathbf{r})-\mu)\,\rho_0(\mathbf{r}) + \mathrm{Tr}_{\mathrm{cl}} f_0\left(\sum_{m=1}^{M}\frac{p_m^2}{2\Gamma}+U+\mathcal{B}^{-1}\ln f_0\right), \tag{2.3.29}$$

or

$$\mathrm{Tr}_{\mathrm{cl}} f_{\min}^{\rho_0}\left(\sum_{m=1}^{M}\frac{p_m^2}{2\Gamma}+U+\mathcal{B}^{-1}\ln f_{\min}^{\rho_0}\right) \geq \mathrm{Tr}_{\mathrm{cl}} f_0\left(\sum_{m=1}^{M}\frac{p_m^2}{2\Gamma}+U+\mathcal{B}^{-1}\ln f_0\right). \tag{2.3.30}$$

However by the very definition of $f_{\min}^{\rho_0}$ the following inequality should also hold,

$$\mathrm{Tr}_{\mathrm{cl}} f_{\min}^{\rho_0}\left(\sum_{m=1}^{M}\frac{p_m^2}{2\Gamma}+U+\mathcal{B}^{-1}\ln f_{\min}^{\rho_0}\right) \leq \mathrm{Tr}_{\mathrm{cl}} f_0\left(\sum_{m=1}^{M}\frac{p_m^2}{2\Gamma}+U+\mathcal{B}^{-1}\ln f_0\right). \tag{2.3.31}$$

The two last equations hold simultaneously, if and only if,

$$\mathrm{Tr}_{\mathrm{cl}} f_{\min}^{\rho_0}\left(\sum_{m=1}^{M}\frac{p_m^2}{2\Gamma}+U+\mathcal{B}^{-1}\ln f_{\min}^{\rho_0}\right) = \mathrm{Tr}_{\mathrm{cl}} f_0\left(\sum_{m=1}^{M}\frac{p_m^2}{2\Gamma}+U+\mathcal{B}^{-1}\ln f_0\right), \tag{2.3.32}$$

or

$$Q[\rho_0] = \mathrm{Tr}_{\mathrm{cl}} f_0\left(\sum_{m=1}^{M}\frac{p_m^2}{2\Gamma}+U+\mathcal{B}^{-1}\ln f_0\right). \tag{2.3.33}$$

As

$$\begin{aligned}\Omega_0 &= \mathrm{Tr}_{\mathrm{cl}} f_0\left(H_M-\mu M+\mathcal{B}^{-1}\ln f_0\right)\\ &= \int \mathrm{d}\mathbf{r}\,(V_{\mathrm{ext}}-\mu)\,\rho_0(\mathbf{r}) + \mathrm{Tr}_{\mathrm{cl}} f_0\left(\sum_{m=1}^{M}\frac{p_m^2}{2\Gamma}+U+\mathcal{B}^{-1}\ln f_0\right),\end{aligned} \tag{2.3.34}$$

inserting equation (2.3.33) into (2.3.34) returns equation (2.3.22). Equation (2.3.33) implies that if ρ is v-representable, then $Q[\rho]=\mathcal{F}[\rho]$. Moreover, $f_0 = f_{\min}^{\rho_0}$ means that f_0 may be obtained directly from ρ_0 even if the $V_{\mathrm{ext}}(\mathbf{r})$ is unknown: find the probability density which yields ρ_0 and minimizes (2.3.19).

An appealing feature of the constrained search method lies in $Q[\rho]$ of equation (2.3.19). It explicitly shows a proper definition of the intrinsic (free energy) functional which does not depend on the external potential. On the other hand, this is not easily observed from $\mathcal{F}[\rho]$ of equation (2.3.12) as a naive interpretation may be given, i.e. the equilibrium probability density is a function of the external potential such that (2.3.12)

should also depend on the external potential. Certainly this is not the case as one may recall the argument above (2.3.12).

Thermodynamics enters by realizing that $\mathcal{F}[\rho_0]$ is the 'intrinsic' Helmholtz free energy of the system, such that the total free energy is

$$F = \int \mathrm{d}\mathbf{r}\rho_0(\mathbf{r})V_{\mathrm{ext}}(\mathbf{r}) + \mathcal{F}[\rho_0], \tag{2.3.35}$$

which includes the contribution of the external potential. Using the variational principle (2.3.17) one obtains,

$$V_{\mathrm{ext}}(\mathbf{r}) + \mu_{\mathrm{in}}[\rho_0;\mathbf{r}] = \mu, \tag{2.3.36}$$

where the intrinsic chemical potential is defined as,

$$\mu_{\mathrm{in}}[\rho;\mathbf{r}] \equiv \frac{\delta\mathcal{F}[\rho]}{\delta\rho(\mathbf{r})}. \tag{2.3.37}$$

Following the theoretical foundation disclosed above, one may move on to the practical application of DFT, which requires determining $\mathcal{F}[\rho]$. Once the (approximate) free energy functional has been constructed, the variational principle (2.3.17) can be employed to obtain the equilibrium one-body density.

It is convenient to split $\mathcal{F}[\rho]$ into two contributions, the ideal free energy, $\mathcal{F}_{\mathrm{id}}[\rho]$ and the excess free energy, $\mathcal{F}_{\mathrm{exc}}[\rho]$, such that

$$\mathcal{F}_{\mathrm{exc}}[\rho] \equiv \mathcal{F}[\rho] - \mathcal{F}_{\mathrm{id}}[\rho]. \tag{2.3.38}$$

The ideal free energy is the free energy of the system with no interaction potential present, $U = 0$, given in the continuum as

$$\mathcal{F}_{\mathrm{id}}[\rho] = \mathcal{B}^{-1}\int \mathrm{d}\mathbf{r}\rho(\mathbf{r})\left(\ln\left(\lambda^3\rho(\mathbf{r})\right) - 1\right), \tag{2.3.39}$$

where the thermal de Broglie wavelength $\lambda = \left(h^2\mathcal{B}/(2\Gamma\pi)\right)^{1/2}$ and h is the Planck constant. The excess free energy is the free energy due to interactions between particles. This is the part of the free energy which has to be determined in almost all cases by means of approximations. Using the variational principle (2.3.17) with (2.3.38) and (2.3.39) gives,

$$\mathcal{B}\mu_{\mathrm{in}}[\rho;\mathbf{r}] = \mathcal{B}\frac{\delta\mathcal{F}[\rho]}{\delta\rho(\mathbf{r})} = \ln\left[\lambda^3\rho(\mathbf{r})\right] - c[\rho;\mathbf{r}], \tag{2.3.40}$$

where

$$\mathcal{B}^{-1}c[\rho;\mathbf{r}] = -\frac{\delta\mathcal{F}_{\mathrm{exc}}[\rho]}{\delta\rho(\mathbf{r})}, \tag{2.3.41}$$

is the one-body direct correlation function. Finally, using (2.3.36) one obtains the formal expression for the equilibrium one-body density as

$$\rho_0(\mathbf{r}) = z \exp\left(-\mathcal{B}V_{\text{ext}}(\mathbf{r}) + c[\rho_0;\mathbf{r}]\right), \tag{2.3.42}$$

where $z = \lambda^{-3}\exp(\mathcal{B}\mu)$ is the fugacity of the system and the quantity $\beta^{-1}c[\rho_0;\mathbf{r}]$ is an effective one-body potential which determines the equilibrium one-body density self-consistently.

In the practical application of classical DFT, almost all $\mathcal{F}[\rho]$ construction is of approximate in nature. In fact, according to [69] there are no exact solutions provided within statistical mechanics for any continuum models in three dimension. As a consequence, there are no models whereby $\mathcal{F}[\rho]$ is determined exactly in three dimension. However, a different situation occurs in one dimension. As the nature of interactions is less complicated, there are some exactly solvable equilibrium models in 1D, e.g. the continuous hard rod model [69, 71, 106, 107] described in Section 2.4.1.

2.3.2 Lattice Fundamental Measure Theory (LFMT)

Fortunately, classical DFT may also be formulated for discrete spaces of d-dimensional lattice systems, $\mathcal{L}^d$. The grand potential of a multicomponent system in a d-dimensional lattice system $\mathcal{L}^d$, as a functional of the density field may be expressed as

$$\Omega[\rho_1(\mathbf{i}),\rho_2(\mathbf{i}),\ldots,\rho_{M_p}(\mathbf{i})] = \mathcal{F}[\rho_1(\mathbf{i}),\rho_2(\mathbf{i}),\ldots,\rho_{M_p}(\mathbf{i})] - \sum_{p=1}^{M_p}\sum_{\mathbf{i}\in\mathcal{L}^d}\rho_p(\mathbf{i})u_p(\mathbf{i}), \tag{2.3.43}$$

where

$$u_p(\mathbf{i}) = \mu_p - V_{\text{ext},p}(\mathbf{i}), \tag{2.3.44}$$

where $p = 1,2,\ldots,M_p$ labels the type (species) of particles in the system, $\mathcal{F}[\rho_p(\mathbf{i})]$ is the free energy functional, $\rho_p(\mathbf{i})$ is the one-body density at site $\mathbf{i}$ of species p, μ_p is the chemical potential of species p, and $V_{\text{ext},p}(\mathbf{i})$ is the one-body external potential of species p. Moreover, as in equation (2.3.38), the free energy functional may be separated into the ideal and excess parts, that is $\mathcal{F}_{\text{id}}$ and $\mathcal{F}_{\text{exc}}$, respectively, such that

$$\mathcal{F}_{\text{exc}}[\rho_1(\mathbf{i}),\rho_2(\mathbf{i}),\ldots,\rho_{M_p}(\mathbf{i})] = \mathcal{F}[\rho_1(\mathbf{i}),\rho_2(\mathbf{i}),\ldots,\rho_{M_p}(\mathbf{i})] - \mathcal{F}_{\text{id}}[\rho_1(\mathbf{i}),\rho_2(\mathbf{i}),\ldots,\rho_{M_p}(\mathbf{i})]. \tag{2.3.45}$$

In the lattice system, the ideal free energy functional which comes from the non-interacting (ideal gas) contribution of the free energy, may be written as

$$\mathcal{BF}_{\mathrm{id}}[\rho_p(\mathbf{i})] = \sum_{p=1}^{M_p} \sum_{\mathbf{i}\in\mathcal{L}^d} \rho_p(\mathbf{i})[\ln(\rho_p(\mathbf{i})) - 1], \tag{2.3.46}$$

similar to that of its continuous (ideal free energy) counterpart in (2.3.39).

An attractive and mathematically elegant method for constructing the excess quantity, $\mathcal{F}_{\mathrm{exc}}$, is employing the lattice fundamental measure theory (LFMT) [108–110]. One of the key principles in LFMT is the notion of the 0D cavity, i.e. a cavity that can only be occupied by maximally one particle. Further definitions of cavities and 0D cavities for the lattice systems are addressed. In a multicomponent system a cavity, $\mathbf{C}(\mathbf{i})$, is a collection of sets of lattice sites in $\mathcal{L}^d$, i.e.: $\mathbf{C}(\mathbf{i}) \equiv \big(\mathcal{C}_1(\mathbf{i}), \mathcal{C}_2(\mathbf{i}), \ldots, \mathcal{C}_p(\mathbf{i}), \ldots, \mathcal{C}_{M_p}(\mathbf{i})\big)$. Hence, a 0D cavity, $\mathcal{C}_{p,0\mathrm{D}}$, is a set of sites, one for each species, p, such that if a particle of any species occupies one of the points (vertices) of its corresponding set, no other particle of the same or different species may be placed at any point of its corresponding set [108].

An essential property of the 0D cavity is that its excess (over ideal) free energy has the same form for all 0D cavities, viz.:

$$\mathcal{BF}_{\mathrm{exc}}(\eta) = \Phi_0(\eta) = (1-\eta)\ln(1-\eta) + \eta, \tag{2.3.47}$$

with $0 \leq \eta \leq 1$ the average occupancy of the 0D cavity. Moreover, every $\mathcal{C}_{0\mathrm{D}}(\mathbf{i})$ is associated with its average occupancy $\bar{\rho}(\mathbf{i}) = \big(\rho_1(\mathbf{i}), \rho_2(\mathbf{i}), \ldots, \rho_{M_p}(\mathbf{i})\big)$ where $\rho_p(\mathbf{i})$ is the density profile of $\mathcal{C}_{p,0\mathrm{D}}(\mathbf{i})$ associated to species p at site $\mathbf{i}$.

Based on the knowledge of the 0D cavity above, the d-dimensional excess free energy functional of the multicomponent hard core lattice fluids may be expressed as [110]:

$$\mathcal{BF}_{\mathrm{exc}}[\rho] = \sum_{\mathbf{i}\in\mathcal{L}^d} \sum_{k\in\mathcal{K}} C_k \Phi_0\left(w^{(k)}(\mathbf{i})\right), \tag{2.3.48}$$

where $\mathcal{K}$ is a set of indices suitably chosen to label every weighted densities $w^k(\mathbf{i})$, Φ_0 is the excess free energy of the 0D cavity, i.e. equation (2.3.47), and the C_k are integer coefficients. The weighted density $w^{(k)}(\mathbf{i})$ is defined as

$$w^{(k)}(\mathbf{i}) \equiv \sum_{p=1}^{M_p} \sum_{\mathbf{t}\in\mathcal{C}^{(k)}_{p,0\mathrm{D}}(\mathbf{i})} \rho_p(\mathbf{t}), \tag{2.3.49}$$

where $\mathcal{C}_{p,0\mathrm{D}}^{(k)}$ is the k-th subset of $\mathbf{i} \in \mathcal{L}^d$, i.e. $\mathcal{C}_{p,0\mathrm{D}}^{(k)} \subset \mathcal{L}^d$, which corresponds to its appropriate 0D cavity of species p.

In the practical application of LFMT, there are three methods which are provided to construct $\mathcal{F}_{\mathrm{exc}}[\rho]$ of (2.3.48). These are 1) the algebraic method, 2) the diagrammatic method, and 3) the Möbius inversion method. The first two methods consist of systematic iteration procedures, whereas the third method uses the knowledge of the abstract lattice theory of posets (partially ordered sets) [111, 112]. In Appendix A the algebraic method is used to calculate the excess free energy functional of the hard core lattice fluid mixtures in 2D. A brief discussion of the hard core fluid models dealt via DFT is given in the following Section.

2.4 Hard Core Models in Equilibrium

In order to fully describe a model fluid, the interatomic potential (in continuum), U, in the Hamiltonian (2.3.9) has to be specified. Purely-hard core fluids exert one of the simplest models of interatomic potentials. This potential as a function of the distance, r, may be written in a simple form as [47]:

$$U(r) = \begin{cases} \infty, & \text{if } 0 \leq r \leq \sigma \\ 0, & \text{if } r \geq \sigma, \end{cases} \tag{2.4.1}$$

where σ is the distance (range) of the infinite repulsive potential. Equation (2.4.1) states that an infinite repulsive potential is subjected between any two particles such that the particles may not overlap. This is, in fact, where the term 'hard core' originates, i.e. particles behave as hard particles such that any two particles cannot get closer than a distance σ to each other. However they are effectively non-interacting at distances greater than σ. This model is an idealization of the physical fact that at some separation distance, σ, particles tend to repel each other such that the diameter of the particles is effectively σ. 'Hard sphere', 'hard disc', and 'hard rod' are terms which are given to objects (particles) in three dimension, two dimension, and one dimension, respectively. The hard core potential of monocomponent particles is illustrated in Figure 2.9.

Equilibrium hard core fluid models which are relevant to this project are i) the continuous hard rod model in 1D, and ii) hard core lattice fluids, especially in 2D. The former model and the hard core lattice fluids in 1D have been solved exactly for the one-body densities in [106, 107, 113] and in [108], respectively.

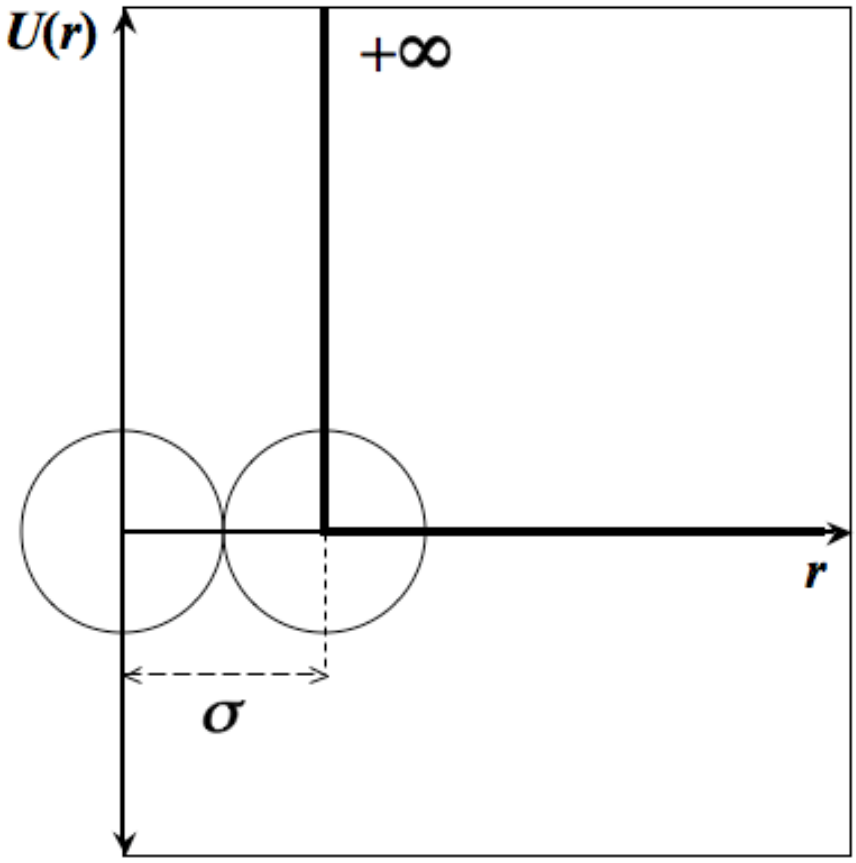

Figure 2.9: Purely-hard core potential as a function of the distance, i.e. $U(r)$. The vertical axis is the value of the potential, while the horizontal axis is the distance variable, r, with origin at $r = 0$. For $0 \leq r \leq \sigma$ there is an infinite repulsive potential, $U = \infty$. For $\sigma \leq r \leq \infty$, the potential is zero, i.e.: $U = 0$. Two (identical) particles (depicted by the circles) may not come close less than a distance σ to each other. However the particles are non-interacting at distances larger than σ. Hence the particles act as hard core particles with diameter σ.

2.4.1 Continuous hard rod model in 1D

An exact solution for the one-body density profile of the hard rod model (with diameter σ) in an arbitrary external potential $V_{\text{ext}}(x)$ was derived in [106], which is expressed in integral equations. Furthermore, a free energy functional of the same model in bulk is constructed in [107]. An example of a configuration of a polydisperse hard rod model is illustrated in Figure 2.10. In order to investigate the hard rod model via DFT (Section

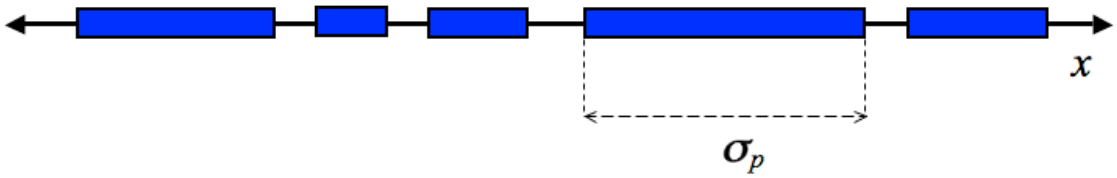

Figure 2.10: The 1D continuous hard rods model. This model consists of a continuous 1D space spanned in the horizontal axis. The hard rods, each with diameter σ_p, where p denotes different species, are depicted by the filled dark rectangles occupying the 1D continuous space. Each particle may not overlap with others.

2.3), we first assert the grand potential functional of the model as follows

$$\Omega_V[\rho] = \mathcal{F}_{\text{id}}[\rho] + \mathcal{F}_{\text{exc}}[\rho] - \int \mathrm{d}x u(x)\rho(x), \tag{2.4.2}$$

where $u(x) = \mu - V_{\text{ext}}(x)$. The excess free energy is given as

$$\mathcal{F}_{\text{exc}}[\rho] \equiv \mathcal{F}^{\text{hr}}_{\text{exc}}[\rho] = -\mathcal{B}^{-1} \int \mathrm{d}x \rho(x) \ln[1 - \zeta(x)], \tag{2.4.3}$$

with $\zeta(x) = \int_{x-\sigma}^{x} \rho(x)\mathrm{d}x$. Hence, applying the functional derivative of (2.3.17) for equation(2.4.2) yields Percus's equation for the one-body density [69]:

$$\mathcal{B}u(x) = \ln \frac{\lambda\rho(x)}{1-\zeta(x)} + \int_{x}^{x+\sigma} \mathrm{d}y \frac{\rho(y)}{1-\zeta(y)}. \tag{2.4.4}$$

Higher order correlation functions may be obtained via further functional derivatives of functional (2.4.2). There is, however, another similar version of the exact excess free energy of the hard rod model. This version is based purely upon the geometric properties of the model, i.e. the fundamental measure theory [113], where the excess free energy functional of the polydisperse particles is written as

$$\mathcal{B}\mathcal{F}_{\text{exc}}[\rho] = \int \mathrm{d}x \left[-n_0(x) \ln\left(1 - n_1(x)\right)\right], \tag{2.4.5}$$

where

$$n_\nu(x) = \int_0^\infty \mathrm{d}\sigma \int \mathrm{d}x' \omega_\nu(\sigma, x - x')\rho(\sigma, x'), \qquad \nu = 0, 1, \tag{2.4.6}$$

is a set of weighted densities, and

$$\omega_0(\sigma, x) = \frac{1}{2}\left[\delta\left(x - \frac{\sigma}{2}\right) + \delta\left(x + \frac{\sigma}{2}\right)\right], \tag{2.4.7}$$

$$\omega_1(\sigma, x) = \Omega\left(|x| - \frac{\sigma}{2}\right), \tag{2.4.8}$$

are weights associated with the ends (the 'surface') and the volume of the rods, respectively, with diameter σ (as a variable) [71]. Equations (2.4.5)-(2.4.8) are used later in the subsequent Chapter.

2.4.2 Hard core lattice fluids

In this model, instead of continuous points in space, a discrete space is considered, which is constituted by a regular d-dimensional lattice $\mathcal{L}^d$. The lattice $\mathcal{L}^d$ consists of points (sites) labelled by a vector $\mathbf{i}$. The distance between two adjacent labelled points is called a lattice spacing, a. A particle may occupy a specific point on the lattice, that is sit on one of the vertices of $\mathcal{L}^d$. Therefore, each site $\mathbf{i}$ may be occupied by a (hard core) particle or may be simply empty. As a consequence of particles 'sitting' only on lattice sites, the kinetic energy in the Hamiltonian (2.3.9) may be neglected leaving only their effective interatomic potential.

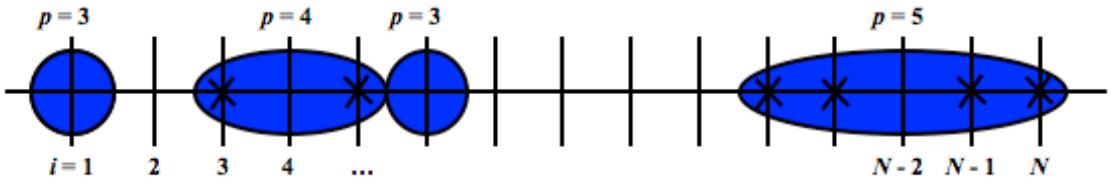

Figure 2.11: An illustration of hard core particles occupying a 1D lattice $\mathcal{L}$. The lattice sites are denoted by the vertical tick marks, and labelled by $i = 1, 2, 3, 4, \ldots, N-2, N-1, N$. The filled blue circles and ovals are the hard core particles. p denotes different species of the particles. There are two species 3 ($p = 3$) particles located at sites $i = 1$ and $i = 6$. These particles exclude their own sites such that the diameter of these particles is a (i.e.: the lattice spacing). A particle at site $i = 4$ ($p = 4$) excludes its nearest neighbours, i.e. sites $i = 3$ and $i = 5$. A bigger particle that excludes its nearest and next nearest neighbour sites ($p = 5$) is located at site $N - 2$. These particles may not overlap.

The potential of the purely-hard core lattice fluids may be stated as

$$U(\mathbf{i},\mathbf{i}') = \begin{cases} \infty, & \text{if } 0 \leq |\mathbf{i}-\mathbf{i}'| \leq \sigma, \\ 0, & \text{otherwise.} \end{cases} \tag{2.4.9}$$

with $\mathbf{i},\mathbf{i}' \in \mathcal{L}^d$, and $U(\mathbf{i},\mathbf{i}')$ is the pairwise interaction potential between two particles on sites $\mathbf{i}$ and $\mathbf{i}'$. The infinite repulsive potential may be thought of as the number of sites being excluded by the particles. Hence, the particles may be regarded as having hard cores of diameter proportional to the number of sites being excluded. Examples of hard core particles on a 1D lattice are given in Fig. 2.11. First, consider a particle occupying site $i \in \mathcal{L}$ that excludes only its own site to other particles. Hence the diameter of the particle is $\sigma = a$. In Fig. 2.11, particles ($p = 3$) occupying sites $i = 1$ and $i = 6$ are examples of hard core particles with only site exclusion. Furthermore, let the range of the repulsive potential be extended to one lattice spacing, i.e.: a. This means that a particle excludes its nearest neighbours, viz.: the particle excludes one site, each to the left and right of the site being occupied. Thus the diameter of the particle is $\sigma = 3a$. An example of this species ($p = 4$) is given in Fig. 2.11 occupying site $i = 4$. In order to obtain a bigger particle diameter (with the same lattice spacing a), the range of the hard repulsive potential may be increased further to $2a$, such that a particle (sitting at site i) excludes its nearest and next nearest neighbours, i.e. sites $i = i-2, i-1, i+1, i+2$. An example of this particle ($p = 5$) is given in Fig. 2.11 occupying site $i = N-2$.

In Section 3.3 of this thesis the object of interest is the 2D hard core lattice fluids consisting of a mixture of a monomer (site exclusion), and 2 dimers (particles with right and upper nearest neighbour exclusions). Examples of these are shown in Fig. 2.12. In two dimension the sites are labelled by $\mathbf{i} = i_x\hat{\mathbf{e}}_x + i_y\hat{\mathbf{e}}_y = (i_x, i_y)$, $\forall \mathbf{i} \in \mathcal{L}^2$ where $i_x, i_y = 1, 2, 3, \ldots, N$, $\hat{\mathbf{e}}_x$ and $\hat{\mathbf{e}}_y$ are the unit vectors along the horizontal and vertical-axes, respectively. In Fig. 2.12, the particles of interest are species 1, 2, and 3. Species 3 ($p = 3$) is the monomer shown at site $(2, 3)$, species 1 ($p = 1$) is the dimer that excludes its right nearest neighbour site depicted at sites $(N-3, 2)$ and $(N-3, 3)$, and species 2 ($p = 2$) is the dimer that excludes its upper nearest neighbour site also shown at sites $(N-1, 3)$ and $(N, 1)$. The position of species 1 and 2 are set to be the left and the lower site of the excluded sites, respectively.

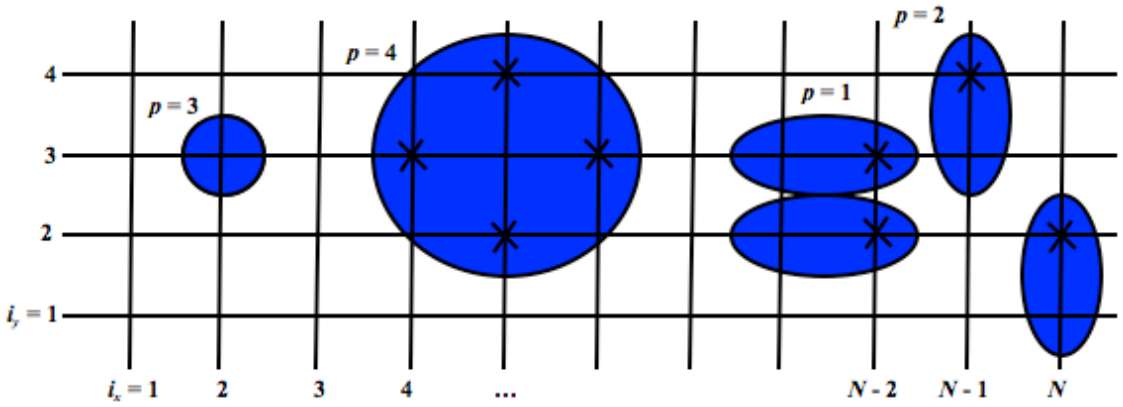

Figure 2.12: An illustration of hard core particles occupying 2D lattice, $\mathcal{L}^2$. The lattice sites are labelled by (i_x, i_y) with $i_x, i_y = 1, 2, 3, \ldots, N$. The filled blue objects are the hard core particles with various diameters. Species 1 ($p = 1$) are particles with right nearest neighbour site exclusion with examples shown at sites $(N-3, 2)$ and $(N-3, 3)$. Species 2 ($p = 2$) are particles that exclude their upper nearest neighbour sites, shown at sites $(N-1, 3)$ and $(N, 1)$. $p = 3$ and $p = 4$ label particles with site exclusion and nearest neighbour exclusion, located at sites $(2, 3)$ and $(5, 3)$, respectively.

2.5 Dynamical Density Functional Theory

Here, the dynamical density functional theory (DDFT) is derived from the Smoluchowski equation following refs. [81, 114]. In the Smoluchowski picture, consider a quantity $\varrho(\mathbf{r}_1, \mathbf{r}_2, \ldots, \mathbf{r}_M, t)$ as the probability to find particles $1, 2, \ldots, M$ at positions $\mathbf{r}_1, \mathbf{r}_2, \ldots, \mathbf{r}_M$, respectively, at time t. Hence, the Smoluchowski equation (without hydrodynamic interactions) may be written as

$$\frac{\partial \varrho}{\partial t} = \frac{1}{\xi} \sum_{m=1}^{M} \nabla_m \cdot \left[\mathcal{B}^{-1} \nabla_m + \nabla_m U_{\text{tot}}(\mathbf{r}_1, \mathbf{r}_2, \ldots, \mathbf{r}_M, t) \right] \varrho, \tag{2.5.1}$$

where

$$U_{\text{tot}}(\mathbf{r}_1, \mathbf{r}_2, \ldots, \mathbf{r}_M, t) = \sum_{m=1}^{M} V_{\text{ext}}(\mathbf{r}_m, t) + \sum_{m,m'=1;\, m<m'}^{M} U(|\mathbf{r}_m - \mathbf{r}_{m'}|), \tag{2.5.2}$$

where we have specialized to model with pairwise interactions: $U(|\mathbf{r}_m - \mathbf{r}_{m'}|)$ is the pairwise interaction potential between particle m and m' that only depends on the distance between the two particles [114]. By integrating out $M - 1$ degrees of freedom

of $\varrho(\mathbf{r}_1, \mathbf{r}_2, \ldots, \mathbf{r}_M)$, the one particle density is obtained as follows:

$$\rho(\mathbf{r}_1, t) = M \int \mathrm{d}^3\mathbf{r}_2 \int \mathrm{d}^3\mathbf{r}_3 \ldots \int \mathrm{d}^3\mathbf{r}_M \varrho(\mathbf{r}_1, \mathbf{r}_2, \ldots, \mathbf{r}_M, t), \tag{2.5.3}$$

and therefore the two-particle density function is given by,

$$\rho^{(2)}(\mathbf{r}_1, \mathbf{r}_2, t) = M(M-1) \int \mathrm{d}^3\mathbf{r}_3 \ldots \int \mathrm{d}^3\mathbf{r}_M \varrho(\mathbf{r}_1, \mathbf{r}_2, \ldots, \mathbf{r}_M, t). \tag{2.5.4}$$

Integrating both sides of the Smoluchowski equation (2.5.1) by $M \int \mathrm{d}^3\mathbf{r}_2 \ldots \int \mathrm{d}^3\mathbf{r}_M$, yields

$$\begin{aligned}
\xi \frac{\partial \rho(\mathbf{r}_1, t)}{\partial t} &= M \int \mathrm{d}^3\mathbf{r}_2 \ldots \int \mathrm{d}^3\mathbf{r}_M \left\{ \sum_{m=1}^{M} \left(\mathcal{B}^{-1} \nabla_m^2 \varrho(\mathbf{r}_1, \mathbf{r}_2, \ldots, \mathbf{r}_M, t) \right.\right. \\
&\quad \left. + \nabla_m \left(\nabla_m V_{\mathrm{ext}}(\mathbf{r}_m, t) \varrho(\mathbf{r}_1, \mathbf{r}_2, \ldots, \mathbf{r}_M, t) \right) \right) \\
&\quad \left. + \sum_{m=1;\, m<m'}^{M} \nabla_m \left(\nabla_m \left(U(|\mathbf{r}_m - \mathbf{r}_{m'}|) \varrho(\mathbf{r}_1, \mathbf{r}_2, \ldots, \mathbf{r}_M, t) \right) \right) \right\} \\
&= \mathcal{B}^{-1} \nabla_1^2 \rho(\mathbf{r}, t) + \nabla_1 \left(\rho(\mathbf{r}, t) \nabla_1 V_{\mathrm{ext}}(\mathbf{r}, t) \right) \\
&\quad + \nabla_1 \int \mathrm{d}^3\mathbf{r}_2 \ldots \mathrm{d}^3\mathbf{r}_M \rho^{(2)}(\mathbf{r}_1, \mathbf{r}_2) \nabla_1 U(|\mathbf{r}_1 - \mathbf{r}_2|).
\end{aligned} \tag{2.5.5}$$

Now, setting $\frac{\partial \rho(\mathbf{r}_1, t)}{\partial t} = 0$ for the equilibrium case and dropping the index 1 and 2 in $\mathbf{r}$, i.e.: $\mathbf{r}_1 = \mathbf{r}$ and $\mathbf{r}_2 = \mathbf{r}'$, we obtain from (2.5.5),

$$0 = \mathcal{B}^{-1} \nabla \rho(\mathbf{r}) + \rho(\mathbf{r}) \nabla V_{\mathrm{ext}}(\mathbf{r}) + \int \mathrm{d}^3\mathbf{r}' \rho^{(2)}(\mathbf{r}, \mathbf{r}') \nabla U(|\mathbf{r} - \mathbf{r}'|). \tag{2.5.6}$$

Equation (2.5.6) is known as the first member of the Yvon-Born-Green (YBG) hierarchy. The above equation provides a procedure to calculate the one-body, two-body, ..., N-body densities. The one-body density, $\rho(\mathbf{r})$, may be determined if the two-body density, $\rho(\mathbf{r}, \mathbf{r}')$, is known. However in order to calculate $\rho(\mathbf{r}, \mathbf{r}')$, the three-body density must be calculated beforehand, and so forth. Thus, in order to calculate $\rho(\mathbf{r})$ exactly, all other higher-order correlation functions must be known in advance. Hence, the YBG hierarchy is not a practical equation to calculate the one-body density.

Invoking again the results from the equilibrium DFT, i.e. combining equations (2.3.36), (2.3.37), and (2.3.40), yields

$$\mu - V_{\mathrm{ext}}(\mathbf{r}) = \mathcal{B}^{-1} \ln \left(\lambda^3 \rho(\mathbf{r}) \right) - c[\rho; \mathbf{r}]. \tag{2.5.7}$$

Taking the gradient of the above equation returns,

$$\nabla V_{\mathrm{ext}}(\mathbf{r}) + \mathcal{B}^{-1} \frac{\nabla \rho(\mathbf{r})}{\rho(\mathbf{r})} - \nabla c[\rho; \mathbf{r}] = 0. \tag{2.5.8}$$

Combining the YBG hierarchy (2.5.6) and equation (2.5.8), gives

$$\int \mathrm{d}^3\mathbf{r}'\rho^{(2)}(\mathbf{r},\mathbf{r}')\nabla U(|\mathbf{r}-\mathbf{r}'|) = -\rho(\mathbf{r})\nabla c[\rho;\mathbf{r}]. \tag{2.5.9}$$

Now an important assumption is unveiled, which is at the heart of the dynamical DFT, i.e. equation (2.5.9) holds also in non-equilibrium condition. Thus, non-equilibrium correlations are approximated by equilibrium ones at the same $\rho(\mathbf{r},t)$ via a given $V_{\mathrm{ext}}(\mathbf{r})$ in equilibrium.

Hence, based upon the assumption above, inserting equation (2.5.9) back into the (non-equilibrium) Smoluchowski equation gives,

$$\xi\frac{\partial\rho(\mathbf{r},t)}{\partial t} = \nabla\left(\mathcal{B}^{-1}\nabla\rho(\mathbf{r},t) + \rho(\mathbf{r},t)\nabla V_{\mathrm{ext}}(\mathbf{r},t) - \rho(\mathbf{r},t)\nabla c[\rho;t]\right), \tag{2.5.10}$$

or

$$\xi\frac{\partial\rho(\mathbf{r},t)}{\partial t} = \nabla\rho(\mathbf{r},t)\nabla\left(\frac{\delta\Omega[\rho]}{\delta\rho(\mathbf{r},t)}\right). \tag{2.5.11}$$

Equation (2.5.11) is the main DDFT equation which is a scheme for investigating various non-equilibrium systems. This scheme is applied to selective solvation in mixed solvents[85], freezing, glass transitions, and crystal growth as well as Brownian dynamic simulations [114].

Chapter 3

Various Phenomenological Results for the TASEP

3.1 Analytical Solutions of the TASEP with a Single Site

In this Section we present an example of the master equation in action. The master equation (2.1.1) is applied to the TASEP with open boundaries and consists of only one site. We wish to determine explicit expressions for the probabilities, including the one-body and current densities. Although it is a trivial model, the explicit solutions for its probabilities, one-body and current densities at any time t, to our knowledge, cannot be found in the literature. Note also that this model is a specific case of a more general model of the two-state systems. These are systems that consist of only two configurational (microscopic) states. Hence, there are only two probabilities associated to two transition rates. These systems have been studied, e.g. in [115, 116].

A particle may enter the (empty) site with an input rate $\alpha(t)$ and exit the (occupied) site with an output rate $\beta(t)$. In this case, we have $n = \{\tau_1\} \equiv 1, 2$ where $n = 1 = \{\tau_1 = 1\}$ is the microscopic state where the site is occupied by a particle, and $n = 2 = \{\tau_1 = 0\}$ is the state where the site is empty. Thus, the probability of the site being occupied by a particle or empty is $P_1(t)$ and $P_2(t)$, respectively. The system is assumed to start evolving from $t = 0$ with given initial conditions of $P_1(t = 0) = P_1(0)$ and $P_2(t = 0) = P_2(0)$. These probabilities satisfy the normalization condition,

$$\sum_n P_n(t) = P_1(t) + P_2(t) = 1, \tag{3.1.1}$$

at any time t. The transition rates are given as $w_{12}(t) = \alpha(t)$ and $w_{21}(t) = \beta(t)$. An illustration of the TASEP with one site is depicted in Figure 3.1.

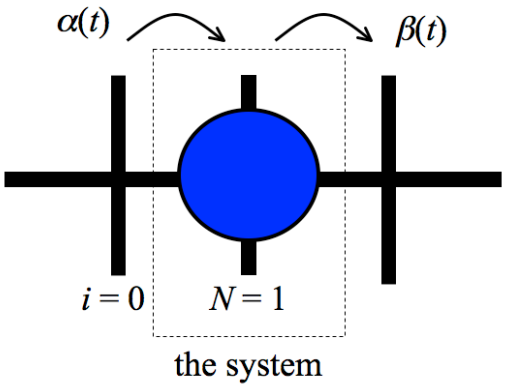

Figure 3.1: The TASEP with open boundaries and consists of only a single site. The lattice sites are depicted by vertical dark thick marks labelled by $i = 0, 1$. The filled (blue) circle occupying site $N = 1$ is a hard core particle. The system under consideration is given inside the dashed box. A particle may enter site $N = 1$ from the zero-th site ($i = 0$) with rate $\alpha(t)$ [arrow to the left of the site] if there is no particle at site $N = 1$. If there is a particle at site $N = 1$, the particle may leave the site with rate $\beta(t)$ [arrow to the right of the site].

Henceforth, the master equations are as follows

$$\begin{aligned} \frac{\partial P_1(t)}{\partial t} &= w_{12}(t)P_2(t) - w_{21}(t)P_1(t) \\ &= \alpha(t)P_2(t) - \beta(t)P_1(t), \end{aligned} \tag{3.1.2}$$

and

$$\begin{aligned} \frac{\partial P_2(t)}{\partial t} &= w_{21}(t)P_1(t) - w_{12}(t)P_2(t) \\ &= \beta(t)P_1(t) - \alpha(t)P_2(t). \end{aligned} \tag{3.1.3}$$

Using the normalization condition (3.1.1) and rearranging, equations (3.1.2) and (3.1.3) may be written as

$$\frac{\mathrm{d}P_1(t)}{\mathrm{d}t} + [\alpha(t) + \beta(t)]P_1(t) = \alpha(t), \tag{3.1.4}$$

and

$$\frac{\mathrm{d}P_2(t)}{\mathrm{d}t} + [\alpha(t) + \beta(t)]P_2(t) = \beta(t). \tag{3.1.5}$$

Equations (3.1.4) and (3.1.5) are inhomogeneous first-order linear ordinary differential equations. The partial derivatives on the LHS of equations (3.1.2) and (3.1.3) are modi-

fied into full derivatives in equations (3.1.4) and (3.1.5) since for given microscopic states, $P_1(t)$ and $P_2(t)$ are functions of time only.

The main task now is to solve the master equations (3.1.4) and (3.1.5) in order to obtain closed expressions for $P_1(t)$ and $P_2(t)$. These equations may be solved by multiplying both sides of the equations by a factor of

$$\exp\left(\int_0^t [\alpha(t') + \beta(t')]\mathrm{d}t'\right).$$

In the following we only consider equation (3.1.4) to be solved explicitly, while equation (3.1.5) may be solved using exactly the same method as (3.1.4). Thus,

$$\mathrm{e}^{\int_0^t [\alpha(t')+\beta(t')]\mathrm{d}t'}\frac{\mathrm{d}P_1(t)}{\mathrm{d}t}+\mathrm{e}^{\int_0^t [\alpha(t')+\beta(t')]\mathrm{d}t'}[\alpha(t)+\beta(t)]P_1(t) = \alpha(t)\mathrm{e}^{\int_0^t [\alpha(t')+\beta(t')]\mathrm{d}t'}. \quad (3.1.6)$$

On the other hand, the following equation is obtained via the product rule,

$$\frac{\mathrm{d}}{\mathrm{d}t}\left(\mathrm{e}^{\int_0^t [\alpha(t')+\beta(t')]\mathrm{d}t'}P_1(t)\right) = \mathrm{e}^{\int_0^t [\alpha(t')+\beta(t')]\mathrm{d}t'}\frac{\mathrm{d}P_1(t)}{\mathrm{d}t} + \mathrm{e}^{\int_0^t [\alpha(t')+\beta(t')]\mathrm{d}t'}[\alpha(t) + \beta(t)]P_1(t). \quad (3.1.7)$$

Thus, inserting equation (3.1.7) into (3.1.6), yields

$$\frac{\mathrm{d}}{\mathrm{d}t}\left(\mathrm{e}^{\int_0^t [\alpha(t')+\beta(t')]\mathrm{d}t'}P_1(t)\right) = \alpha(t)\mathrm{e}^{\int_0^t [\alpha(t')+\beta(t')]\mathrm{d}t'}. \quad (3.1.8)$$

Hence, equation (3.1.4) has been modified to yield equation (3.1.8), which is more conveniently integrated. In order to do so, both sides of (3.1.8) are multiplied by $\mathrm{d}t$, and then integrated from 0 to t, yielding:

$$\mathrm{e}^{\int_0^t [\alpha(t')+\beta(t')]\mathrm{d}t'}P_1(t) = \int_0^t \alpha(t)\mathrm{e}^{\int_0^t [\alpha(t')+\beta(t')]\mathrm{d}t'}\mathrm{d}t + \mathcal{A}_1, \quad (3.1.9)$$

or

$$P_1(t) = \mathrm{e}^{-\int_0^t [\alpha(t')+\beta(t')]\mathrm{d}t'}\left\{\int_0^t \alpha(t)\mathrm{e}^{\int_0^t [\alpha(t')+\beta(t')]\mathrm{d}t'}\mathrm{d}t + \mathcal{A}_1\right\}. \quad (3.1.10)$$

One may also solve the master equation (3.1.5) via the same method used to derive equation (3.1.4). This yields,

$$P_2(t) = \mathrm{e}^{-\int_0^t [\alpha(t')+\beta(t')]\mathrm{d}t'}\left\{\int_0^t \beta(t)\mathrm{e}^{\int_0^t [\alpha(t')+\beta(t')]\mathrm{d}t'}\mathrm{d}t + \mathcal{A}_2\right\}, \quad (3.1.11)$$

where $\mathcal{A}_1$ and $\mathcal{A}_2$ are constant coefficients of the probabilities, $P_1(t)$ and $P_2(t)$, respectively. These coefficients may be determined from the initial conditions, $P_1(0)$ and $P_2(0)$. Thus, setting $t = 0$ for equations (3.1.10) and (3.1.11) yields,

$$\mathcal{A}_1 = P_1(0), \qquad \text{and} \qquad \mathcal{A}_2 = P_2(0). \quad (3.1.12)$$

Equations (3.1.10) and (3.1.11) are the final products for the probabilities, which are closed and depend only upon the explicit expressions of some given $\alpha(t)$ and $\beta(t)$.

Next, the average one-body density may be calculated over possible events and histories [7, 34, 36], via equation (2.2.9), producing

$$\begin{aligned}\rho_1(t) &= \sum_{n=1,2} \tau_{1,n} P_n(t) = P(1,t) \\ &= \mathrm{e}^{-\int_0^t [\alpha(t')+\beta(t')]\mathrm{d}t'} \left\{ \int_0^t \alpha(t) \mathrm{e}^{\int_0^t [\alpha(t')+\beta(t')]\mathrm{d}t'} \mathrm{d}t + \rho_1(0) \right\},\end{aligned} \tag{3.1.13}$$

where $\rho_1(0) = P_1(0)$. From equation (3.1.13) it may be observed that the one-body density only depends upon the hopping rates. Furthermore, the dynamics of the TASEP can be traced through the time evolution of the time-dependent one-body density, i.e.:

$$\frac{\mathrm{d}\rho_1(t)}{\mathrm{d}t} = \frac{\mathrm{d}P_1(t)}{\mathrm{d}t} = \alpha(t)[1-\rho_1(t)] - \beta(t)\rho_1(t). \tag{3.1.14}$$

The above equation is attained by inserting the first line of equation (3.1.13), i.e.: $\rho_1(t) = P_1(t)$, into (3.1.4) and rearranging. More importantly, equation (3.1.14) is a continuity equation of the form (2.2.7), that is

$$\frac{\mathrm{d}\rho_1(t)}{\mathrm{d}t} = -[J_{\mathrm{out}}(t) - J_{\mathrm{in}}(t)], \tag{3.1.15}$$

where

$$J_{\mathrm{in}}(t) = \alpha(t)[1-\rho_1(t)], \tag{3.1.16}$$

and

$$J_{\mathrm{out}}(t) = \beta(t)\rho_1(t), \tag{3.1.17}$$

are the current densities of particles entering and exiting the site, respectively. Hence, invoking again equation (3.1.13) one obtains from equations (3.1.16) and (3.1.17),

$$J_{\mathrm{in}}(t) = \alpha(t) \left[1 - \mathrm{e}^{-\int_0^t [\alpha(t')+\beta(t')]\mathrm{d}t'} \left\{ \int_0^t \alpha(t) \mathrm{e}^{\int_0^t [\alpha(t')+\beta(t')]\mathrm{d}t'} \mathrm{d}t + \rho_1(0) \right\} \right], \tag{3.1.18}$$

and also,

$$J_{\mathrm{out}}(t) = \beta(t) \left[\mathrm{e}^{-\int_0^t [\alpha(t')+\beta(t')]\mathrm{d}t'} \left\{ \int_0^t \alpha(t) \mathrm{e}^{\int_0^t [\alpha(t')+\beta(t')]\mathrm{d}t'} \mathrm{d}t + \rho_1(0) \right\} \right]. \tag{3.1.19}$$

In the form of (3.1.18) and (3.1.19), the current densities do not depend upon the one-body density. The dependency only comes from the input and output hopping rates, $\alpha(t)$ and $\beta(t)$.

Next we look at special cases. First, consider the case where the hopping rates are independent of time, i.e.: $\alpha(t) = \alpha$ and $\beta(t) = \beta$. From equation (3.1.13), the one-body density has a simpler form of

$$\begin{aligned}\rho_1(t) &= \mathrm{e}^{-\int_0^t[\alpha+\beta]\mathrm{d}t'}\left\{\int_0^t \alpha \mathrm{e}^{\int_0^t[\alpha+\beta]\mathrm{d}t'}\mathrm{d}t + \rho_1(0) - \frac{\alpha}{\alpha+\beta}\right\} \\ &= \frac{\alpha}{\alpha+\beta} + \left(\rho_1(0) - \frac{\alpha}{\alpha+\beta}\right)\mathrm{e}^{-[\alpha+\beta]t}, \end{aligned} \tag{3.1.20}$$

and the probability of the system to be empty becomes,

$$P_2(t) = \frac{\beta}{\alpha+\beta} - \left(P_2(0) - \frac{\beta}{\alpha+\beta}\right)\mathrm{e}^{-[\alpha+\beta]t}. \tag{3.1.21}$$

There are two terms on the RHS of equation (3.1.20). The first term is a time-independent constant, which is the ratio between the input rate and the sum of the input and output hopping rates. The second term is a function of time, which decreases exponentially as time increases (evolves). In the latter term, $(\alpha+\beta)$ on the exponential factor is the decay constant which acts as a time scale for the relaxation of the densities to steady state. The current densities can also be obtained as

$$J_{\mathrm{in}}(t) = \frac{\alpha\beta}{\alpha+\beta} - \alpha\left(\rho_1(0) - \frac{\alpha}{\alpha+\beta}\right)\mathrm{e}^{-[\alpha+\beta]t}, \tag{3.1.22}$$

and

$$J_{\mathrm{out}}(t) = \frac{\alpha\beta}{\alpha+\beta} + \beta\left(\rho_1(0) - \frac{\alpha}{\alpha+\beta}\right)\mathrm{e}^{-[\alpha+\beta]t}. \tag{3.1.23}$$

If the initial one-body density is set to be zero, i.e.: $\rho_1(0) = 0$, then the current densities at time $t = 0$ (the initial current densities) are $J_{\mathrm{in}}(0) = \alpha$ and $J_{\mathrm{out}}(0) = 0$, respectively. As time evolves, particles occupy site $N = 1$ such that $J_{\mathrm{in}}(t)$ decreases, while $J_{\mathrm{out}}(t)$ and $\rho_1(t)$ increase. Once a particle occupies the site, the probability of a particle coming into the site is zero (0) because of the hard core repulsion (except if the particle jumps out of the site) hence the decrease of $J_{\mathrm{in}}(t)$ (and the increase of $J_{\mathrm{out}}(t)$). After a considerably long time evolution, the current densities J_{in} and J_{out} coincide and become constant, such that the system reaches stationary state. Furthermore, the decay constant of $(\alpha+\beta)$ in equations (3.1.22) and (3.1.23) govern the rate of the system to reach steady state, i.e.: the larger the value of $(\alpha+\beta)$, the faster the system approaches steady state.

At steady state, setting $t \to \infty$ for equation (3.1.20) gives the one-body density as

$$\rho_1|_{t\to\infty} = \frac{\alpha}{\alpha+\beta}, \tag{3.1.24}$$

where only the first constant term of (3.1.20) survives and the second term decays exponentially to zero (0) as time approaches infinity. Moreover, the current densities at steady state are attained from equations (3.1.22) and (3.1.23), that is

$$J_{\text{in}}|_{t\to\infty} = J_{\text{out}}|_{t\to\infty} = J = \frac{\alpha\beta}{\alpha+\beta}. \tag{3.1.25}$$

It is clear from (3.1.25) that the current densities are non-zero and become constant with respect to space (sites) and time. Hence, the system reaches a steady state condition of

$$\frac{\mathrm{d}\rho_1(t)}{\mathrm{d}t} = 0 \qquad \text{for} \qquad t \to \infty,$$

according to equations (3.1.15) and (3.1.25). And it is because of this non-zero current density that maintains the TASEP in out-of-equilibrium regime. Furthermore, the results for ρ_1, J_{in} and J_{out} in steady state above are exact [35] and do not depend on the initial conditions of the system.

One may compare the steady state results above to the exact recursion formula [36]. By invoking equation (2.2.25), the one site TASEP partition function from (2.2.23) reads,

$$Z_{N=1} = \sum_{n=1,2} f_{n,N=1} = f_{1,1} + f_{2,1} = \alpha + \beta, \tag{3.1.26}$$

and applying equation (2.2.28) gives

$$T_{i=1,N=1} = \sum_{n=1,2} \tau_{i=1,n} f_{n,N=1} = f_{1,N=1} = \alpha. \tag{3.1.27}$$

Hence, following equation (2.2.27) the one-body density is obtained as

$$\rho_{i=1,N=1} = \frac{T_{i=1,N=1}}{Z_{N=1}} = \frac{\alpha}{\alpha+\beta}, \tag{3.1.28}$$

which agrees with equation (3.1.24).

3.2 TASEP with Time-Dependent Input and Output Rates

As outlined in Chapter 1, many studies have been carried out for the TASEP with constant input and output rates, and correspondences to many interesting physical system can be motivated. Here an extension of the TASEP is explored, where both input and output rates are (periodically) time-dependent, viz.: $\alpha(t)$ and $\beta(t)$. The current Section is mainly motivated by trying to extend the TASEP to time-dependent boundary rates using a framework similar to DFT, i.e. using functionals of the current density, in

Chapter 5. This model may be of interest for modeling traffic, where traffic light are switch periodically. Investigation of such generalizations of the TASEP are still scarce, e.g. in [117] where the ASEP model is studied by coupling the exit site to a reservoir with time-dependent density.

In this case, we go further by varying periodically both the input and output rates. The general form of these are given as

$$\alpha(t) = \alpha_0 + \alpha_{\text{str}} \cos\left(\frac{2\pi t}{T_\alpha}\right), \tag{3.2.1}$$

and

$$\beta(t) = \beta_0 + \beta_{\text{str}} \cos\left(\frac{2\pi t}{T_\beta}\right), \tag{3.2.2}$$

where $\alpha(t)$ and $\beta(t)$ are the time-dependent input and output rates at time t, respectively. α_0 and β_0 are the initial (time-independent) input and output rates, respectively, with values $0 \leq \alpha_0, \beta_0 \leq 1$. α_{str} and β_{str} are the strength of the oscillations for the input and output rates, respectively, with values $0 \leq \alpha_{\text{str}}, \beta_{\text{str}} \leq 1$, depending upon α_0 and β_0 such that $0 \leq \alpha(t), \beta(t) \leq 1$ at any time t. T_α and T_β are the periods of the oscillations of the input and output hopping rates, respectively. As there are many parameters that have to be taken into account in equations (3.2.1) and (3.2.2), this discussion is restricted by considering equal periods of the hopping rates, i.e.:

$$T_\alpha = T_\beta = T. \tag{3.2.3}$$

For some cases, we also consider equal initial rates and strengths, that is $\alpha_0 = \beta_0$ and $\alpha_{\text{str}} = \beta_{\text{str}}$. Time (t) is considered discrete throughout. The dynamical rules considered are the (random) sequential and parallel updating. Some results of these dynamical set up are discussed separately.

Random number generators are used in the simulations. The densities are obtained by averaging over 10000 replicas (ensemble) of the TASEP taken after a long time evolution of $t = 10^5$ time steps (or longer). Furthermore, alternating occupied and empty lattice sites are set as the initial configuration for each replica such that the initial one-body density is 0.5. The time evolution starts at $t = 0$ for both the mean-field and simulations.

We emphasis that this Section is not intended for a full disclosure of the phase diagram of the TASEP with time-dependent input and output rates. There is no specific (physical) reason as to why we choose these specific examples for $\alpha(t)$ and $\beta(t)$ in equations (3.2.1) and (3.2.2). Instead, we would like to present some examples that show

interesting feature of this model compared to the TASEP with constant input and output rates.

3.2.1 One-body and current densities for sequential dynamics

The governing equation for the sequential dynamics is based upon the continuity equation (2.2.38), that is

$$\rho_i(t+1) = \rho_i(t) - \frac{1}{N+1}[J_{i(i+1)}(t) - J_{(i-1)i}(t)],$$

where

$$J_{i(i+1)}(t) = k_{i(i+1)}(t)\rho_i(t)[1 - \rho_{i+1}(t)],$$

is the mean-field current density. Specifications of the hopping rates are in order. Inside the lattice sites, i.e. $1 \leq i \leq (N-1)$, the hopping rates are constant with value 1, that is

$$k_{12} = k_{23} = \ldots = k_{(N-1)N} = 1. \tag{3.2.4}$$

This means that a particle occupying site i jumps to site $i+1$ with certainty (probability 1) if site i is chosen and there is no particle at site $i+1$. Thus for $1 \leq i \leq (N-1)$, the current density above is modified into

$$J_{i(i+1)}(t) = \rho_i(t)[1 - \rho_{i+1}(t)]. \tag{3.2.5}$$

The interesting physics are produced by the boundary conditions where the current densities are given by,

$$J_{01}(t) = J_{\text{in}}(t) = \alpha(t)[1 - \rho_1(t)], \tag{3.2.6}$$

by setting $k_{01}(t) = \alpha(t)$ and

$$J_{N(N+1)}(t) = J_{\text{out}}(t) = \beta(t)\rho_N(t), \tag{3.2.7}$$

by inserting $k_{N(N+1)} = \beta(t)$. The time parameter is considered discrete with 1 time step is set to be the smallest time interval. The time evolution, i.e. $t \to t+1$, of the densities are deterministic. The total number of lattice sites is $N = 100$. At the boundaries, if the chosen site is $i = 0$ (zero-th site) and there is no particle at site $i = 1$, then a particle may enter site $i = 1$ with a hopping rate $\alpha(t)$, otherwise site $i = 1$ stays empty. Moreover, if the chosen site is $N = 100$ and there is a particle at the site, then the particle may exit the lattice sites with rate $\beta(t)$, otherwise the particle stays at the site.

Hence, consider first a case of equal rates at the boundaries, where $\alpha_0 = \beta_0 = 0.5$ and $\beta_{\text{str}} = \alpha_{\text{str}} = 0.5$. The periods of the oscillation are varied, that is $T = 100$ time steps, $T = 10^4$ time steps, and $T = 10^6$ time steps. An initial condition of alternating empty and occupied lattice sites is used such that the initial average density (over an ensemble of identical systems) is 0.5. The objective of this case is to investigate the effect of the oscillation period upon the densities of the TASEP.

There is a reason as to why the periods above are chosen. In order to explain this we need to consider an empty lattice sites as an initial condition. The first particle that enters the lattice sites (from the left) would minimally take 100 time steps to exit the sites. This is an extreme condition where the chosen site is always the site where the particle is sitting. There is another extreme condition in order for a particle to travel throughout the lattice sites. In this case only after 100 trials of randomly choosing sites, the site where the particle is sitting gets to be chosen such that the total time to travel $\mathcal{L}$ is 100×100 time steps. These (extreme) time scales, i.e.: $T = 100$ time steps and $T = 10^4$ time steps, may be used as the period of the input and output hopping rates.

In Figure 3.2, some comparison between the mean-field and simulation results of the one-body and current densities are shown. The densities are taken after a long time evolution of 10^5 time steps.

For $T = 100$ time steps the density profiles are given in Figure 3.2(i). In general, the one-body and current density profiles are flat with values of 0.5 and 0.25, respectively. The mean-field one-body and current density profiles are given by the solid red line and dashed green line, respectively, while the simulation results are given by the blue cross (+) points and pink cross (x) points, respectively. No variation of the densities are detected, except a very small variation at the edges of the sites, i.e.: at sites $i = 1$ and $N = 100$. Hence, the oscillation period is not large enough to affect the densities in the bulk.

However when the period is increased to 10^4 time steps in Figure 3.2(ii), there is a significant changes in the one-body and current density profiles. The one-body density profiles are given by the solid red line and blue cross (+) points, for the mean-field and simulation results. There is a qualitative agreement between the mean-field and the simulation. Both profiles show a high density value near the entrance of the lattice site, which then decreases to some value under 0.5 (low density) and increases again over 0.5 (high density) and finally decreases at the exit of $\mathcal{L}$. Henceforth, one would expect many

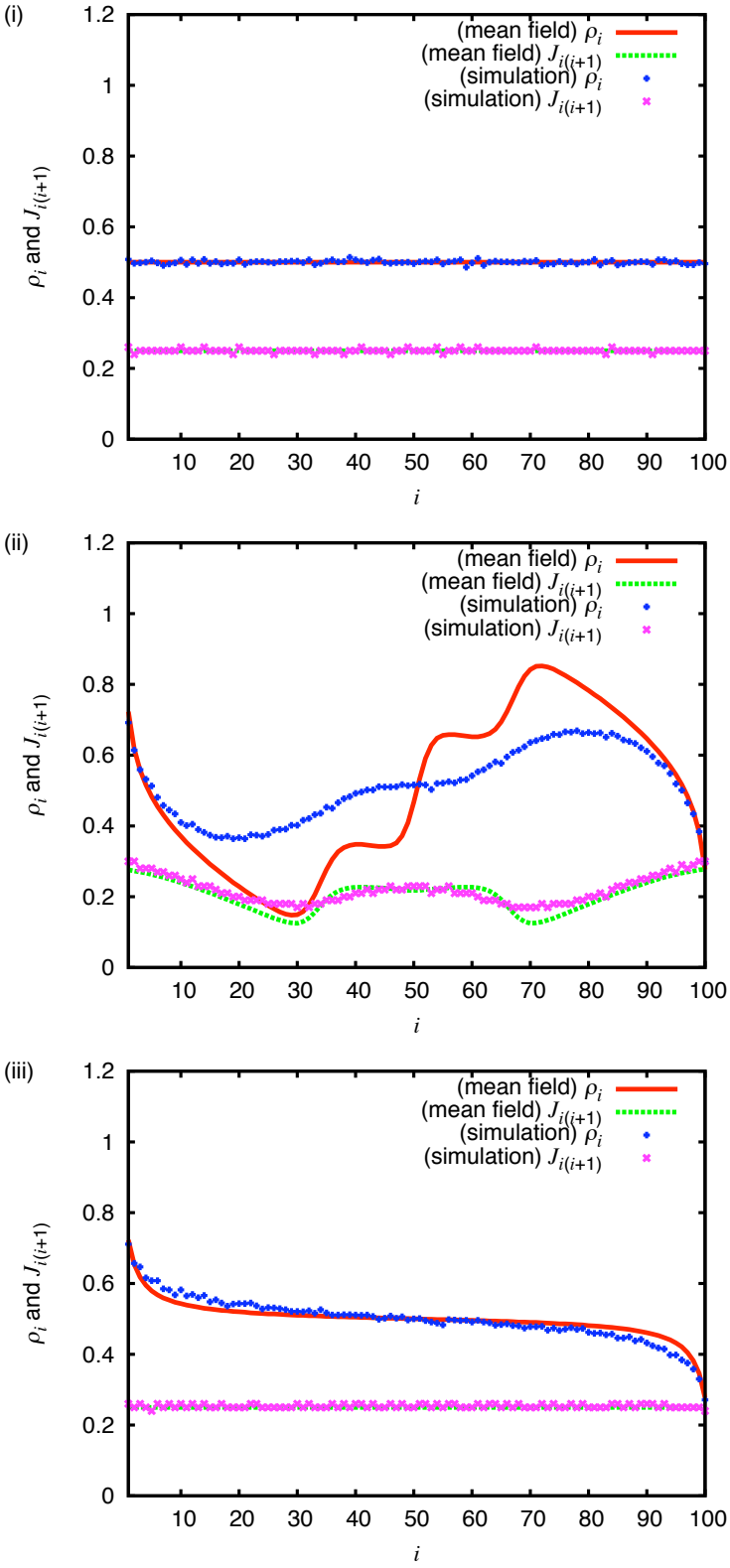

Figure 3.2: The one-body and current densities of the TASEP with sequential updating and time-dependent boundary rates. The input and output rates are specified as $\alpha(t) = \beta(t) = 0.5 + 0.5\cos(2\pi t/T)$. The profiles are obtained from the mean-field and simulation results and taken after a long time evolution of 10^5 time steps. The main variable being varied is the period, i.e. $T = 10^2$ (i), $T = 10^4$ (ii), and $T = 10^6$ (iii).

particles piling up near the entrance, and then decreases going further along the sites. Then particles diffuse around the middle of the sites, and would expect particles piling up again, and finally decreases around the exit sites. This resembles a coexistence phase between low and high densities, where the mean-field result shows a structured step profile. Clearly the period is large enough to affect the outcome of the density profiles across the lattice site $\mathcal{L}$.

The current density profiles are shown by the dashed green line (mean-field) and pink cross points (simulation). The agreement between the mean-field and simulation is good. It may be observed from Fig. 3.2(ii) that the current densities vary with respect to the sites.

Now the period is increased further to $T = 10^6$ time steps in Fig. 3.2(iii). The one-body density profiles are obtained from the mean-field theory (solid red line) and simulation (blue +'s). The profiles show a qualitative agreement of a maximal current phase. On the other hand, the current density profiles are flat throughout $\mathcal{L}$ with value of 0.25.

Next we consider a case where snapshots of the one-body and current densities are taken in one period after a long time evolution (10^5 time steps). The input and output rates are equal with $\alpha_0 = \beta_0 = 0.2$ and $\alpha_{\rm str} = \beta_{\rm str} = 0.2$. Figure 3.3 are profiles of the one-body and current densities of this present case. This Figure shows the evolution of the one-body and current densities through one cycle at times $t = 10^5$ time steps [Fig. 3.3(i)], $t = 10^5 + 1250$ time steps [Fig. 3.3(ii)], $t = 10^5 + 2500$ time steps [Fig. 3.3(iii)], $t = 10^5 + 7500$ time steps [Fig. 3.3(iv)], and $t = 10^5 + 10000$ time steps [Fig. 3.3(v)]. It can be observed that the profiles in Fig. 3.3(i) is exactly similar to that of Fig. 3.3(v), which shows that the profiles will repeat itself after one period. Again this is due to the periodic time-dependent boundary conditions of the hopping rates. In general, there are qualitative agreements between the mean-field and simulation results for both one-body and current densities in all of the profiles from Fig. 3.3(i)-(v).

Furthermore, an example of the density profiles obtained from the mean-field calculations by varying $\alpha_{\rm str}$ is presented. Here, the input and output hopping rates are equal with $\alpha_0 = \beta_0 = 0.5$ and $T = 10000$ time steps. $\alpha_{\rm str}$ is varied from 0.1 to 0.5, that is 0.1, 0.2, 0.3, 0.4, and 0.5. The one-body and current density profiles are given in Figure 3.4. For $\alpha_{\rm str} = 0.1$ [Fig. 3.4(i)] the one-body density is nearly flat throughout the lattice sites with an average value of 0.5, except at the ends of $\mathcal{L}$, which is similar to

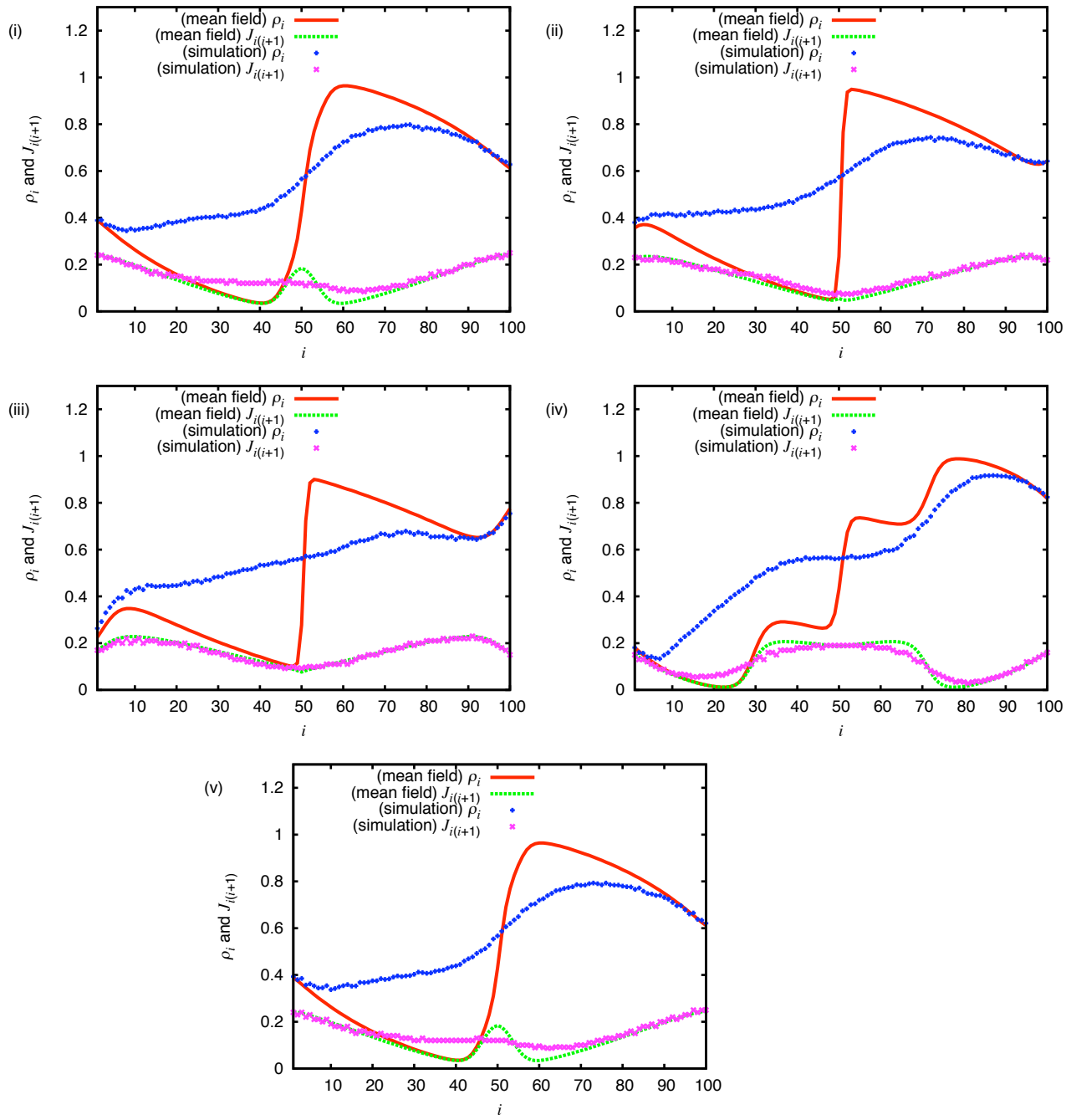

Figure 3.3: Time evolution (in one period) of the one-body and current density profiles of the sequential updating TASEP in 1D with time-dependent input and output hopping rates. The boundary hopping rates are set to be $\alpha(t) = \beta(t) = 0.2 + 0.2\cos(2\pi t/T)$, where $T = 10^4$ time steps. The above Figures are snapshots attained from the mean-field and simulation results taken after a long time evolution, i.e. after $t = 10^5$ time steps (i), $t = 10^5 + 1250$ time steps (ii), $t = 10^5 + 2500$ time steps (iii), $t = 10^5 + 7500$ time steps (iv), and $t = 10^5 + 10^4$ time steps (v).

the maximal current phase. As the oscillation strength is increased there is a transition from a flat profile of 0.5 (maximal current phase) to a coexistence phase between high and low densities. The current density profiles in Fig. 3.4(ii) also change as the strength of oscillation is varied. It may be observed that as the oscillation strength is increased the current density profiles exhibit two minima, whereas the middle sites are almost flat.

The last example is given in Figure 3.5. In this interesting case, we set $\alpha_0 = 0.4$, $\alpha_{\rm str} = 0.3$, $\beta_0 = 0.3$, $\beta_{\rm str} = 0.05$, and $T = 15 \times 10^3$ time steps. One reason for studying this particular case is the different values of the input and output hopping rates at their minimum and maximum values. For $t = uT$, where $u = 0, 1, 2, \ldots$, $\cos\left(\frac{2\pi t}{T}\right)$ will be equal to the maximum value of 1, such that $\alpha(t = uT) = 0.7$ and $\beta(t = uT) = 0.35$. This is a condition for the boundary rates to produce a high density phase. The values of $\cos\left(\frac{2\pi t}{T}\right)$ also reach a minimum value of -1.0 when $t = \frac{(2u+1)T}{2}$, giving $\alpha\left(\frac{(2u+1)T}{2}\right) = 0.1$ and $\beta\left(\frac{(2u+1)T}{2}\right) = 0.25$. This produces a low density phase. Thus there is a competition between boundary rates at their minimum and maximum values that produce low and high one-body densities, respectively, at each cycle.

The profiles in Figure 3.5 show the one-body densities, which are depicted by the solid red line (mean-field) and blue (+) points (simulation). At the beginning of the lattice sites, i.e. $1 \leq i \leq 10$, the profile clearly lies within the low density regime. In fact the mean-field and simulation results agree qualitatively. At the far right of $\mathcal{L}$, i.e. near the exit sites, the mean-field and simulation results agree on a high density regime with a value around 0.7. Interestingly, two coexistence phases are possibly exhibited around the middle of the sites, i.e.: $20 \leq i \leq 80$. From the mean-field theory, the coexistence phases can be recognized from two walls (shock profiles) at sites $20 \leq i \leq 25$ and $50 \leq i \leq 60$, whereas the simulation shows two straight lines at sites $10 \leq i \leq 30$ and $30 \leq i \leq 80$. This means that instead of one straight line stretching from the entrance to the exit sites as shown in Fig. 2.7, one may identify two lines (in Fig. 3.5) which should correspond to two phase transitions with two expected shock profiles. These shocks move stochastically within their appropriate regimes. The true locations of the shocks are not detected by the mean-field result. The first transition occurs between sites $10 \leq i \leq 30$ which looks like a transition between two low density (LD) phases (LD-LD phase transition). The second transition occurs between sites $30 \leq i \leq 80$, which is a transition between low (LD) and high density (HD) phases (LD-HD phase transition). Hence, the input and output hopping rates fix low and high one-body densities near the entrance and exit sites of $\mathcal{L}$,

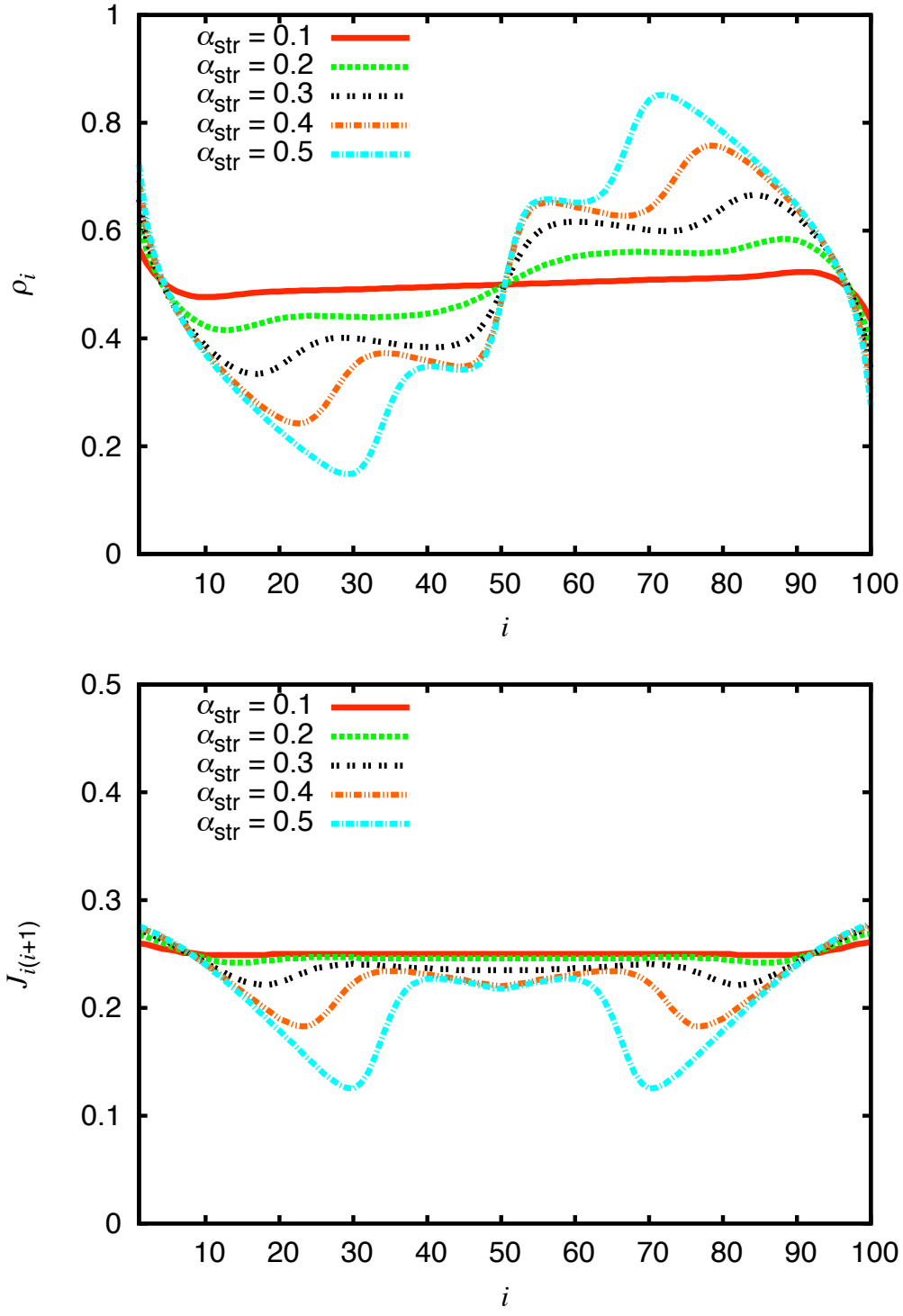

Figure 3.4: The mean-field one-body and current densities of the TASEP with sequential updating obtained by varying the oscillation strength, i.e. $\alpha_{\rm str}$. The input and output hopping rates are given as $\alpha(t) = \beta(t) = 0.5 + \alpha_{\rm str}\cos(2\pi t/T)$, where $T = 10^4$ time steps. The densities are plotted after 10^5 time steps with oscillation strength variation of 0.1, 0.2, 0.3, 0.4, and 0.5.

respectively, such that coexistence phases exist between the two profiles. Furthermore, the current densities are given by the dashed (green) line (mean-field) and the (pink) cross points (simulation). The agreement between the mean-field and simulation results for the current density is better than that of the one-body density.

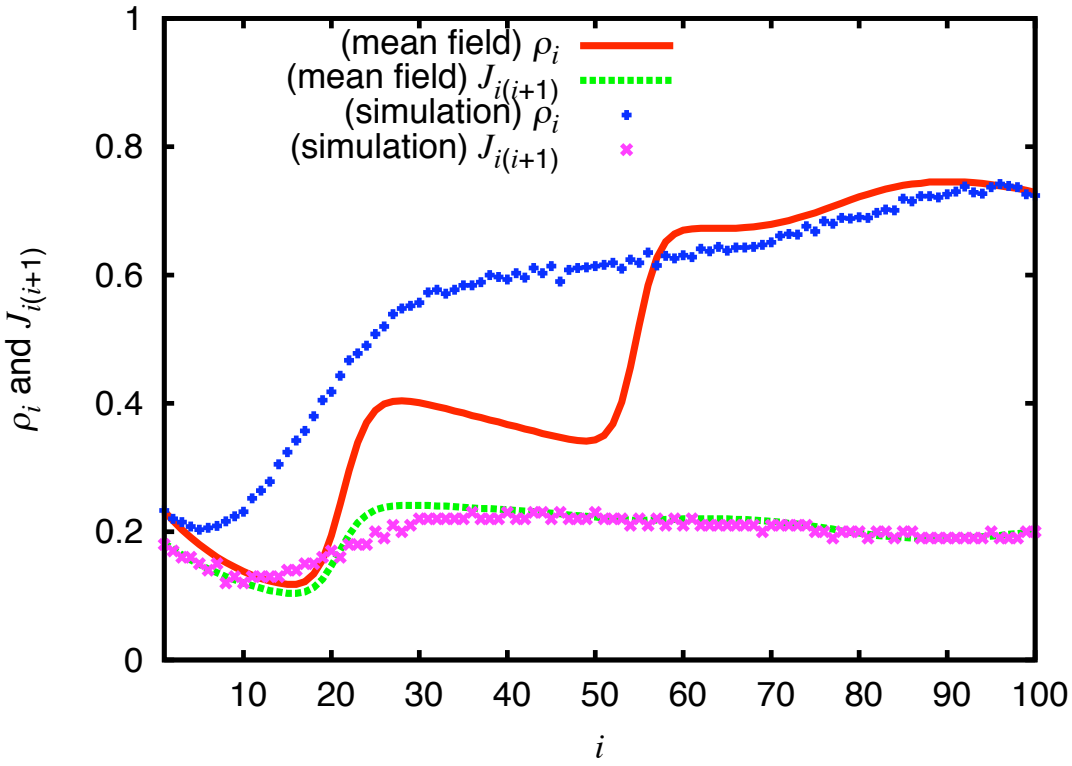

Figure 3.5: The one-body and current densities of the TASEP with sequential dynamics obtained from mean-field and simulation results. The input hopping rate is given by $\alpha(t) = 0.4 + 0.3\cos(2\pi t/T)$, and the output hopping rate is $\beta(t) = 0.3 + 0.05\cos(2\pi t/T)$. The period of oscillation is $T = 15 \times 10^3$ time steps. The above profiles are taken after 10^5 time steps.

Based on the result in Fig. 3.3, it is important to note that for the case of $\alpha(t) = 0.4 + 0.3\cos(2\pi t/T)$ and $\beta(t) = 0.3 + 0.05\cos(2\pi t/T)$, the density profiles should reach a periodic steady state (after a long time evolution). Consequently, the density profiles change within one period. Hence, the one-body and current densities of Fig. 3.5 are strictly just a snapshot taken after a long time evolution of 10^5 time steps. These particular profiles will be obtained again after one period, i.e. $10^5 + 15000$ time steps. Here, other profiles of this case within one period are not shown.

In summary, we have given four example cases for sequential updating of this model, viz. in Figs. 3.2-3.5. These figures show one-body and current density profiles that are very different to those for the TASEP with constant boundary rates. Fig. 3.2 shows that varying the period of $\alpha(t)$ and $\beta(t)$ generates interesting profiles of the one-body and current density. In this particular case, the one-body density profiles undergo phase changes as the period is increased. In the next example, i.e. Fig. 3.3, we show that after a long time evolution, the system reaches a periodic steady state condition. Here, over the time interval of one period, the one-body and current density profiles change. But, after one period the same profiles are attained. This differs from the TASEP with constant boundary rates, where the one-body and current densities are stationary at any time in steady state. In Fig. 3.4 the one-body density profiles undergo a phase transition from a maximal current phase to a coexistence phase, as the strength of oscillation is increased from 0.1 to 0.5. Again, this feature is not observed in the TASEP with constant input and output rates. Another interesting feature of this model is shown in Fig. 3.5 where two shocks occur in the system. The low and high density features around the entrance and the end of the lattice, respectively, are a distinctive feature compare to Fig. 3.2(ii) and Fig. 3.4, where at both ends the one-body density profiles are fixed at high values.

3.2.2 One-body and current densities for parallel dynamics

The main equation used in the parallel updating TASEP is the continuity equation (2.2.7), i.e.:

$$\frac{\partial \rho_i(t)}{\partial t} = J_{(i-1)i}(t) - J_{i(i+1)}(t),$$

where the mean-field current density, $J_{i(i+1)}(t)$, is given by equation (3.2.5). The current densities at the entrance and exit sites are given by equations (3.2.6) and (3.2.7), respectively. A discrete time parameter is considered where 1 time step is the smallest time interval. The time evolution of the densities are deterministic. The total number of lattice sites is 100 sites.

Here, once again the total number of lattice sites, N, is used as a comparison to the time scale of the oscillation in order to set the period of the oscillation of the input and output hopping rates, T. Particularly in this case, T is chosen equal to N as the minimum period of the oscillation, that is $T = N = 100$ time steps. To illustrate this, consider first an empty lattice site $\mathcal{L}$. Assume also that the system is in a low density regime, such that only after a particle exits $\mathcal{L}$ another particle may enter $\mathcal{L}$. Equal input

and output hopping rates are considered with $\alpha_0 = \beta_0 = 0.5$ and $\alpha_{\rm str} = \beta_{\rm str} = 0.5$. At time $t = 0$ a particle will enter site $i = 1$ with probability 1. But because the time is discrete and the dynamics is parallel updating, the particle hops at each time step along $\mathcal{L}$ until it eventually reaches the right most site at time $t = 99$ time steps. Finally, at $t = 100$ time steps the particle jumps out of $\mathcal{L}$ with certainty (according to the output hopping rate), while another particle enters $\mathcal{L}$. Thus, it takes 100 time steps for a particle to travel $\mathcal{L}$ where the input and output hopping rates act as 'gates' that open and close each period. The period of oscillation may be varied to investigate the effect of T on the one-body and current densities of the system.

For the first case, the boundary hopping rates are set to be equal with $\alpha_0 = \beta_0 = 0.09$, $\alpha_{\rm str} = \beta_{\rm str} = 0.09$, and $T = 100$ time steps. Since $0 \leq \cos(\theta) \leq 1$, then the maximum value of $\alpha(t)$ and $\beta(t)$ is 0.18, and their minimum value is 0. Thus this is an example of oscillation in the low rate regime. The density profiles specified by these hopping rates are given in Figure 3.6. These figures are snapshots at specific times of the one-body and current densities in one cycle (1 period) resulted from the mean-field and simulation results after a long time evolution of $t = 10^5$. The specific times of snapshots are 10^5[Fig. 3.6(i)], $10^5 + 12$ [Fig. 3.6(ii)], $10^5 + 25$ [Fig. 3.6(iii)], $10^5 + 50$ [Fig. 3.6(iv)], $10^5 + 75$ [Fig. 3.6(v)], and $10^5 + 100$ [Fig. 3.6(vi)] time steps.

At any time of the snapshots the one-body densities exhibit a coexistence phase between the low and high density regimes. At the bulk, a wall is observed in the mean-field result at the middle of the lattice sites. The detail profiles of the high and low density areas change as time progress. Other than that the height of the wall appears to change at each time of snapshot. The simulations of the one-body density consistently support a coexistence phase. However the curve of the profiles changes at each time of snapshot. The current density profiles are also obtained from mean-field and simulation results. There are good (qualitative) agreement between these results in all snapshots.

The oscillation strength of the input and output rates is also varied. In this case, the input and output rates are equal where $\alpha_0 = \beta_0 = 0.2$ and $T = 100$ time steps. The strength of oscillation is varied with values 0.05, 0.15, and 0.2. The density profiles for this case are given in Figure 3.7. It is clear that increasing the oscillation strength does not change the general feature of the one-body and current densities. All of the one-body density profiles clearly exhibit coexistence phases. According to the mean-field results, the strength of oscillation modifies the profiles of the low and high density regimes.

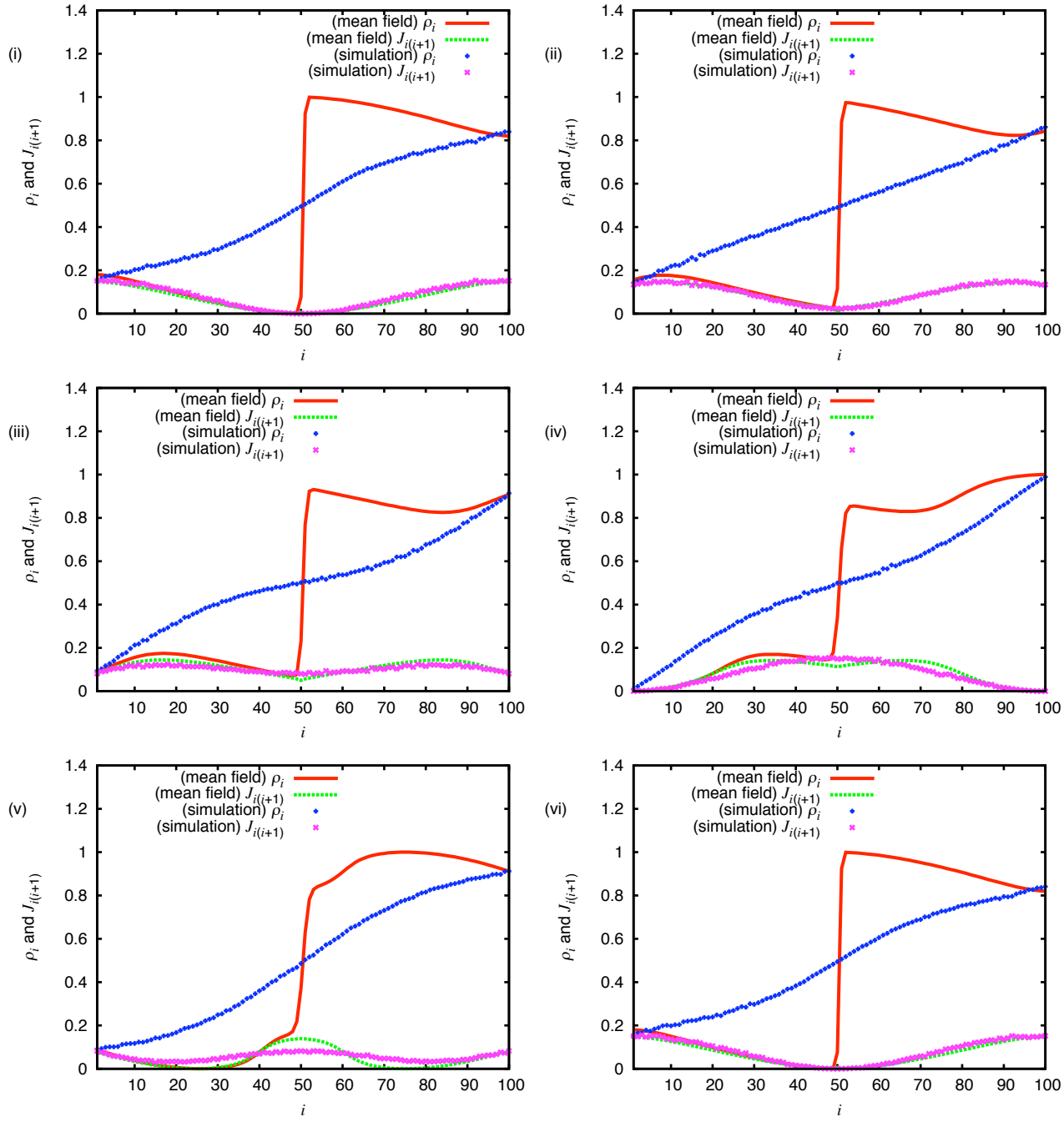

Figure 3.6: The time evolution (in one period) of the one-body and current densities of the TASEP in 1D with parallel updating. The input and output hopping rates are given by $\alpha(t) = \beta(t) = 0.09 + 0.09\cos(2\pi t/T)$ where $T = 100$ time steps. The above figures are densities giving the mean-field and simulation results taken after 10^5 time steps (i), $10^5 + 12$ time steps (ii), $10^5 + 25$ time steps (iii), $10^5 + 50$ time steps (iv), $10^5 + 75$ time steps (v), and $10^5 + 100$ time steps (vi).

According to the simulation results, there are areas which the one-body densities show considerably flat profiles as the oscillation strength is increased, i.e. near the boundaries. This seems to show that stronger oscillation strength constrains the position of the wall (shock) to a smaller region of the sites.

Lastly, we show the effect of varying the oscillation period, T, upon the densities of the system. The input and output rates are specified by $\alpha_0 = \beta_0 = \alpha_{\text{str}} = 0.1$, $\beta_{\text{str}} = 0.05$. T is varied with values 100 time steps, 10^4 time steps, and 10^6 time steps. The one-body and current densities for this case are depicted in Figure 3.8.

For $T = 100$ time steps, the simulation result shows a straight line for the one-body density, which extends from the center (site $i = 50$) to the end of $\mathcal{L}$. This is the coexistence region where a shock moves stochastically each time step. The mean-field result also shows a wall near the exit of $\mathcal{L}$ which indicates a coexistence phase. However, the region of the coexistence phase appears to be suppressed by a low density regime (from the entrance site until the centre of the sites).

When the period is increased to 10^4 time steps in Figure 3.8(ii), a high density of the one-body density starts to form around the exit sites. This is supported both by the mean-field and simulation results. Near the entrance sites a coexistence phase is clearly exhibited. Hence, the coexistence phase region appears to be shifted toward the entrance as the high density starts to dominate at the end of the lattice sites. The mean-field and simulation of the current densities agrees very well and shows a straight line with a constant value.

The period is increased further to 10^6 time steps. Figure 3.8(iii) clearly shows the one-body density profile is fully dominated by a high density phase. Again the agreement between the mean-field and simulation is quite good at the far-right boundary to the bulk sites but then it gets worse near the entrance.

Hence, with the specified boundary rates above, increasing the period changes the one-body density profile from a low density-coexistence phase (LD-CP) regime to a high density (HD) phase. At large period, e.g. 10^6 time steps, the oscillation is slow compared to the total number of lattice sites. Therefore, after a long time evolution the density should be influenced only by the maximum values of the input and output hopping rate, viz.: 0.2 and 0.15, which gives a high density phase.

As in previous Section, examples of density profiles for the TASEP with parallel dynamics are given, i.e. in Figs. 3.6-3.8. Here, we only consider low $\alpha(t)$ and $\beta(t)$ such

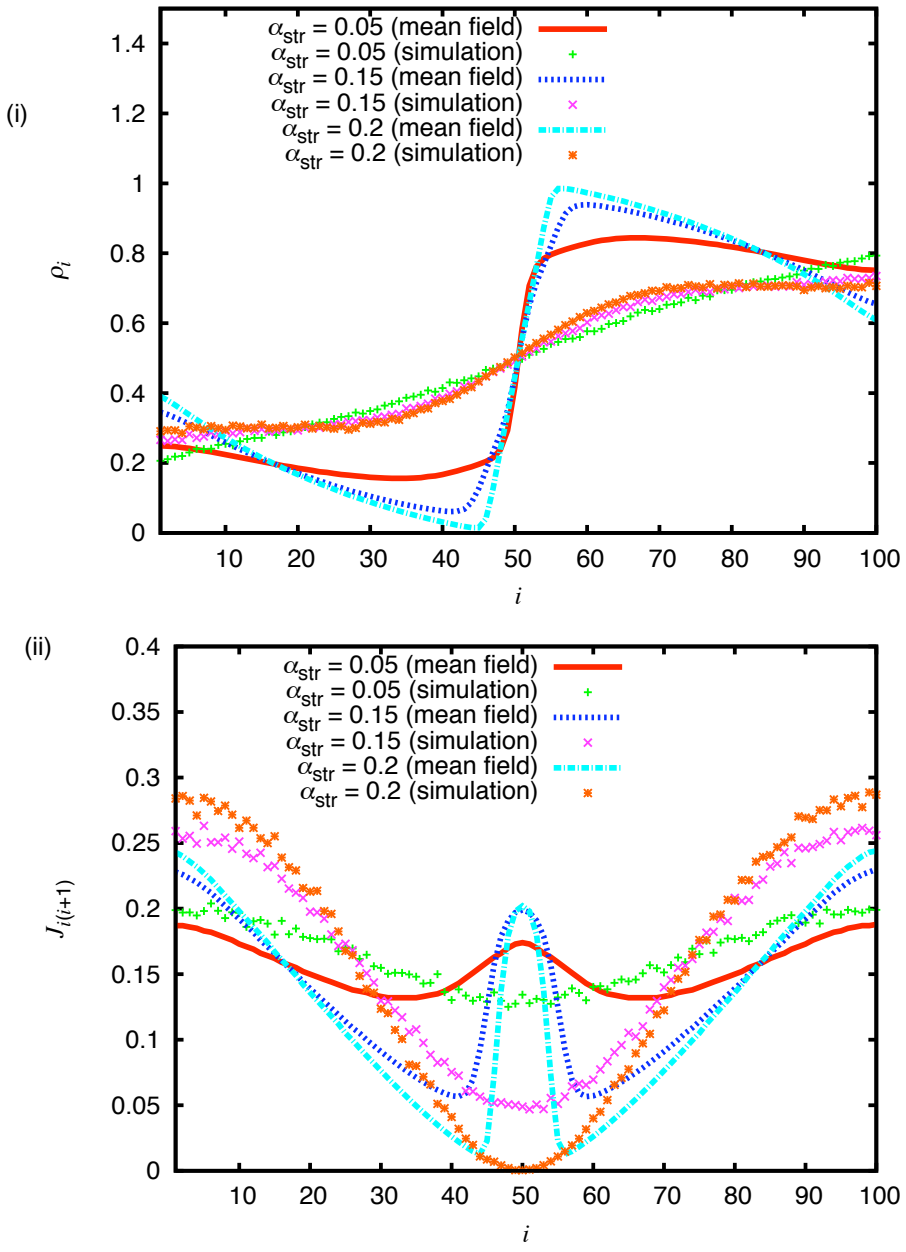

Figure 3.7: The mean-field one-body and current densities of the TASEP with parallel updating obtained by varying the oscillation strength, viz.: $\alpha_{\rm str}$. The boundary hopping rates are specified as $\alpha(t) = \beta(t) = 0.2 + \alpha_{\rm str}\cos(2\pi t/T)$, where $T = 100$ time steps. The figures above are the mean-field and simulation results of the one-body and current density profiles, respectively, after a long time evolution of 10^5 time steps.

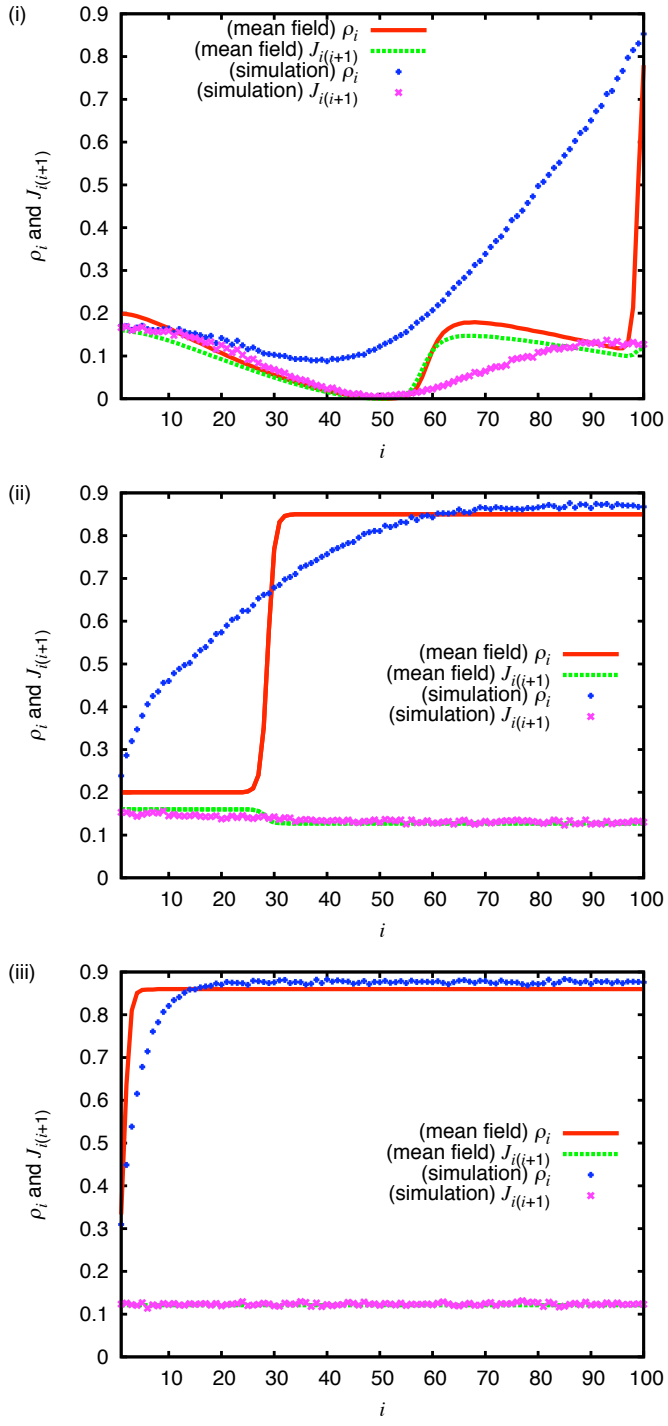

Figure 3.8: The one-body and current densities of the TASEP with parallel updating in 1D where the period (T) is varied. The input and output rates are given by $\alpha(t) = 0.1 + 0.1\cos(2\pi t/T)$ and $\beta(t) = 0.1 + 0.05\cos(2\pi t/T)$, respectively. The figures above are taken after 10^5 time steps obtained from mean-field and simulation results with oscillation periods $T = 100$ time steps (i), $T = 10^4$ time steps (ii), and $T = 10^6$ time steps (iii).

that low (density) current flows through the system. These are the cases where the mean-field approximations is valid. For higher values of $\alpha(t)$ and $\beta(t)$, the mean-field results deviate significantly from simulation results. We obtain interesting profiles of the one-body and current densities of the model, which are not obtained from the TASEP with constant boundary rates. After a long time evolution, the system reaches a periodic steady state condition, e.g. see Fig. 3.6. Varying the parameters of $\alpha(t)$ and $\beta(t)$, which is in this case the oscillation strength and period changes the behaviour of the one-body and current densities, e.g. see Figs. 3.7 and 3.8, respectively.

Here, we aim at presenting interesting examples of density profiles for the TASEP with time-dependent input and output rates, both for sequential and parallel dynamics. These examples give new features for density profiles which differ from the TASEP with constant boundary rates. However, we do not attempt in providing a full behaviour of the model, e.g. the full phase diagram. Hence, further investigation may be conducted upon this model in future work.

3.3 Mean-Field One-Body and Current Densities of the TASEP in 2D with Open Boundaries

In this section the TASEP is extended to a 2D square lattice $\mathcal{L}^2$. This is motivated by a correspondence between the TASEP and the lattice fluid mixtures proposed in [45]. This correspondence relies on a relationship between some calculated quantities in the equilibrium model and the desired quantities of the TASEP. Thus, one may obtain the one-body and current densities of the TASEP using the knowledge of the lattice fluid mixtures. With regard to this Section, the correspondence is further applied to higher dimensions, especially in two dimensions. It is important to note that at this present stage we do not discuss the interpretation of the one-body and current densities of the TASEP upon the equilibrium model. The calculation of one-body densities of the equilibrium model, via DFT, is given in Appendix A. Furthermore, two examples of the one-body and current density profiles of the TASEP with open boundaries at steady state are given in Figs. 3.10 and 3.11.

Here, employing the sequential dynamics scheme, at each time step $t \to t+1$ (discrete time), a site $\mathbf{i} = i_x\hat{\mathbf{e}}_x + i_y\hat{\mathbf{e}}_y = (i_x, i_y) \in \mathcal{L}^2$ is chosen randomly with proba-

bility[1] $1/[N(N+2)]$. N^2 is the total number of lattice sites in the square lattice, $(i_x, i_y) = 1, \ldots, N$, $\hat{\mathbf{e}}_x$ and $\hat{\mathbf{e}}_y$ are unit vectors in x and y-axes, respectively. If there is a particle on that chosen site, the (hard core) particle may jump to its right nearest neighbour site (along the x-axis) or its upper nearest neighbour site (along the y-axis) with hopping rates $k^{\mathrm{r}}_{\mathbf{i}(\mathbf{i}+\hat{\mathbf{e}}_x)}(t)$ and $k^{\mathrm{u}}_{\mathbf{i}(\mathbf{i}+\hat{\mathbf{e}}_y)}(t)$, respectively. The jump only occurs if the nearest neighbour site is empty. The particle may also stay on the site with probability $1-\frac{\left[k^{\mathrm{r}}_{\mathbf{i}(\mathbf{i}+\hat{\mathbf{e}}_x)}(t)+k^{\mathrm{u}}_{\mathbf{i}(\mathbf{i}+\hat{\mathbf{e}}_y)}(t)\right]}{N(N+2)}$. Here, the boundary condition employed is the open boundaries.

The average one-body density, $\rho_{\mathbf{i}}(t)$, and the current densities to the right and to the upper sites, i.e.: $J^{\mathrm{r}}_{\mathbf{i}(\mathbf{i}+\hat{\mathbf{e}}_x)}(t)$ and $J^{\mathrm{u}}_{\mathbf{i}(\mathbf{i}+\hat{\mathbf{e}}_y)}(t)$, respectively, are determined. In order to do so, a relationship between the TASEP in 2D and the lattice fluid mixtures in accordance with [45] is established. Here, the particles of the TASEP and their possible movements are associated as particles in the lattice fluid mixtures. This yields (see Fig. 3.9):

1) Particles that hop to their right nearest neighbours are associated to particles with site exclusion that exclude particles from their right nearest neighbours (species 1).

2) Particles that hop to the upper nearest neighbours are associated to particles with site exclusion that exclude particles from their upper nearest neighbours (species 2).

3) Particles that do not move in the TASEP are associated to particles with only site exclusion in the lattice fluid mixtures (small particles or species 3).

As a consequence of the above correspondence, the physical quantities of the two (different) models are associated as well. This is attained by identifying the (linearized) one-body densities of the equilibrium lattice fluid mixture with the one-body and current densities of the TASEP, giving[35, 45]:

$$\rho_3(\mathbf{i}) \longrightarrow \rho_{\mathbf{i}}(t), \tag{3.3.1}$$

$$\rho_1(\mathbf{i}) \longrightarrow J^{\mathrm{r}}_{\mathbf{i}(\mathbf{i}+\hat{\mathbf{e}}_x)}(t), \tag{3.3.2}$$

$$\rho_2(\mathbf{i}) \longrightarrow J^{\mathrm{u}}_{\mathbf{i}(\mathbf{i}+\hat{\mathbf{e}}_y)}(t), \tag{3.3.3}$$

[1] $1/[N(N+2)]$ means that there are as many as N^2+2N sites to be chosen randomly at each time step. The $2N$ term comes from sites $(i_x, 0)$ and $(0, i_y)$ along the y and x-axes, respectively, where $1 \leq i_x, i_y \leq N$. These sites may be considered as reservoirs where a particle may enter the lattice sites. Therefore, these sites can also be chosen (randomly).

$$\frac{e^{\beta(\mu_1 - V_1^{\rm ext}(\mathbf{i}))}}{e^{\beta(\mu_3 - V_3^{\rm ext}(\mathbf{i}))}} \longrightarrow k^{\rm r}_{\mathbf{i}(\mathbf{i}+\hat{\mathbf{e}}_x)}(t), \tag{3.3.4}$$

and

$$\frac{e^{\beta(\mu_2 - V_2^{\rm ext}(\mathbf{i}))}}{e^{\beta(\mu_3 - V_3^{\rm ext}(\mathbf{i}))}} \longrightarrow k^{\rm u}_{\mathbf{i}(\mathbf{i}+\hat{\mathbf{e}}_y)}(t). \tag{3.3.5}$$

The next step is to conduct some calculations in the equilibrium lattice fluids mixture, i.e.: i) constructing the excess free energy functional of the model via LFMT, and then ii) calculating the direct correlation function for each species considered in the model. From these calculations, the (linearized) one-body densities of the model are obtained in equations (A.3.7), (A.3.8), and (A.3.9) in Appendix A. Finally, applying the correspondences (3.3.1)-(3.3.5) for equations (A.3.7)-(A.3.9), one obtains the desired TASEP quantities as,

$$J^{\rm r}_{\mathbf{i}(\mathbf{i}+\hat{\mathbf{e}}_x)}(t) = k^{\rm r}_{\mathbf{i}(\mathbf{i}+\hat{\mathbf{e}}_x)}(t)\rho_{\mathbf{i}}(t)\left[1 - \rho_{\mathbf{i}+\hat{\mathbf{e}}_x}(t)\right], \tag{3.3.6}$$

and

$$J^{\rm u}_{\mathbf{i}(\mathbf{i}+\hat{\mathbf{e}}_y)}(t) = k^{\rm u}_{\mathbf{i}(\mathbf{i}+\hat{\mathbf{e}}_y)}(t)\rho_{\mathbf{i}}(t)\left[1 - \rho_{\mathbf{i}+\hat{\mathbf{e}}_y}(t)\right], \tag{3.3.7}$$

where $J^{\rm r}$ and $J^{\rm u}$ are components of the current vector field $\mathbf{J}_{\mathbf{i}}(t) = J^{\rm r}_{\mathbf{i}(\mathbf{i}+\hat{\mathbf{e}}_x)}(t)\hat{\mathbf{e}}_x + J^{\rm u}_{\mathbf{i}(\mathbf{i}+\hat{\mathbf{e}}_y)}(t)\hat{\mathbf{e}}_y$. The time evolution of the one-body density distribution can be obtained from the continuity equation, viz.:

$$\begin{aligned}\frac{\partial\rho_{\mathbf{i}}(t)}{\partial t} &= -\frac{1}{N(N-2)}\nabla\cdot\mathbf{J}_{\mathbf{i}}(t) = -\frac{1}{N(N-2)}\left[\nabla_x J^{\rm r}_{\mathbf{i}(\mathbf{i}+\hat{\mathbf{e}}_x)}(t) + \nabla_y J^{\rm u}_{\mathbf{i}(\mathbf{i}+\hat{\mathbf{e}}_y)}(t)\right] \\ &\equiv \frac{1}{N(N-2)}\left\{\left[J^{\rm r}_{(\mathbf{i}-\hat{\mathbf{e}}_x)\mathbf{i}}(t) - J^{\rm r}_{\mathbf{i}(\mathbf{i}+\hat{\mathbf{e}}_x)}(t)\right] + \left[J^{\rm u}_{(\mathbf{i}-\hat{\mathbf{e}}_y)\mathbf{i}}(t) - J^{\rm u}_{\mathbf{i}(\mathbf{i}+\hat{\mathbf{e}}_y)}(t)\right]\right\}.\end{aligned} \tag{3.3.8}$$

The steady state is obtained if $\partial\rho_{\mathbf{i}}(t)/\partial t = 0$. The results of the density and current distributions from this correspondence are of the mean-field type. The size of this cubic lattice is 100×100 sites. A particle may enter the lattice through sites $(i_x, 0)$ with probability α_1 and exit from sites $(i_x, 100)$ with probability β_1 where $i_x = 1, \ldots, 100$. A particle may also enter the lattice through sites $(0, i_y)$ with probability α_2 and exit the lattice after reaching sites $(100, i_y)$ with probability β_2 where $i_y = 1, \ldots, 100$. The constant input and output hopping rates are varied in these figures. The hopping rates in the bulk are constant and uniform with $k^{\rm r} = k^{\rm u} = 0.5$. The continuity equation (3.3.8) is integrated forward in time with an initial condition of empty lattice sites until a steady state is reached (in 10^6 time steps).

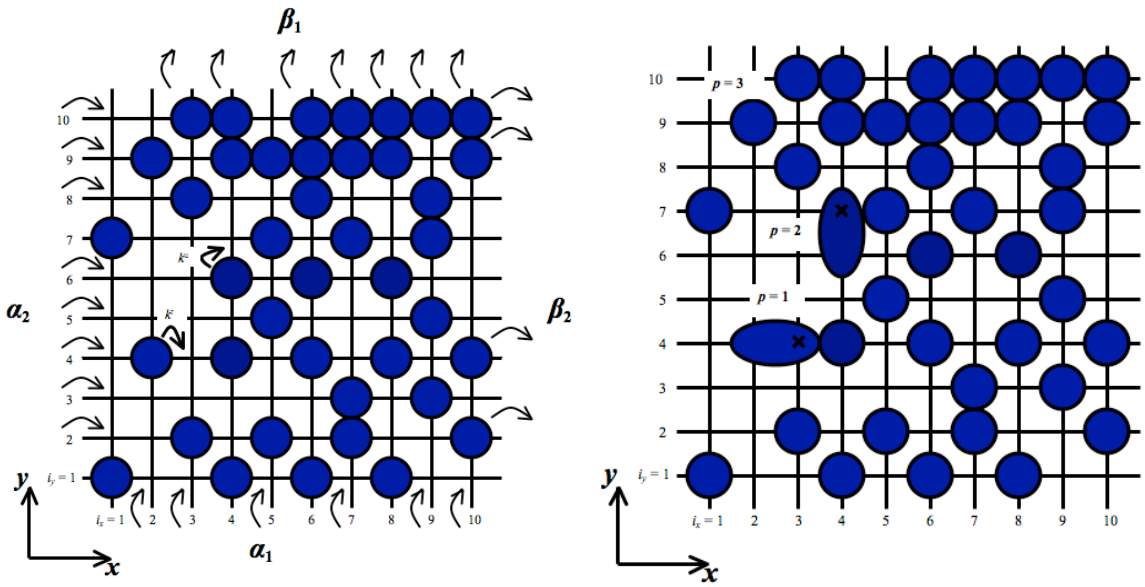

(i) (ii)

Figure 3.9: Illustrations of the TASEP with constant boundary hopping rates (i), and the hard core lattice fluid mixtures (ii) in 2D. The sites are labelled by $\mathbf{i} = i_x\hat{\mathbf{e}}_x + i_y\hat{\mathbf{e}}_y$ where $i_x, i_y = 1, 2, \ldots, N$, $\hat{\mathbf{e}}_x$ and $\hat{\mathbf{e}}_y$ are the unit vectors to the x and y-axes, respectively. The cubic lattice above consists of 10×10 sites. The filled blue circles are the hard core particles. In (i), at the boundaries, particles may enter the lattice sites with hopping rates α_1 and α_2 from sites $(i_x, 1)$ and $(1, i_y)$, respectively. In the bulk, a particle may jump to its right or upper nearest neighbour site with a hopping rate k^{r} or k^{u}, respectively. Particles may exit $\mathcal{L}^2$ with hopping rates β_1 and β_2 from sites (i_x, N) and (N, i_y). Figure (ii) is a possible configuration of the hard core fluid mixtures. There are 3 species defined for the model. The first species is a hard core particle that excludes its right nearest neighbour site ($p = 1$). The second species excludes its upper nearest neighbour site ($p = 2$), and the third species is subjected to only site exclusion ($p = 3$). Species 1 ($p = 1$) in (ii) is associated to the particle that jumps to the right nearest neighbour in (i), e.g.: site $(2, 4)$. Species 2 in (ii) is associated to the particle that jumps to the upper nearest neighbour site in (i), e.g.: site $(4, 6)$, and species 3 in (ii) is associated to all particles that do not move in (i).

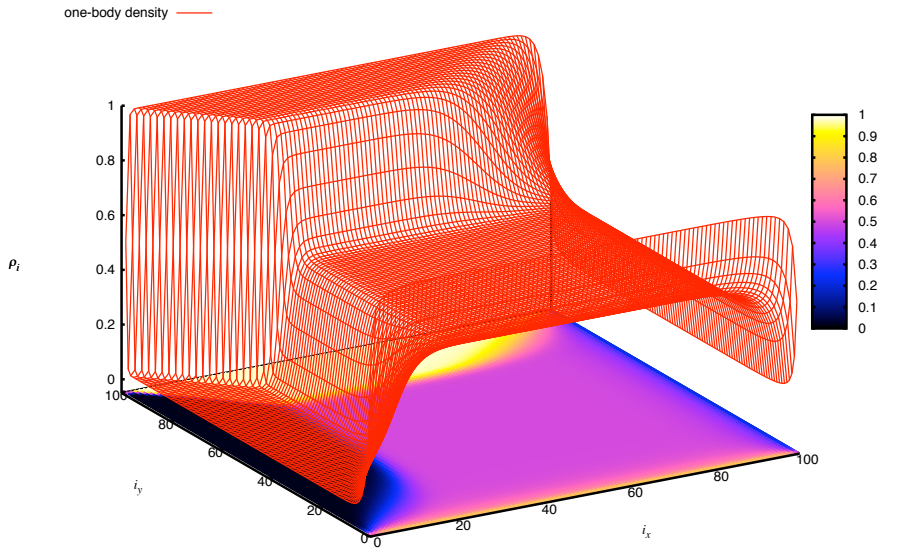

(i)

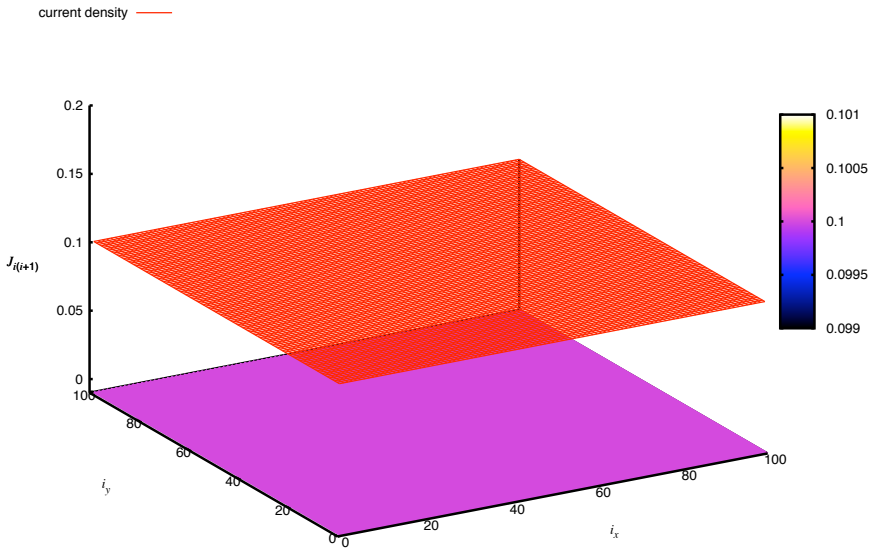

(ii)

Figure 3.10: The steady state one-body and current density distributions of the TASEP with open boundaries in 2D as functions of the lattice sites. Along the x-axis, a particle can enter sites $(1, i_y)$ with rate $\alpha_2 = 0.1$ and exit sites $(100, i_y)$ with rate $\beta_2 = 0.9$. And along the y-axis, a particle may enter sites $(i_x, 1)$ with rate $\alpha_1 = 0.9$ and exit sites $(i_x, 100)$ with rate $\beta_1 = 0.1$. The one-body and current density profiles are of mean-field type and taken after a long time evolution of 10^6 time steps.

The first case is given in Figure 3.10. The input and output hopping rates specified for this case are given by,

$$k^{\mathrm{u}}_{(i_x,0)(i_x,1)} = \alpha_1 = 0.9, \qquad \text{and} \qquad k^{\mathrm{u}}_{(i_x,100)(i_x,101)} = \beta_1 = 0.1, \tag{3.3.9}$$

and

$$k^{\mathrm{r}}_{(0,i_y)(1,i_y)} = \alpha_2 = 0.1, \qquad \text{and} \qquad k^{\mathrm{r}}_{(100,i_y)(101,i_y)} = \beta_2 = 0.9. \tag{3.3.10}$$

Taking an analogy from the TASEP in 1D, particles traveling along the x-axis ($\alpha_2 = 0.1$ and $\beta_2 = 0.9$) should produce low density regimes, while particles traveling along the y-axis (with $\alpha_1 = 0.9$ and $\beta_1 = 0.1$) should end up in high density regimes. Hence there is a competition between high density (along the y-axis) and low density (along the x-axis) phases on the 2D lattice sites. The mean-field one-body density of this case is given by Figure 3.10(i). Here, the profile seems to be quite structured with a shape similar to a saddle (although it is not symmetric). There are regions of high density phase especially along the x-axis and at the far end of the y-axis. There are regions of low density phase as well around the beginning of the x-axis and along the y-axis. Thus the density profile exhibits a coexistence phase (between the high and low density regimes). Interestingly, around the middle of the sites, the density profile is flat with value nearing 0.5 which means that particles diffuses around the center of the lattice sites.

The current density of this case is obviously constant and uniform throughout the lattice sites with a value equal to 0.01, see Figure 3.10(ii). This also confirms that the system reaches a steady state condition.

Next we take a look at another case where the boundary hopping rates are given as:

$$k^{\mathrm{r}}_{(0,i_y)(1,i_y)} = \alpha_2 = k^{\mathrm{u}}_{(i_x,0)(i_x,1)} = \alpha_1 = 0.1, \tag{3.3.11}$$

and

$$k^{\mathrm{r}}_{(100,i_y)(101,i_y)} = \beta_2 = k^{\mathrm{u}}_{(i_x,100)(i_x,101)} = \beta_1 = 0.1. \tag{3.3.12}$$

The mean-field one-body and current density profiles in steady state are given in Figure 3.11(i) and (ii), respectively. Recalling again the TASEP in 1D by setting $\alpha = \beta = 0.1$ the one-body density should yield a coexistence phase. Figure 3.11(i) is somewhat the 2D version of the coexistence phase. There are areas of low density phase, i.e.: along the xy-plane around the beginning of the lattice sites, and areas of high density phase at the far end of the sites. Similar to the previous case, the middle sites appears to be a flat profile with a value of 0.5. Furthermore, the current density profile in Fig. 3.11(ii) is flat and uniform over the sites with a value of 0.1.

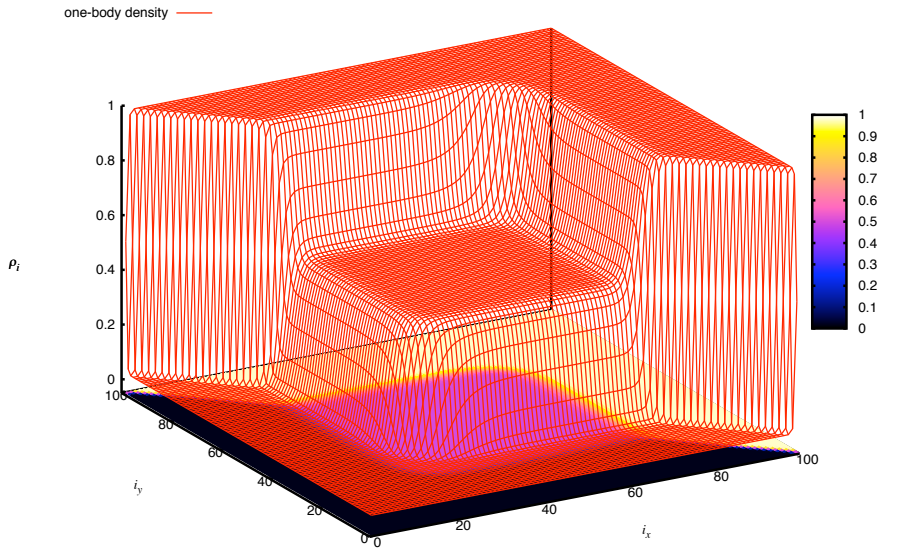

(i)

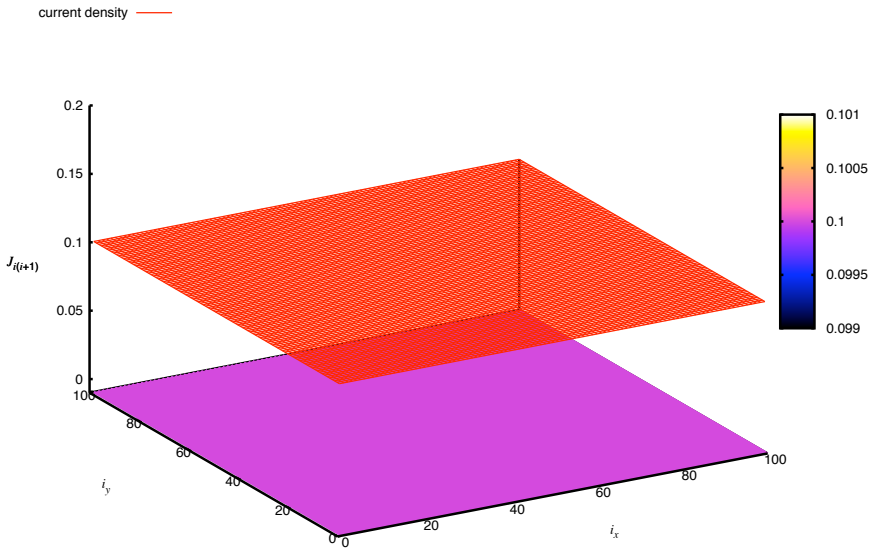

(ii)

Figure 3.11: A steady state one-body and current density distributions of the TASEP with open boundaries in a coexistence phase. Along the xy-plane a particle may enter and exit the sites with equal rates, in this case $\alpha_1 = \alpha_2 = \beta_1 = \beta_2 = 0.1$. The input and output hopping rates along the sides of the xy-plane create a coexistence phase regions, which is a coexistence between low and high density regions. The corresponding one-body and current density profiles are mean-field and taken after a long time evolution of 10^6 time steps.

3.4 TASEP with a Junction

An interesting variation of the TASEP in 2D is to consider only specific sites in the xy-plane such that a junction is formed. This model may be of some interest in studying the densities of vehicles on a road with a junction, or of insects on trails that form a junction.

The main objective of this Section is to give some examples of the one-body and current density profiles of the TASEP with a junction. One point that we would like to put across is to show that interesting one-body density profiles may be obtained from this model. These profiles differ from the typical one-body density profiles of the TASEP in 1D with open boundaries and constant boundary rates at steady state. Hence, we are not attempting in providing a full account of this model, e.g. the full phase diagram, although in our view this model deserve to be investigated in future work. Furthermore, as these density profiles are obtained via the mean-field approximation, the validity of these results should be justified following the numerical comparison (between mean-field and simulation results) in Section 2.2.8.

Here we have a square lattice of $N \times N$ sites with N are odd total number of lattice sites. The total number of lattice sites used throughout this model is $N = 101$ sites. One way to build a junction is to apply inhomogeneous hopping rates upon the lattice sites.

The hopping rate to the right of the lattice sites, i.e.: $\mathbf{i}$ to $\mathbf{i} + \hat{\mathbf{e}}_x$, is given by

$$k^{\mathrm{r}}_{\mathbf{i}(\mathbf{i}+\hat{\mathbf{e}}_x)} = \begin{cases} 0; & 1 \leq i_y \leq (\frac{[N+1]}{2} - 1), \\ k^{\mathrm{r}} = 0.5; & i_y = \frac{[N+1]}{2}, \\ 0; & \left(\frac{[N+1]}{2} + 1\right) \leq i_y \leq N, \end{cases} \tag{3.4.1}$$

for $1 \leq i_x \leq N - 1$. This corresponds to the equilibrium fluid model by setting the external potential $V_1^{\mathrm{ext}}(\mathbf{i})$ as

$$V_1^{\mathrm{ext}}(i_x, i_y) = \begin{cases} \infty; & 1 \leq i_y \leq (\frac{[N+1]}{2} - 1), \\ V_1^{\mathrm{ext}}; & i_y = \frac{[N+1]}{2}, \\ \infty; & \left(\frac{[N+1]}{2} + 1\right) \leq i_y \leq N, \end{cases} \tag{3.4.2}$$

for $\forall i_x$.

The hopping rate to the upper site (along the y-axis), i.e.: $\mathbf{i}$ to $\mathbf{i}+\hat{\mathbf{e}}_y$, is given by

$$k^{\mathrm{u}}_{\mathbf{i}(\mathbf{i}+\hat{\mathbf{e}}_y)} = \begin{cases} 0; & 1 \le i_x \le (\frac{[N+1]}{2} - 1), \\ k^{\mathrm{u}} = 0.5; & i_x = \frac{[N+1]}{2}, \\ 0; & \left(\frac{[N+1]}{2} + 1\right) \le i_x \le N, \end{cases} \tag{3.4.3}$$

$1 \le i_y \le N-1$. Again the hopping rate of (3.4.3) is related to the equilibrium model by setting $V_2^{\mathrm{ext}}(\mathbf{i})$ as

$$V_2^{\mathrm{ext}}(i_x, i_y) = \begin{cases} \infty; & 1 \le i_x \le (\frac{[N+1]}{2} - 1), \\ V_2^{\mathrm{ext}}; & i_x = \frac{[N+1]}{2}, \\ \infty; & \left(\frac{[N+1]}{2} + 1\right) \le i_x \le N, \end{cases} \tag{3.4.4}$$

$\forall i_y$.

According to equation (3.4.1) all hopping rates to the right nearest neighbours are zeros, $k^{\mathrm{r}} = 0$, except for sites $\left(1, \frac{[N+1]}{2}\right)$ to $\left(N-1, \frac{[N+1]}{2}\right)$, which is $k^{\mathrm{r}} = 0.5$. And according to equation (3.4.3) all hopping rates to the upper nearest neighbour sites are zeros, except at sites $\left(\frac{[N+1]}{2}, 1\right)$ to $\left(\frac{[N+1]}{2}, N-1\right)$, which is $k^{u} = 0.5$. A particle may enter site $\left(1, \frac{[N+1]}{2}\right)$ or $\left(\frac{[N+1]}{2}, 1\right)$, and exit site $\left(N, \frac{[N+1]}{2}\right)$ or $\left(\frac{[N+1]}{2}, N\right)$ with constant rates α_2, α_1, β_2 and β_1, respectively[2]. Therefore, this junction has two entering and exiting sites [see Figure 3.12(i)].

The junction TASEP above may be thought as a combination (interaction) of one dimensional TASEPs. Therefore, the density profiles of the TASEP with a junction may be discussed using known density profiles of the TASEP in 1D. In this case, instead of a single TASEP with hopping rates α_2 and β_2 another 1D TASEP with hopping rates α_1 and β_1 is embedded at their center site. The interaction between the two 1D TASEPs may modify the (known) density profiles of the individual 1D TASEP. Hence, this is similar to studying the effect of adding sites (with different boundary rates) to a 1D TASEP. Figure 3.12 shows the designated models where only the sites with non-zero values of the hopping rates are considered. Figure 3.12(i) illustrates the TASEP with a junction involving four paths (lane) whereby particles may travel through the lattice sites. Path I is a 1D TASEP along the x-axis with boundary hopping rates α_2 and β_2. This path interacts with path II, which is another 1D TASEP with hopping rates α_1

[2]However, this junction TASEP contains too many control parameters, i.e. $\alpha_1, \beta_1, \alpha_2$, and β_2. In order to reduce these parameters the junction is further modify into a simpler junction, which consists of only one entering site and two exiting sites.

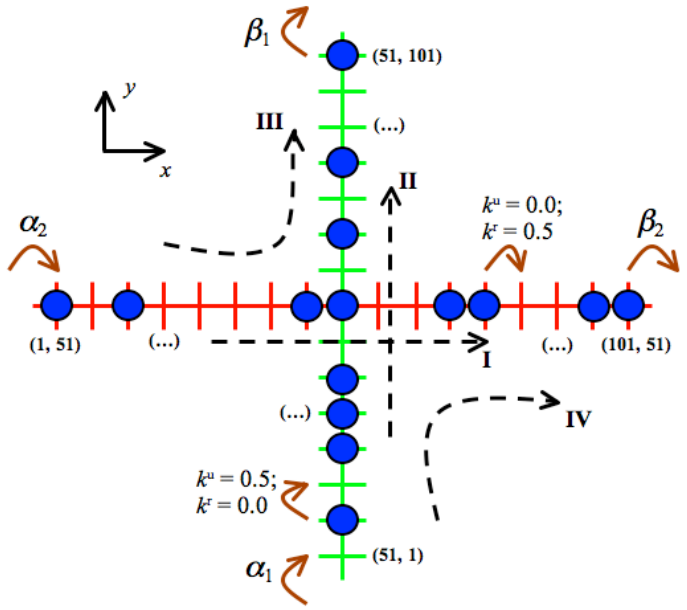

(i)

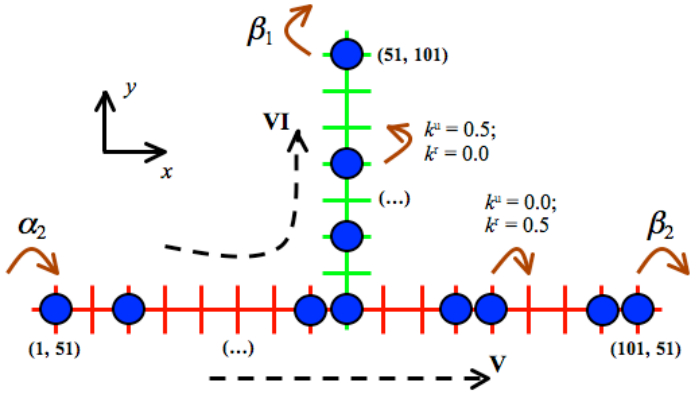

(ii)

Figure 3.12: A sketch of the TASEP with a junction. The lattice sites on the x-axis is given by the solid red line, whereas the lattice sites on the y-axis is given by the solid green line. The tick marks on the xy-plane are the sites which are labelled as $\mathbf{i} = (i_x, i_y)$. The filled (blue) circles are the hard core particles. In (i) a particle may enter the lattice from site $(1, 51)$ with rate α_2 or site $(51, 1)$ with rate α_1. If there is a particle at site $(101, 51)$ or $(51, 101)$, the particle may exit the site with rate β_2 and β_1, respectively. Particles may travel through the lattice sites by following one of the possible given paths (lanes), viz. paths I - IV, with a hopping rate of 0.5. In (ii), α_1 is set to be 0. Thus, particles may only enter the lattice from site $(1, 51)$. The particles may travel along path V or path VI with rate 0.5.

and β_1. Path II is drawn vertically, i.e.: it lies on the y-axis. Thus, one may discuss the effect of adding path II toward the density profiles of path I, and vice versa. However, one may also consider different paths, i.e.: path III and path IV. Path III is a 1D TASEP with rates α_2 and β_1, which interacts with another TASEP along path IV with α_1 and β_2.

Figure 3.12(ii) is a further simplification of the TASEP with a junction where α_1 is set to be 0. Hence, the paths to be considered are reduced to two paths, viz.: V and VI. Each path is a 1D TASEP, which is affected by an addition of sites with a particular output rate. Path V is a 1D TASEP along the x-axis with α_2 and β_2, which is modified by additional sites ending with β_1, whereas path VI is a 1D TASEP with hopping rates α_2 and β_1 with an additional branch (sites) ending with β_2.

The first example is depicted in Figure 3.13 where $\alpha_1 = \beta_2 = 0.1$ and $\alpha_2 = \beta_1 = 0.4$. Consider first from Figure 3.13(i) the one-body density profile along path I with $\alpha_2 = 0.4$ and $\beta_2 = 0.1$, which is given by the solid (red) line. The density profile starts from a low linear density of $\rho = 0.4 < 0.5$, then suddenly jumps to a high density of $\rho = 0.9 > 0.5$ at the junction site $(51, 51)$ until the end of the lattice sites. This shows that the density profile is in a coexistence phase. Next, we observe the density profile along path II with $\alpha_1 = 0.1$ and $\beta_1 = 0.4$, which is given by the dashed (green) line. Here the density profile starts from a low linear density of $\rho = 0.1$ then suddenly jumps to a higher density of $\rho = 0.6$ until the end of the lattice sites. This shows that the density profile is also in a coexistence phase. Other paths may be considered, i.e. paths III and IV. Along path IV [Figure 3.13(iii)], the density profile is in a coexistence phase starting from a low density of $\rho = 0.1$ (dashed [green] line) then suddenly jumps to a high density of $\rho = 0.9$ (solid [red] line). The density profile of path III starts from a low density of $\rho = 0.4$ (solid [red] line) then jumps to $\rho = 0.6$ (dashed [green] line), which is also a coexistence phase.

A TASEP in 1D with $\alpha = 0.4$ and $\beta = 0.1$ should only produce a high density phase, which is different from the one-body density profile along path I in Fig. 3.13. Moreover, the density profile of a TASEP with $\alpha = 0.1$ and $\beta = 0.4$ should only be a low density phase, which is different from the one-body density profile along path II. The present of path II at the center of path I modifies the one-body density of path I into a coexistence phases (CP). However, for $\alpha = \beta = 0.4 < 0.5$, the resulting density profile is the coexistence phase, similar to the density profile of path III. A TASEP in 1D with $\alpha = \beta = 0.1$ gives a coexistence phase, which is the same to that of the one-body density

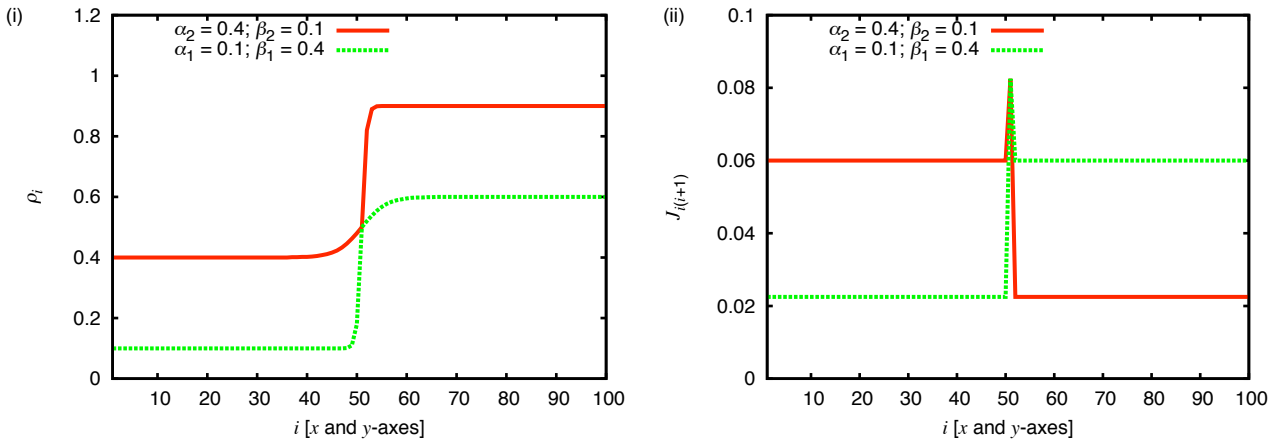

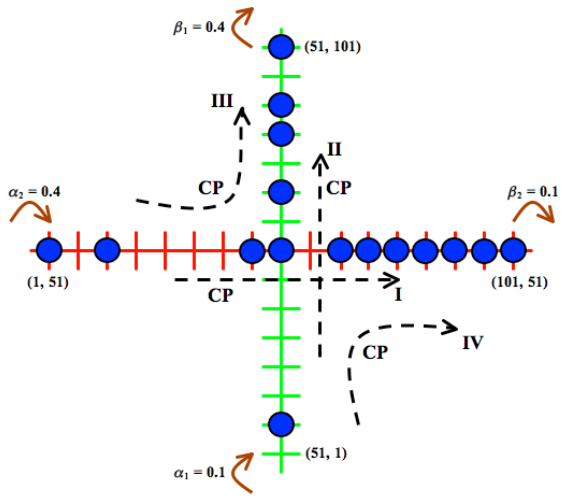

(iii)

Figure 3.13: The TASEP with a junction specified by input and output hopping rates of $\alpha_2 = \beta_1 = 0.4$ and $\alpha_1 = \beta_2 = 0.1$. In Figure 3.13(i), the vertical axis is the one-body density profile and the horizontal axis is the overlapped x and y-axis of the lattice sites with $N = 101$. The junction is on site $(51, 51)$ where the paths are intersected. The solid (red) line is the one-body density of path I. The dashed (green) line is a coexistence phase along path II. The corresponding current density profiles are given in Figure 3.13(ii). Figure 3.13(iii) gives the steady state phases corresponding to each path. Paths I to IV end up in coexistence phases (CP). The filled circles are the (hard core) particles.

profile of path IV. Thus, adding path IV to path III, or vice versa does not affect the one-body density of each path.

The current density profiles of this case are shown in Figure 3.13(ii). The current density of path I is given by the solid (red) line. Starting from the entrance, the current density profile is constant with a value of 0.06. Then at site $(51, 51)$ it jumps to a higher value just above 0.08, but falls to a value below 0.03 at the remaining sites. This means that particles travel faster in the first half of the lattice sites as not many particles occupy the sites, whereas they travel slower from the center until the end of the sites because many particles are occupying the junction up to the exit sites. Now opposite to that of path I, the current density of path II [dashed (green) line] starts with a low value of 0.02 until the junction site. Then it jumps to a higher value of 0.06 for the remaining sites. The current density is low at the entrance because not many particles are entering the site (low input rate). The current densities of paths III and IV are flat except at the center site. The density of path III is higher than that of path IV. This indicates that the mobility of particles moving along path III is higher than that of path IV.

The case above is further modified by turning off one of the input hopping rate, i.e.: $\alpha_1 = 0$, such that no particles may enter the sites from it. The corresponding one-body and current densities are shown in Figure 3.14(i) and (ii), respectively. First we look at path V [Fig. 3.14(iii)]. At the entrance site where the input rate is $\alpha_2 = 0.4$ the profile is flat with a value equal to the input hopping rate. Around the centre, the one-body density dips to a value of 0.2, then increases suddenly to a flat high density of 0.9 until the end of the lattice sites. For path VI, from the junction to the exiting site (with $\beta_1 = 0.4$) the one-body density is flat with a low density value of 0.2 but then increases at the exiting site. The dip at the junction is caused by the existence of two output rates. Furthermore, the path with lower output rate gives a higher one-body density. One may compare this to cases of the TASEP in 1D. For $\alpha = \beta = 0.4 < 0.5$ the one-body density should be in a coexistence phase. However, path VI produces a low density phase (LD) [Fig. 3.14(i)]. On the other hand, for $\alpha = 0.4$ and $\beta = 0.1$ the one-body density should be a purely high density phase. In this case, the present of path VI modifies the profile of path V into a coexistence phase (CP).

Moreover, the current density profiles [Fig. 3.14(ii)] of paths V and VI from the entrance to the junction are flat with a value of 0.06. Then they decrease with values 0.04 (for path VI) and around 0.02 (for path V) until the end of the sites. Thus, particles

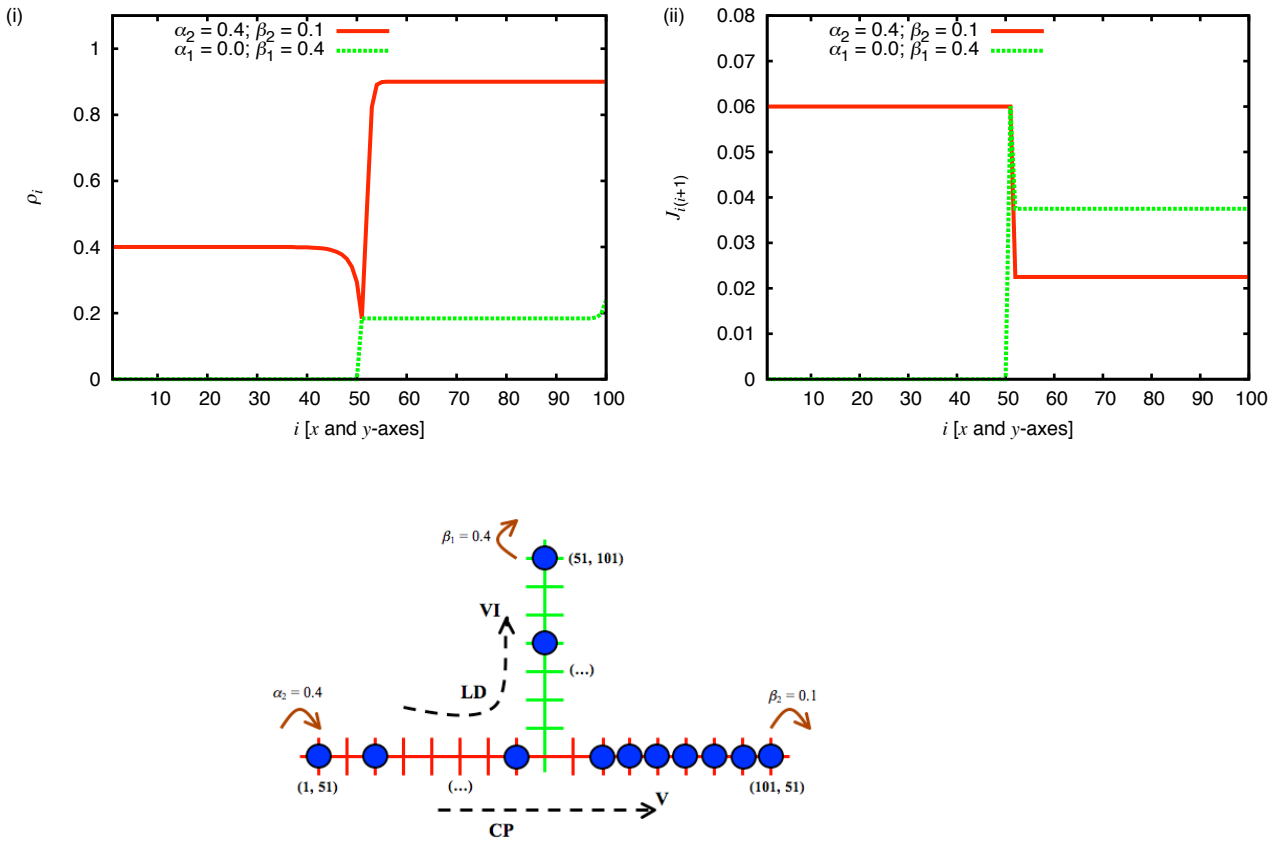

(iii)

Figure 3.14: A modification of the TASEP with a junction by setting $\alpha_1 = 0.0$. The other input and output hopping rates are the same as the aforementioned case, viz.: $\beta_1 = 0.4$, and $\alpha_2 = 0.4$; $\beta_2 = 0.1$. The one-body and current density profiles are provided in Fig. 3.14(i) and (ii), respectively. The vertical axes are the one-body and current densities, respectively, while the horizontal axis is the sites of the paths. The densities of path V are given by the solid (red) line. The density of path IV is given by the solid (red) line from the entrance to the junction and the dashed (green) line from the junction to the exit site. Sites $(51, 51)$ is the position of the junction. Fig. 3.14(iii) gives the resulting phases of the one-body density for each path in steady state. Path V turns out to reach a coexistence phase (CP), while path VI becomes a low density phase.

travel fastest at the first half of the lattice sites, then they move slower at either path for the rest of the lattice sites. Particles travel slower on path V as a consequence of the lower output rate. Particles tend to pile up at the junction to the exit sites (corresponding to a high density), hence slowing down the current flow of the particles.

In Table 3.1, various phases for this particular case are given. α_2 and β_2 are set to be 0.4 and 0.1, respectively. α_1 and β_1 are varied.

Table 3.1: Various Phases of the TASEP with a junction where $\alpha_2 = 0.4$ and $\beta_2 = 0.1$. Note that paths II and III are labeled as V and VI for cases where $\alpha_1 = 0.0$. LD, HD, MC, and CP are abbreviations for low density, high density, maximal current, and coexistence phases.

No.	α_1	β_1	path I (V) $[\alpha_2, \beta_2]$	path II (α_1, β_1)	path III (VI) $[\alpha_2, \beta_1]$	path IV (α_1, β_2)
1.	0.0	0.2	CP	-	LD	-
2.	0.0	0.4	CP	-	LD	-
3.	0.0	0.6	CP	-	LD	-
4.	0.0	0.9	CP	-	LD	-
5.	0.1	0.05	HD	CP	HD	CP
6.	0.1	0.1	HD	CP	HD	CP
7.	0.1	0.2	HD-HD	CP	HD	CP
8.	0.1	0.4	CP	CP	CP	CP
9.	0.1	0.5	CP	LD-LD	LD	CP
10.	0.1	0.9	CP	LD-LD	LD	CP
11.	0.5	0.1	HD	HD	HD	HD
12.	0.5	0.2	HD	HD	HD	HD
13.	0.5	0.5	HD-HD	HD-MC	HD-MC	HD-HD
14.	0.5	0.9	HD-MC	HD-HD	HD-HD	HD-MC
15.	0.9	0.1	HD	HD	HD	HD
16.	0.9	0.2	HD	HD	HD	HD
17.	0.9	0.5	HD-HD	HD-MC	HD-MC	HD-HD
18.	0.9	0.9	HD-HD	HD-MC	HD-MC	HD-HD

Another case of the TASEP with a junction is given in Figure 3.15. Here the boundary hopping rates are specified as $\alpha_2 = \beta_2 = 0.5$ and $\alpha_1 = 0.1$; $\beta_1 = 0.2$ for paths I and

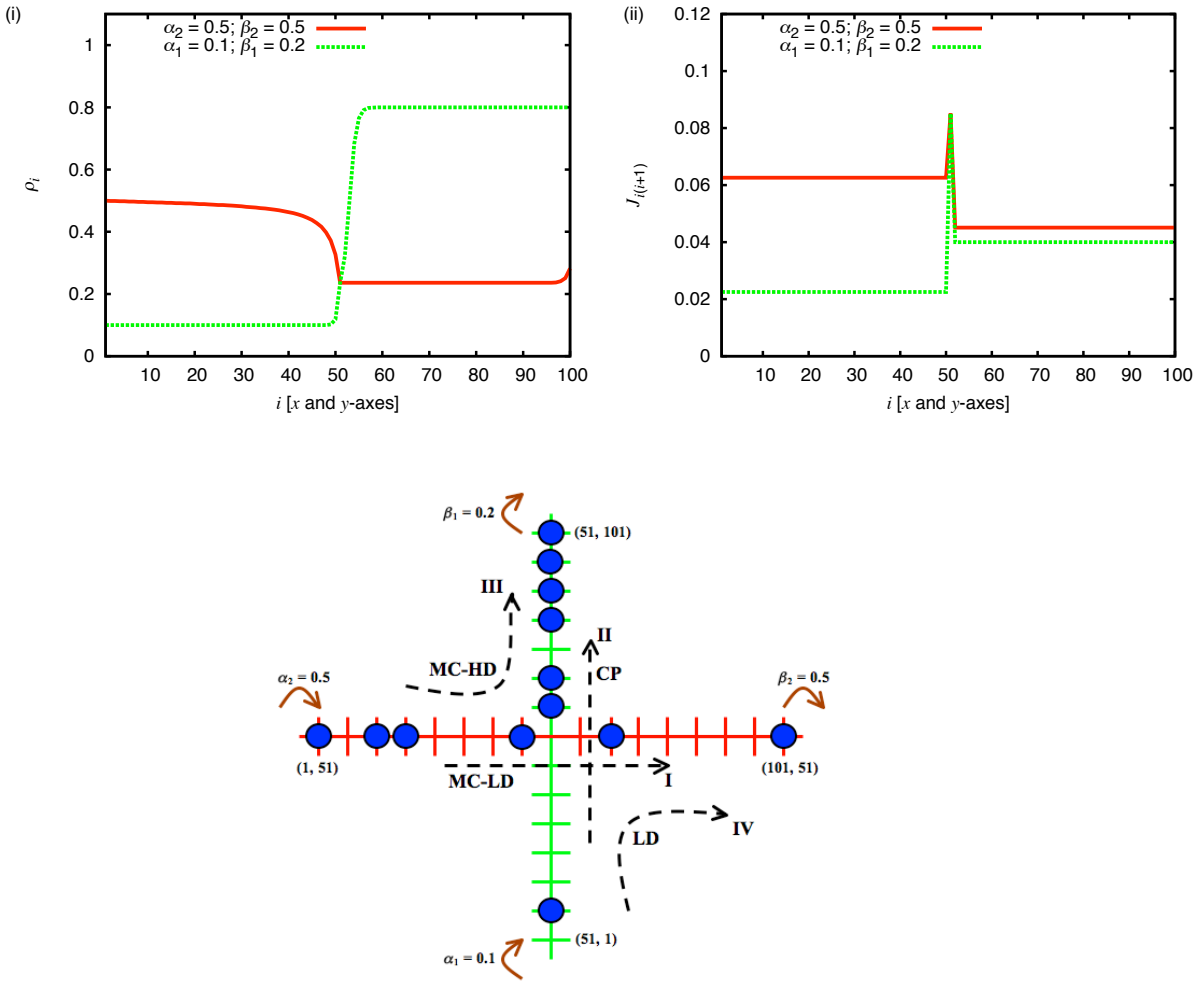

(iii)

Figure 3.15: The one-body and current density distributions of the TASEP with a junction where $\alpha_1 = 0.1$; $\beta_2 = 0.2$, and $\alpha_2 = \beta_2 = 0.5$. The one-body and current density profiles are given in Fig. 3.15(i) and (ii), respectively. The steady state phases of the one-body density on each path is illustrated in Fig. 3.15(iii). Path I ends up in a coexistence between a maximal current and a low density phases (MC-LD), path II returns a coexistence phase (CP), path III gives a coexistence between maximal current and high density phases (MC-HD), and finally path IV ends up in a low density phase (LD).

II, respectively. The one-body and current densities are given in Figure 3.15(i) and (ii), respectively. For a TASEP in 1D with $\alpha = \beta = 0.5$, the one-body density profile are flat everywhere with a value of 0.5. However adding path II causes a change in the one-body density profile of path I. Along the first half of the lattice sites, the profile stays flat with a value of 0.5. Then near the junction the profile decreases, and maintained in a low density regime until the end of the sites. Thus, adding path II has an effect in lowering the one-body density profile of path I from the junction until the end of the sites. But one may also look at path II which should be a low density phase given the input and output hopping rates. However, in present of path I it becomes a coexistence phase where a low density of 0.1 coexist with a high density regime of 0.8. Furthermore, a 1D TASEP with $\alpha = 0.5$ and $\beta = 0.2$ should produce a high density phase. However, path III shows a coexistence between a maximal current phase of 0.5 and a flat high density phase of 0.8. Finally, a 1D TASEP with $\alpha = 0.1$ and $\beta = 0.5$ should produce a flat profile with a low value of the one-body density. Path IV produces also a low density regime, however there is a jump occurring at the junction.

Furthermore, the current density profile of path I shows a decrease of values from (just) above 0.06 (at the entrance to the junction) to a value just above 0.04 [from the junction to the exit sites]. For path II, the current density is flat with a value of just above 0.02 (from the entrance until the junction), and then increases at the remaining sites to a value of 0.04.

This case is varied by setting $\alpha_1 = 0.0$. The resulting one-body and current density profiles at steady state are shown in Figure 3.16(i) and (ii), respectively. For path V with $\alpha_2 = \beta_2 = 0.5$, instead of a flat profile of 0.5 throughout the sites, a profile similar to path I in Figure 3.16(i) is obtained, where the profile is flat with values nearly 0.5, but then collapses to a flat low density regime just below 0.3, and increases at the end of the lattice sites. A similar profile is obtained for path VI with $\alpha_2 = 0.5$ and $\beta_1 = 0.2$ but with a higher one-body density profile at the exit sites. Hence, considering path V, adding a junction at its mid point (path VI) causes a dip in the one-body profile, such that a coexistence between maximal current and low density phases (MC-LD) occurs. The current density profiles between the two paths are the same. There is a jump at the junction from a value of above 0.06 to a lower value of 0.03.

Finally, we provide a list of various phases of this case in Table 3.2. In this Table we set $\alpha_2 = \beta_2 = 0.5$ is set in Table 3.2. α_1 and β_1 are varied.

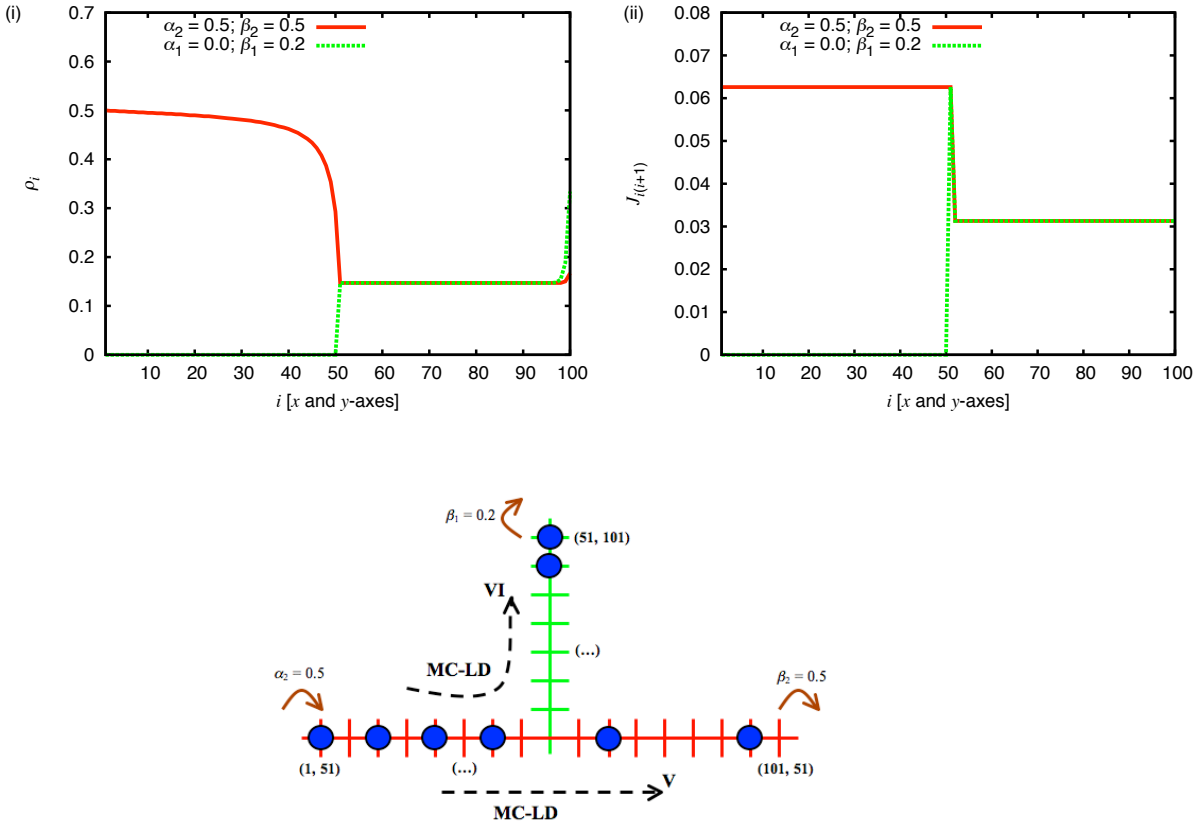

(iii)

Figure 3.16: Variation of the TASEP with a junction by setting $\alpha_1 = 0.0$; $\beta_1 = 0.2$ and $\alpha_2 = \beta_2 = 0.5$. The one-body and current density profiles are given in Fig. 3.16(i) and (ii), respectively. Paths V and VI give the same phase of the one-body density profile in steady state, i.e.: a coexistence between maximal current and low density phases (MC-LD).

Table 3.2: Various Phases of the TASEP with a junction where $\alpha_2 = \beta_2 = 0.5$. Note that paths II and III are labeled as V and VI for cases where $\alpha_1 = 0.0$. LD, HD, MC, and CP are abbreviations for low density, high density, maximal current, and coexistence phases.

No.	α_1	β_1	path I (V) $[\alpha_2, \beta_2]$	path II (α_1, β_1)	path III (VI) $[\alpha_2, \beta_1]$	path IV (α_1, β_2)
1.	0.0	0.2	MC-LD	-	MC-LD	-
2.	0.0	0.4	MC-LD	-	MC-LD	-
3.	0.0	0.6	MC-LD	-	MC-LD	-
4.	0.0	0.9	MC-LD	-	MC-LD	-
5.	0.1	0.05	HD-MC	CP	HD-HD	LD-MC
6.	0.1	0.1	MC (0.5)	CP	MC-HD	LD-MC
7.	0.1	0.2	MC-LD	CP	MC-HD	LD-LD
8.	0.1	0.4	MC-LD	LD-LD	MC-LD	LD-LD
9.	0.1	0.5	MC-LD	LD-LD	MC-LD	LD-LD
10.	0.1	0.9	MC-LD	LD-LD	MC-LD	LD-LD
11.	0.5	0.2	HD-MC	HD-HD	HD-HD	HD-MC
12.	0.5	0.4	HD-MC	HD	HD	HD-MC
13.	0.5	0.9	MC (0.5)	MC	MC (0.5)	MC
14.	0.9	0.1	HD-MC	HD-HD	HD-HD	HD-MC
15.	0.9	0.2	HD-MC	HD-HD	HD-HD	HD-MC
16.	0.9	0.5	HD-MC	HD-MC	HD-MC	HD-HD

To conclude, it may be observed from Tables 3.1 and 3.2 that rich phases are produced from this model. It is reiterated here that these Tables are not yet a full representation of the phase diagram of the TASEP with a junction. However, the point here is that adding an additional TASEP (in 1D) to another 1D TASEP at their center such that it creates a junction modifies the one-body and current density profiles of each 1D TASEP. Another interesting result is the existence of various coexistence phases other than the LD-HD coexistence appearing in the single TASEP in 1D, e.g.: MC-LD, HD-MC, LD-LD, and HD-HD, for the appropriate values of the boundary rates. We would also like to point out that the above results show the flexibility of the method given in [45] in providing insights to variants of the TASEP, especially the TASEP in higher dimensions.

Chapter 4

Correspondence Between the TASEP and Continuous Hard Rod Model

In this chapter a correspondence between the TASEP and the continuous hard rod model is investigated. Our focus is on the case of open boundaries with constant input and output hopping rates. We start with a single site and proceed to the TASEP with many (N) sites, both restricted to the steady state condition. We especially discuss the continuous hard rod model in the bulk. The motivation behind the correspondence is that one may use the knowledge of the hard rod model to obtain properties of the TASEP, viz. the average occupancy (one-body density), ρ, and the current density, J, at steady state.

4.1 The TASEP with a single site

Trajectories in continuous time

The TASEP with a single site has been discussed in Section 3.1. However it is useful to recall some of the information which is relevant to the present Section. The main difference between Section 3.1 and the present Section is instead of studying the time evolution of the system through the master equation, one look at the trajectory of particles at site $N = 1$. The specification of the TASEP remains, that is a particle may enter the site with input hopping rate α, so long as no other particle occupies the site. If

a particle occupies the site, it may exit the site with output hopping rate β. The system evolves in time, which is assumed to be continuous. Hence, the trajectory of this simple model may be given as follows:

1) A particle enters the lattice site with rate α.

2) The particle stays in the site for a lifetime γ such that no other particle can sit on the site.

3) After a lifetime γ the particle exits the site with rate β.

4) Then the process can repeat.

The above procedure is depicted in Figure 4.1. Furthermore, one defines $P(\gamma)\mathrm{d}\gamma$ as the probability distribution of a particle to occupy the site with lifetime $\mathrm{d}\gamma$. Thus, the differential equation for $P(\gamma)$ is written as

$$\mathrm{d}P(\gamma) \sim -P\beta\mathrm{d}\gamma,$$

such that,

$$P(\gamma) \sim \exp\left(-\beta\gamma\right). \tag{4.1.1}$$

Thus, the one-body density (average occupation) of the particle as a function of the lifetime γ is given by

$$\rho(\gamma) = \mathcal{R}P(\gamma) = \mathcal{R}\exp(-\beta\gamma), \tag{4.1.2}$$

where $\mathcal{R}$ is a normalization constant to be determined.

The continuous hard rod model

The ingredients of the hard rod model are already given in equations (2.4.5)-(2.4.8) in Subsection 2.4.1. Here, the focus is on the bulk case, where $\rho(\sigma, x) = \rho(\sigma)$ and σ is the size of the rods. Therefore, inserting $\rho(\sigma)$ into equation (2.4.6) gives

$$\begin{aligned} n_0 &= \int_0^\infty \sigma\rho(\sigma)\left\{\frac{1}{2}\int\delta\left(x-\frac{\sigma}{2}\right)\mathrm{d}x + \frac{1}{2}\int\sigma\left(x+\frac{\sigma}{2}\right)\mathrm{d}x\right\} \\ &= \int_0^\infty \rho(\sigma)\mathrm{d}\sigma, \end{aligned} \tag{4.1.3}$$

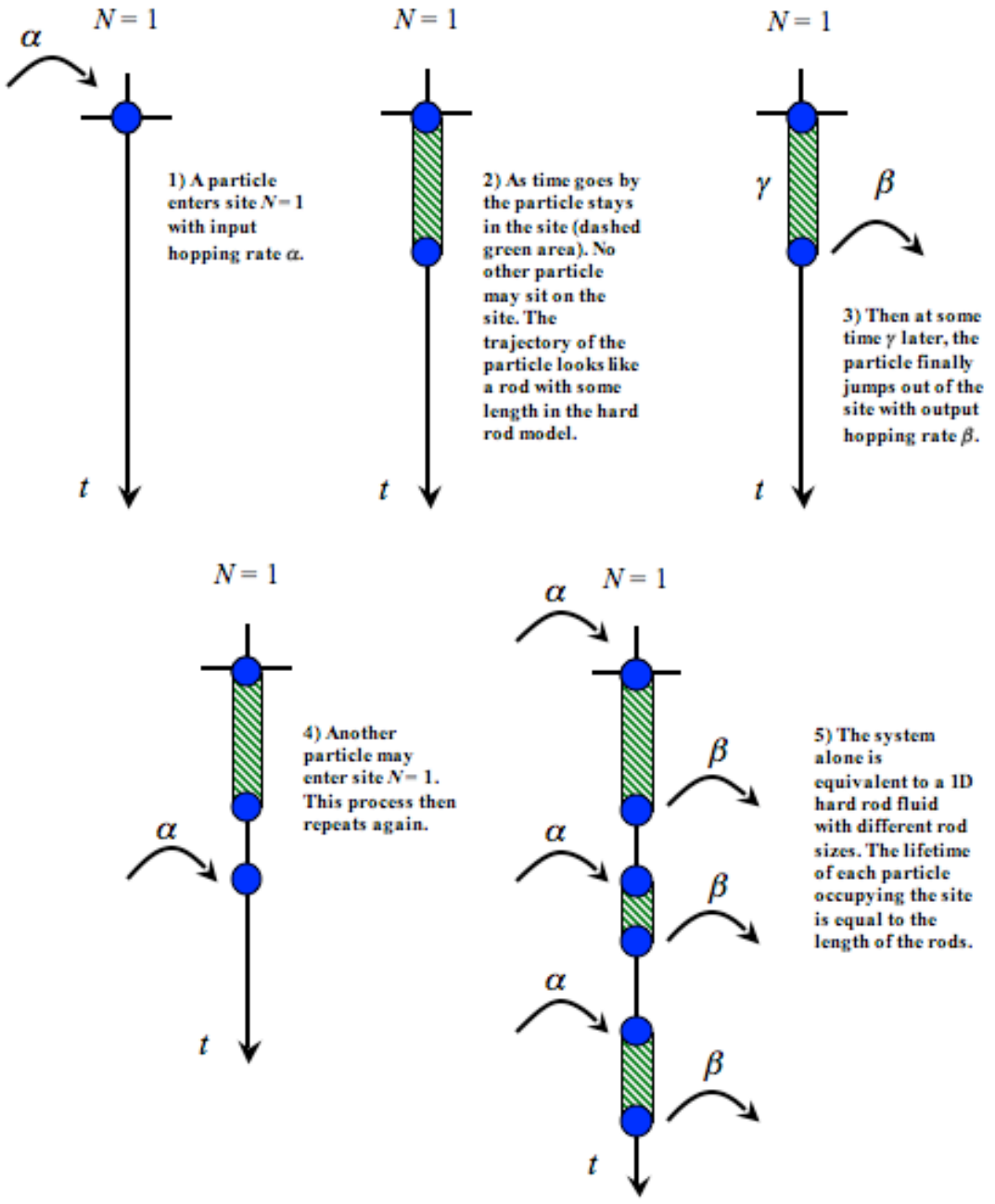

Figure 4.1: A sketch of the trajectories of the TASEP with open boundaries that consists of only a single site. The lattice site, $N = 1$, is depicted by a dark (cross) thick mark. The filled (blue) circles occupying the site is the hard core particle. The vertical axis is the time parameter, t. A particle may enter the site with a constant input rate α [black arrow at the left of the site] if there is no particle at the site. The particle occupies the site with a lifetime of γ represented by the dashed (green) area. The particle may exit the site with an output rate β [dark arrow at the right of the site].

and

$$\begin{aligned} n_1 &= \int_0^\infty \rho(\sigma)\mathrm{d}\sigma \int_{-\infty}^{\infty} \Theta\left(|x| - \frac{\sigma}{2}\right) \mathrm{d}x \\ &= \int_0^\infty \rho(\sigma)\mathrm{d}\sigma \left\{ \int_{-\infty}^{0} \Theta\left(-x - \frac{\sigma}{2}\right) \mathrm{d}x + \int_0^\infty \Theta\left(x - \frac{\sigma}{2}\right) \mathrm{d}x \right\} \\ &= \int_0^\infty \sigma\rho(\sigma)\mathrm{d}\sigma, \end{aligned} \tag{4.1.4}$$

where n_0 and n_1 are the total density and total packing fraction of the system, respectively. In the bulk, where $n_0(x) = n_0$ and $n_1(x) = n_1$ [according to equations (4.1.3) and (4.1.4)], the excess free energy functional of the hard rod model with total length L becomes

$$\begin{aligned} \mathcal{F}_{\mathrm{exc}}[\rho] &= k_{\mathrm{B}}\mathcal{T} \int_{-\frac{L}{2}}^{+\frac{L}{2}} \mathrm{d}x \left[-n_0 \ln(1 - n_1)\right] \\ &= -k_{\mathrm{B}}\mathcal{T}L \left[n_0 \ln(1 - n_1)\right], \end{aligned}$$

or

$$\Upsilon \equiv \frac{\mathcal{F}_{\mathrm{exc}}[\rho]}{k_{\mathrm{B}}\mathcal{T}L} = -n_0 \ln\left(1 - n_1\right). \tag{4.1.5}$$

Another important quantity is the equation of state. In order to calculate the total pressure of the system one needs to determine the excess chemical potential, μ_{exc}. This is obtained via (functional) derivative of Υ w.r.t. $\rho(\sigma)$, i.e.:

$$\begin{aligned} \mu_{\mathrm{exc}}(\sigma') &= \frac{\delta\Upsilon}{\delta\rho(\sigma')} = \frac{\delta}{\delta\rho(\sigma')} \left\{ \left(- \int_0^\infty \rho(\sigma)\mathrm{d}\sigma \right) \ln\left(1 - \int_0^\infty \sigma\rho(\sigma)\mathrm{d}\sigma\right) \right\} \\ &= \left(- \int_0^\infty \frac{\delta\rho(\sigma)}{\delta\rho(\sigma')}\mathrm{d}\sigma \right) \ln\left(1 - \int_0^\infty \sigma\rho(\sigma)\mathrm{d}\sigma\right) + \frac{\int_0^\infty \rho(\sigma)\mathrm{d}\sigma}{\left(1 - \int_0^\infty \sigma\rho(\sigma)\mathrm{d}\sigma\right)} \int_0^\infty \sigma \frac{\delta\rho(\sigma)}{\delta\rho(\sigma')}\mathrm{d}\sigma \\ &= \left(- \int_0^\infty \delta(\sigma - \sigma')\mathrm{d}\sigma \right) \ln\left(1 - \int_0^\infty \sigma\rho(\sigma)\mathrm{d}\sigma\right) + \frac{\left(\int_0^\infty \sigma\delta(\sigma - \sigma')\mathrm{d}\sigma\right) \int_0^\infty \rho(\sigma)\mathrm{d}\sigma}{\left(1 - \int_0^\infty \sigma\rho(\sigma)\mathrm{d}\sigma\right)} \\ &= -\ln\left(1 - \int_0^\infty \sigma\rho(\sigma)\mathrm{d}\sigma\right) + \frac{\sigma' \int_0^\infty \rho(\sigma)\mathrm{d}\sigma}{\left(1 - \int_0^\infty \sigma\rho(\sigma)\mathrm{d}\sigma\right)}, \end{aligned} \tag{4.1.6}$$

or using again equations (4.1.3) and (4.1.4), and dropping the prime signs yields

$$\mu_{\mathrm{exc}}(\sigma) = -\ln\left(1 - n_1\right) + \frac{\sigma n_0}{1 - n_1}. \tag{4.1.7}$$

The excess part of the pressure is then given by,

$$\begin{aligned} -\frac{\mathcal{P}_{\rm exc}}{k_{\rm B}\mathcal{T}} &= \Upsilon - \int_0^\infty {\rm d}\sigma \mu_{\rm exc}(\sigma)\rho(\sigma) \\ &= -n_0 \ln(1-n_1) - \left\{ \int_0^\infty {\rm d}\sigma \rho(\sigma) \left[-\ln(1-n_1) + \frac{\sigma n_0}{1-n_1} \right] \right\} \\ &= -n_0(1-n_1) - \left\{ -n_0 \ln(1-n_1) + \frac{n_0 n_1}{1-n_1} \right\} \\ &= -\frac{n_0 n_1}{1-n_1}. \end{aligned} \tag{4.1.8}$$

Finally, the total pressure may be determined as

$$\mathcal{P}_{\rm tot} = k_{\rm B}\mathcal{T} \left\{ \int_0^\infty {\rm d}\sigma \rho(\sigma) + P_{\rm exc} \right\} = n_0 + \frac{n_0 n_1}{1-n_1}, \tag{4.1.9}$$

or

$$\frac{\mathcal{P}_{\rm tot}}{k_{\rm B}\mathcal{T}} = \frac{n_0}{1-n_1}. \tag{4.1.10}$$

The correspondence

We have explained the two (different) models relevant to the present discussion. Next, a relationship between them is proposed. This is done by identifying the quantities in the TASEP with one site and quantities of the hard rod model, i.e.:

1) The trajectory of the single site TASEP is equivalent to the hard rod fluids such that the lifetime of a particle on the site, γ, may be identified as the length of the rod, σ, or

$$\gamma \leftrightarrow \sigma. \tag{4.1.11}$$

2) The output rate of the TASEP, β, which is the number of ejection events per unit time of the site being occupied corresponds to the number of particles per volume occupied by the particle, viz.:

$$\beta = \frac{\text{number of ejection events}}{\text{time of the site being occupied}} \leftrightarrow \frac{\text{number of particles}}{\text{the volume that the particles occupy}}. \tag{4.1.12}$$

3) The input rate of the TASEP, α, corresponds to the gap size between the rods. In the equilibrium model, increasing the gap between rods means working against the pressure ($\mathcal{P}_{\rm tot}$) of the fluids. Thus, one can identify α to $\mathcal{P}_{\rm tot}$, i.e.:

$$\alpha \leftrightarrow \frac{\mathcal{P}_{\rm tot}}{k_{\rm B}\mathcal{T}}. \tag{4.1.13}$$

Utilizing the identifications above, we determine the one-body and current densities of the TASEP with a single site using the equations for hard rod model. This is done by replacing σ by γ in equations (4.1.3) and (4.1.4), yielding,

$$n_0 = \int_0^\infty \mathrm{d}\gamma\rho(\gamma), \qquad n_1 = \int_0^\infty \gamma\rho(\gamma)\mathrm{d}\gamma. \tag{4.1.14}$$

Inserting equation (4.1.2) into equation (4.1.14) gives

$$n_0 = \int_0^\infty \mathrm{d}\gamma\mathcal{R}e^{-\beta\gamma} = \frac{\mathcal{R}}{\beta} \Rightarrow \mathcal{R} = n_0\beta, \tag{4.1.15}$$

and

$$n_1 = \int_0^\infty \gamma\mathcal{R}e^{-\beta\gamma}\mathrm{d}\gamma = -\mathcal{R}\int_0^\infty \frac{\partial}{\partial\beta}e^{-\beta\gamma}\mathrm{d}\gamma = \mathcal{R}\beta^{-2}. \tag{4.1.16}$$

Hence, inserting equation (4.1.15) into (4.1.16) yields

$$n_1\beta = n_0. \tag{4.1.17}$$

Moreover, inserting the correspondence (4.1.13) into equation (4.1.10) gives

$$\alpha = \frac{n_0}{1-n_1}. \tag{4.1.18}$$

Combining (4.1.17) and (4.1.18) by eliminating n_0 leads to

$$n_1 = \frac{\alpha}{\alpha+\beta} \equiv \rho,$$

which is equivalent to equation (3.1.24). Also, inserting the above equation into (4.1.17) and solving for n_0 yields

$$n_0 = \frac{\alpha\beta}{(\alpha+\beta)} \equiv J,$$

which agrees with equation (3.1.25). Hence, one finds that the average occupancy of the single site, ρ, corresponds to the packing fraction of the hard rod model, i.e.

$$\rho \leftrightarrow n_1, \tag{4.1.19}$$

whereas the current density through the site, J, corresponds to the total density of the hard rod model, or

$$J \leftrightarrow n_0 \tag{4.1.20}$$

Equations (4.1.19) and (4.1.20) are indeed consistent with physical intuition. Recall from above that n_0 and n_1 are the total density and total packing fraction of the system, respectively. n_1 is the ratio between the total volume of particles and the volume that is

available for the particles. This quantity is indeed (intuitively) associated to the average time that the site is occupied, i.e. ρ. Furthermore, the current density, J, according to Fig 4.1 is actually the average number of 'passing' events (with lifetime γ), i.e.: the average number of particles moving through the site. This is physically associated to n_0.

4.2 TASEP consisting of N sites

This correspondence is extended to the TASEP with N sites in steady state. Instead of just a single trajectory of particles occupying a site, each site of the N sites system has its own particle trajectories.

A schematic illustration is given in Figure 4.2. It may be observed that the trajectory of a particle is spanned from one site to its right adjacent site and connected by the arrowed dashed lines. Because of the hard core interactions, the trajectory of two or more particles may not overlap. These dashed lines also represent the correlations between sites. Here, we focus on the bulk sites, viz.: sites $i-1$, i, and $i+1$. Recall the hopping rates from site $i-1$ to site i and from site i to $i+1$ as $k_{(i-1)i}$ and $k_{i(i+1)}$, respectively.

Here a mean-field approximation is assumed where the correlations, i.e. the (arrowed) dashed lines are neglected such that each site becomes uncorrelated 1D 'time rods'. Similar to the first case above $P(i,\gamma)\mathrm{d}\gamma$ is defined as the probability of a particle to be at site i with a lifetime $\mathrm{d}\gamma$ where its differential form may be written as

$$\mathrm{d}P(i,\gamma) \sim -Pk_{i(i+1)}\left[1-n_1(i+1)\right]\mathrm{d}\gamma, \tag{4.2.1}$$

or

$$\frac{\mathrm{d}P(i,\gamma)}{P} \sim -k_{i(i+1)}\left[1-n_1(i+1)\right]\mathrm{d}\gamma. \tag{4.2.2}$$

Solving equation (4.2.2) gives,

$$P(i,\gamma) \sim e^{-k_{i(i+1)}[1-n_1(i+1)]\gamma}. \tag{4.2.3}$$

The exponential factor of $k_{i(i+1)}\left[1-n_1(i+1)\right]$ in relation (4.2.3) represents the inverse time scale of particles to hop from site i to $i+1$. Hence, the one-body density of particles at site i with lifetime γ is proportional to $P(i,\gamma)$ such that

$$\rho(i,\gamma) = \mathcal{R}P(i,\gamma) = \mathcal{R}e^{-k_{i(i+1)}[1-n_1(i+1)]\gamma}. \tag{4.2.4}$$

As a consequence of the mean-field approximation, the particle trajectories at each site may be treated as separate hard rod models. Hence, equations (4.1.3) and (4.1.4)

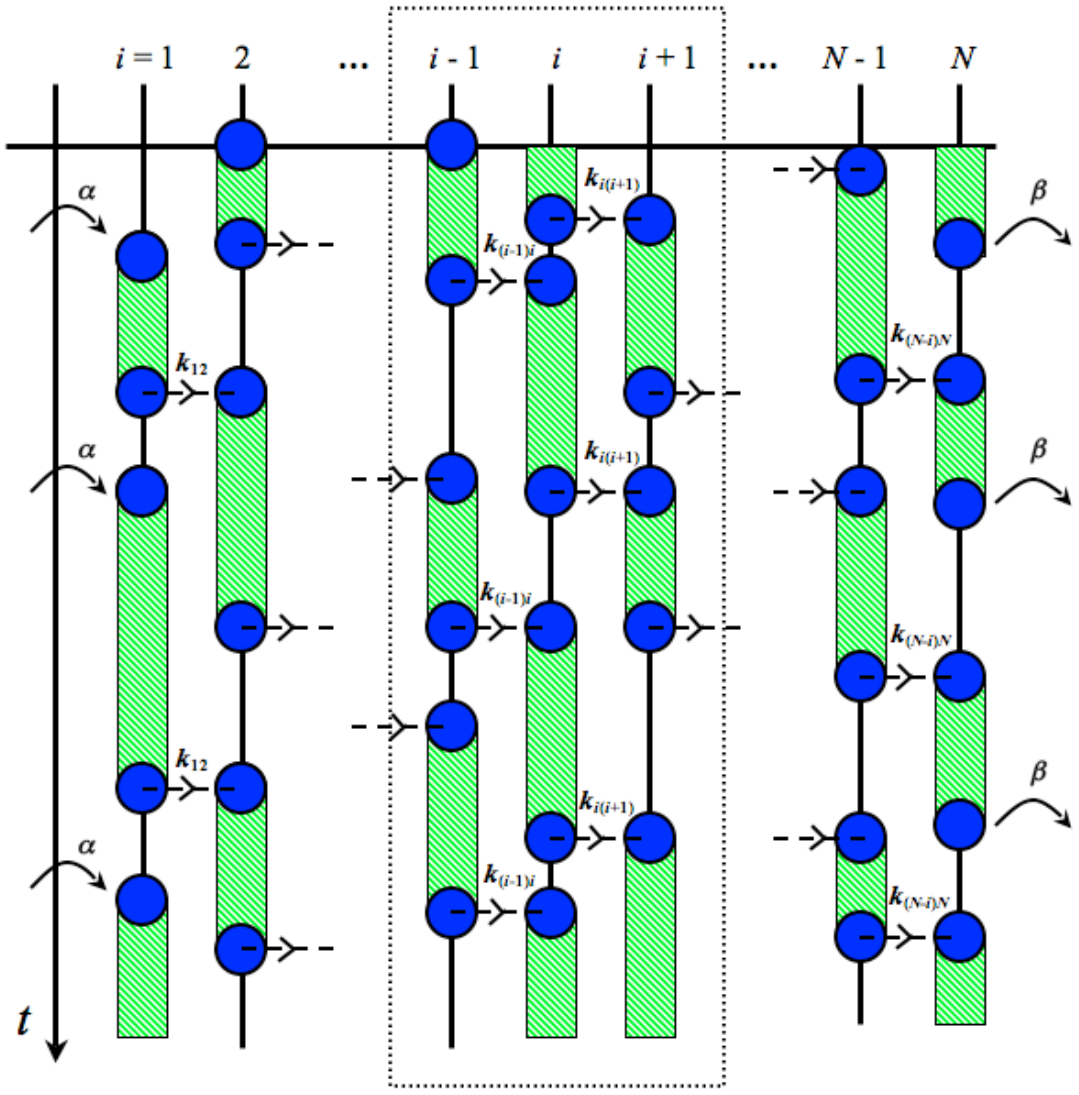

Figure 4.2: A sketch of particle trajectories of the TASEP with open boundaries and consists of N sites. The lattice sites are depicted by solid vertical marks on the horizontal axis, and labeled as $i = 1, 2, 3, \ldots, i-1, i, i+1, \ldots, N-1, N$. The vertical axis indicates the time parameter t. The filled blue circles represent the hard core particles. A particle may enter site $i = 1$ with a constant hopping rate α [black arrow to the left of the site] if there is no particle at the site. The particle occupies the site with a lifetime of γ (dashed [green]) area. Then it may jump to its right nearest neighbour with hopping rate $k_{i(i+1)}$. If there is a particle at site $N-1$, then the particle may hop out of the lattice sites with rate β.

may still be applied but now by inserting equation (4.2.4), giving

$$n_0(i) = \int_0^\infty \mathrm{d}\gamma \mathcal{R} e^{-k_{i(i+1)}[1-n_1(i+1)]\gamma} = \frac{\mathcal{R}}{k_{i(i+1)}\left[1-n_1(i+1)\right]}, \tag{4.2.5}$$

and

$$n_1(i) = \int_0^\infty \gamma \mathcal{R} e^{-k_{i(i+1)}[1-n_1(i+1)]\gamma} = \frac{\mathcal{R}}{k_{i(i+1)}^2\left[1-n_1(i+1)\right]^2}. \tag{4.2.6}$$

Combining equations (4.2.5) and (4.2.6) gives,

$$n_0(i) = k_{i(i+1)} n_1(i)\left[1-n_1(i+1)\right]. \tag{4.2.7}$$

On the other hand, one may also determine a correspondence amidst the gap size between the time rods and the pressure of the hard rod fluids. The gap size of the time rods at site i is related to the quantity $k_{(i-1)i}n_1(i-1)$. By exploiting correspondence (4.1.13), the aforementioned quantity corresponds to the pressure of the hard rod fluids, such that

$$\frac{\mathcal{P}(i)}{k_\mathrm{B}\mathcal{T}} \leftrightarrow k_{(i-1)i}n_1(i-1). \tag{4.2.8}$$

Using further equation (4.1.10), the total pressure of the hard rod fluids at site i is stated as

$$\frac{\mathcal{P}(i)}{k_\mathrm{B}\mathcal{T}} = \frac{n_0(i)}{1-n_1(i)}. \tag{4.2.9}$$

Thus combining equation (4.2.9) and correspondence (4.2.8) yields

$$\frac{n_0(i)}{1-n_1(i)} = k_{(i-1)i}n_1(i-1), \tag{4.2.10}$$

or

$$n_0(i) = k_{(i-1)i}n_1(i-1)\left[1-n_1(i)\right]. \tag{4.2.11}$$

As the LHS of equations (4.2.7) and (4.2.11) are equal to $n_0(i)$, equation (4.2.11) can be inserted into (4.2.7) giving,

$$k_{i(i+1)}n_1(i)\left[1-n_1(i+1)\right] = k_{(i-1)i}n_1(i-1)\left[1-n_1(i)\right]. \tag{4.2.12}$$

And finally, using correspondence (4.1.19) and (4.1.20), gives

$$k_{i(i+1)}\rho_i\left[1-\rho_{i+1}\right] = k_{(i-1)i}\rho_{(i-1)}\left[1-\rho_i\right] = J,$$

which is equivalent to equation (2.2.16), the current density formula for the mean-field TASEP with open boundaries at steady state.

To summarize, this Section proposes an alternative correspondence between the TASEP and the continuous hard rod model. First, an exact correspondence is obtained between the particle trajectories of the TASEP with a single site and the continuous hard rod model. This correspondence is then extended beyond the single site, i.e. TASEP with N sites, within the mean-field approximation where each site of the TASEP is considered as independent 'time rod'. The exact relationship for the latter case is not yet obtained.

Chapter 5

Current Density Functional for the TASEP

The aim of this Chapter is to construct current density functionals for the TASEP. First the exact current density functional of the TASEP with a single site is constructed. Then we proceed constructing the mean field current density functional for N sites.

5.1 The TASEP with a Single Site

The objective here is to find an exact expression of the current density functional for one site, $\mathcal{M}[\tilde{J}_{\text{in}}(t), \tilde{J}_{\text{out}}(t)]$. In order to do so, recall the (exact) equation of motions for this simple model in equations (3.1.16) and (3.1.17), viz.:

$$J_{\text{in}}(t) = \alpha(t)\left[1 - \rho_1(t)\right],$$

and

$$J_{\text{out}}(t) = \beta(t)\rho_1(t),$$

where $J_{\text{in}}(t)$ and $J_{\text{out}}(t)$ are the true current densities going into and going out of site 1, respectively. $\alpha(t)$ and $\beta(t)$ are the time-dependent input and output rates, respectively. $\rho_1(t)$ is the true time-dependent one-body density at the site. The one-body density is treated as an independent variable. An additional constraint is given to determine $\rho_1(t)$, which is in this case the continuity equation (3.1.15), i.e.:

$$\frac{\partial \rho_1(t)}{\partial t} = J_{\text{in}}(t) - J_{\text{out}}(t).$$

Furthermore, by taking the logarithm on both sides of equations (3.1.16) and (3.1.17), yields

$$\ln J_{\text{in}}(t) = \ln \alpha(t) + \ln\left[1 - \rho_1(t)\right] \Rightarrow 0 = \ln J_{\text{in}} - \ln \alpha(t) - \ln\left[1 - \rho_1(t)\right], \tag{5.1.1}$$

and

$$\ln J_{\text{out}}(t) = \ln \beta(t) + \ln \rho_1(t) \Rightarrow 0 = \ln J_{\text{out}} - \ln \beta(t) - \ln \rho_1(t). \tag{5.1.2}$$

Now assume that equations (5.1.1) and (5.1.2) are the Euler-Lagrange equations obtained by minimizing a functional that is yet to be determined. According to classical DFT (Section 2.3), the free energy functional may be split into two terms, that is the ideal and excess parts. Here a similar convention is followed. Based upon the Euler-Lagrange equations (5.1.1) and (5.1.2), consider the first term of each equation to be derived from the 'ideal' part of the functional. Thus, this part of the functional is defined as

$$T_{\text{id}}[\tilde{J}_{\text{in}}, \tilde{J}_{\text{out}}] = \int_0^\infty \mathrm{d}t \left\{ \tilde{J}_{\text{in}}(t) \left[\ln(\tilde{J}_{\text{in}}(t)) - 1\right] + \tilde{J}_{\text{out}}(t) \left[\ln(\tilde{J}_{\text{out}}(t)) - 1\right] \right\}, \tag{5.1.3}$$

where $\tilde{J}_{\text{in}}$ and $\tilde{J}_{\text{out}}$ are trial current densities coming into and out of site $N = 1$. On the other hand, consider the two last terms in equations (5.1.1) and (5.1.2) as resulting from functional derivatives of the excess part of the functional. Thus this part is constructed as

$$T_{\text{exc}}[\tilde{J}_{\text{in}}, \tilde{J}_{\text{out}}] = -\int_0^\infty \mathrm{d}t \left[\tilde{J}_{\text{in}}(t) \ln\left[1 - \rho_1(t)\right] + \tilde{J}_{\text{out}}(t) \ln\left[\rho_1(t)\right] \right]. \tag{5.1.4}$$

Combining functionals (5.1.3) and (5.1.4), a full functional of the TASEP with one site is proposed as

$$\begin{aligned} \mathcal{M}\left[\tilde{J}_{\text{in}}, \tilde{J}_{\text{out}}\right] &= T_{\text{id}}[\tilde{J}_{\text{in}}, \tilde{J}_{\text{out}}] + T_{\text{exc}}[\tilde{J}_{\text{in}}, \tilde{J}_{\text{out}}] \\ &\quad + \int_0^\infty \mathrm{d}t \tilde{J}_{\text{in}}(t) A(t) + \int_0^\infty \mathrm{d}t \tilde{J}_{\text{out}}(t) B(t), \end{aligned} \tag{5.1.5}$$

where $A(t)$ and $B(t)$ are Lagrange multipliers that couple to $\tilde{J}_{\text{in}}(t)$ and $\tilde{J}_{\text{out}}(t)$, respectively. The task now is to determine $A(t)$ and $B(t)$ such that equations (5.1.1) and (5.1.2) are satisfied (upon minimization of (5.1.5)). In this case a variational principle is postulated such that at the true solutions of $J_{\text{in}}(t)$ and $J_{\text{out}}(t)$ one requires

$$\left.\frac{\delta \mathcal{M}}{\delta \tilde{J}_{\text{in}}(t)}\right|_{\tilde{J}_{\text{in}}(t), \rho_1(t)} = 0, \qquad \text{and} \qquad \left.\frac{\delta \mathcal{M}}{\delta \tilde{J}_{\text{out}}(t)}\right|_{\tilde{J}_{\text{out}}(t), \rho_1(t)} = 0. \tag{5.1.6}$$

Thus, carrying out the functional derivative of (5.1.5) with respect to $\tilde{J}_{\rm in}(t)$ and applying the first equation of (5.1.6) gives,

$$\begin{aligned}\frac{\delta\mathcal{M}}{\delta\tilde{J}_{\rm in}(t)} &= \ln J_{\rm in}(t) - \ln\left(1-\rho_1(t)\right) + A(t) = 0 \\ &\Rightarrow \quad A(t) = -\ln\left(\frac{J_{\rm in}(t)}{1-\rho_1(t)}\right). \end{aligned} \tag{5.1.7}$$

Inserting equation (5.1.1) into (5.1.7) gives the Lagrange multiplier for $J_{\rm in}(t)$ as

$$A(t) = -\ln\alpha(t). \tag{5.1.8}$$

Next, $B(t)$ is determined by differentiating (5.1.5) with respect to $\tilde{J}_{\rm out}(t)$ and using the second equation of (5.1.6) which gives,

$$\begin{aligned}\frac{\delta\mathcal{M}}{\delta\tilde{J}_{\rm out}(t)} &= \ln J_{\rm out}(t) - \ln\rho_1(t) + B(t) = 0 \\ &\Rightarrow \quad B(t) = -\ln\left(\frac{J_{\rm out}(t)}{\rho_1(t)}\right) = -\ln\beta(t), \end{aligned} \tag{5.1.9}$$

using equation (5.1.2).

Finally, inserting (5.1.8) and (5.1.9) into (5.1.5) yields the final functional of the TASEP with one site as

$$\begin{aligned}\mathcal{M}\left[\tilde{J}_{\rm in},\tilde{J}_{\rm out}\right] &= T_{\rm id}[\tilde{J}_{\rm in},\tilde{J}_{\rm out}] + T_{\rm exc}[\tilde{J}_{\rm in},\tilde{J}_{\rm out}] \\ &\quad - \int_0^\infty {\rm d}t\tilde{J}_{\rm in}(t)\ln\alpha(t) - \int_0^\infty {\rm d}t\tilde{J}_{\rm out}(t)\ln\beta(t). \end{aligned} \tag{5.1.10}$$

Supported by the continuity equation,

$$\rho_1(t) = \rho_1(0) + \int_0^t {\rm d}t'\left[J_{\rm in}(t') - J_{\rm out}(t')\right], \tag{5.1.11}$$

where $J_{\rm in}(t)$ and $J_{\rm out}(t)$ are the true solutions of the current densities, equation (5.1.10) gives the exact description of one site.

5.2 TASEP with N Sites

Now we seek to find the mean-field functional for the TASEP with N sites where the current density is again taken as the trial field of the functional. The calculation is similar to that above for one site. The mean-field equation of motion for N sites is given by equation (2.2.37), viz.:

$$J_{i(i+1)}(t) = k_{i(i+1)}(t)\rho_i(t)\left[1-\rho_{i+1}(t)\right],$$

where $J_{i(i+1)}(t)$ is the current from site i to site $i+1$ at time t, $k_{i(i+1)}(t)$ is the time-dependent hopping rate from site i to site $i+1$ at time t, and $\rho_i(t)$ is the density at site i at time t, for $i = 0, 1, 2, \ldots, N$. $\rho_i(t)$ is again considered as an independent variable and the true solution of the one-body density, constrained by the continuity equation (2.2.7),

$$\frac{\partial \rho_i(t)}{\partial t} = J_{(i-1)i}(t) - J_{i(i+1)}(t),$$

or

$$\rho_i(t) = \rho_i(0) + \int_0^t \mathrm{d}t \left[J_{(i-1)i}(t) - J_{i(i+1)}(t) \right]. \tag{5.2.1}$$

So now equation (2.2.37) is modified by applying the logarithm on both of its sides, such that

$$\ln J_{i(i+1)}(t) = \ln k_{i(i+1)}(t) + \ln \rho_i(t) \left[1 - \rho_{i+1}(t) \right], \tag{5.2.2}$$

which gives a set of Euler-Lagrange equations in the form of

$$\begin{aligned}
\ln J_{0(1)}(t) &= \ln k_{01}(t) + \ln \rho_0 \left[1 - \rho_1(t) \right], \\
\ln J_{12}(t) &= \ln k_{12}(t) + \ln \rho_1(t) \left[1 - \rho_2(t) \right], \\
\ln J_{23}(t) &= \ln k_{23}(t) + \ln \rho_2(t) \left[1 - \rho_3(t) \right], \\
&\ldots \\
\ln J_{N(N+1)}(t) &= k_{N(N+1)}(t) + \ln \rho_N \left[1 - \rho_{(N+1)} \right],
\end{aligned} \tag{5.2.3}$$

or

$$\begin{aligned}
\ln J_1(t) &= \ln \alpha(t) + \ln \left[1 - \rho_1(t) \right], \\
\ln J_{12}(t) &= \ln k_{12}(t) + \ln \rho_1(t) \left[1 - \rho_2(t) \right], \\
\ln J_{23}(t) &= \ln k_{23}(t) + \ln \rho_2(t) \left[1 - \rho_3(t) \right], \\
&\ldots \\
\ln J_N(t) &= \ln \beta(t) + \ln \rho_N,
\end{aligned} \tag{5.2.4}$$

where we set $\rho_0(t) = 1$, $\rho_{(N+1)}(t) = 0$, $k_{01}(t) = \alpha(t)$, and $k_{N(N+1)} = \beta(t)$.

Now the 'ideal' and 'excess' parts of the functional are constructed, which are given by

$$T_{\mathrm{id}}[\tilde{J}_{i(i+1)}] = \int_0^\infty \mathrm{d}t \sum_{i=0}^{N} \tilde{J}_{i(i+1)}(t) \left[\ln \left(\tilde{J}_{i(i+1)}(t) \right) - 1 \right], \tag{5.2.5}$$

and

$$T_{\mathrm{exc}}[\tilde{J}_{i(i+1)}] = \int_0^\infty \mathrm{d}t \sum_{i=0}^{N} \tilde{J}_{i(i+1)}(t) \left[\rho_i(t) - \rho_i(t) \rho_{i(i+1)}(t) \right], \tag{5.2.6}$$

respectively, where $\tilde{J}_{i(i+1)}(t)$ is the trial current density linking sites i to $i+1$ at time t. Introducing $\nu_i(t)$ as a Lagrange multiplier corresponding to $\tilde{J}_{i(i+1)}(t)$ yields the full mean-field functional as

$$\mathcal{M}[\tilde{J}_{i(i+1)}] = T_{\mathrm{id}}[\tilde{J}_{i(i+1)}] + T_{\mathrm{exc}}[\tilde{J}_{i(i+1)}] + \int_0^\infty \mathrm{d}t \sum_{i=0}^{N} \tilde{J}_{i(i+1)}(t)\nu_i(t). \tag{5.2.7}$$

The postulated variational principle requires that at the true solution, $J_{i(i+1)}(t)$,

$$\left.\frac{\delta\mathcal{M}}{\delta\tilde{J}_{i(i+1)}(t)}\right|_{\tilde{J}_{i(i+1)}(t),\rho_i(t)} = \ln J_{i(i+1)}(t) - \ln\big(\rho_i(t) - \rho_i(t)\rho_{(i+1)}(t)\big) + \nu_i(t) = 0, \tag{5.2.8}$$

or

$$\nu_i(t) = -\ln\left(\frac{J_{i(i+1)}(t)}{\rho_i(t) - \rho_i(t)\rho_{i+1}(t)}\right) = -\ln k_{i(i+1)}(t), \tag{5.2.9}$$

by invoking equation (2.2.37). Thus, inserting equation (5.2.9) into (5.2.7) gives the mean-field functional of the TASEP as

$$\mathcal{M}[\tilde{J}_{i(i+1)}] = T_{\mathrm{id}}[\tilde{J}_{i(i+1)}] + T_{\mathrm{exc}}[\tilde{J}_{i(i+1)}] - \int_0^\infty \mathrm{d}t \sum_{i=0}^{N} \tilde{J}_{i(i+1)}(t) \ln k_{i(i+1)}(t). \tag{5.2.10}$$

Equations (5.2.1) and (5.2.10) give the mean-field description for the TASEP with N sites.

Hence, to sum up the exact current density functional of the TASEP with one site has been derived, as well as the mean-field current density functional of the TASEP with N sites. These functionals are constructed based on the (macroscopic) equation of motions of the TASEP. The latter are assumed to be the Euler-Lagrange equations obtained by minimizing the functional being determined. For the N sites case, as a consequence of the mean-field equation of motion, the functional is also of the mean field type.

Chapter 6

An Argument for the Foundation of the Current Density Functional

Here an argument for the foundation of the current density functional is given starting from the master equation. First, we lay out the mathematical tools needed for the argument, and then apply this to the cases of non-equilibrium and of equilibrium systems.

6.1 The basic mathematical tools

Recall the master equation (2.1.1) as the starting point for the dynamics:

$$\frac{\partial P_n(t)}{\partial t} = \sum_{n'} \left[w_{nn'}(t) P_{n'}(t) - w_{n'n}(t) P_n(t) \right],$$

A formal solution of (2.1.1) is obtained by rearranging (2.1.1) and integrating such that

$$P_n(t) = P_n(0) + \int_0^t \mathrm{d}t' \sum_{n'} \left[j_{nn'}(t') - j_{n'n}(t') \right], \tag{6.1.1}$$

where we have introduced

$$j_{n'n}(t) = w_{n'n}(t) P_n(t), \tag{6.1.2}$$

as the *configurational current* of a transition from state n to state n' at time t. So, according to equation (6.1.1) the probability $P_n(t)$ is the difference between the total incoming microscopic currents to state n and the total outgoing currents from state n integrated over time t. Equation (6.1.1) also suggests using the configurational current, $j_{n'n}(t)$, as the main quantity corresponding to $P_n(t)$ through equation (6.1.2). Furthermore, the

transition rate, $w_{n'n}(t)$, is split into two contributing factors, i.e.:

$$w_{n'n}(t) = w^{\text{int}}_{n'n} w^{\text{ext}}_{n'n}(t), \tag{6.1.3}$$

where $w^{\text{int}}_{n'n}$ is the time-independent 'internal' contribution of the transition rate that depends on the dynamics of the system under consideration. $w^{\text{ext}}_{n'n}(t)$ is the time-dependent 'external' contribution to the transition rate. Especially for particle hopping models on a lattice $\mathcal{L}$ the latter may be defined as

$$w^{\text{ext}}_{n'n}(t) = \exp\left\{ -\sum_{i,k} \tau_{i,n}\tau_{k,n'}[1-\tau_{k,n}][1-\tau_{i,n'}]V^{\text{ext}}_{ik}(t) \right\}, \tag{6.1.4}$$

where $V^{\text{ext}}_{ik}(t)$ is a given external hopping rate linking sites i and k at time t, $\tau_{i,n}$ and $\tau_{k,n'}$ are the occupation numbers of sites i and k in states n and n', respectively, and $i, k \in \mathcal{L}$.

In order to illustrate this, consider the TASEP with open boundaries that consists of N sites. The dynamics follows a continuous time step, i.e.: $t \to t + \mathrm{d}t$ where $\mathrm{d}t$ is an infinitesimal increment of t. A site i is chosen randomly from $N+1$ sites with probability $1/(N+1)$. A particle on the chosen site i (if there is any) can jump to its right nearest neighbour, i.e. site $i+1$, with probability $k(t)\mathrm{d}t$, as long as site $i+1$ is empty. A transition from state n to n', $n \to n'$, may occur with transition rate $w_{n'n}(t) = k(t)$. A microscopic current, $j_{n'n}(t)$, occurs during this transition satisfying equation (6.1.2), i.e. $j_{n'n}(t) = k(t)P_n(t)$. At the left-most site, the transition rate is $w_{n'_l n_l}(t) = \alpha(t)$ such that $j_{n'_l n_l}(t) = \alpha(t)P_{n_l}(t)$ for any transition of $n_l = \{0\tau_2\tau_3\ldots\tau_{N-1}\tau_N\} \to n'_l = \{1\tau_2\tau_3\ldots\tau_{N-1}\tau_N\}$. And at the right-most site, the transition rate is $w_{n'_r n_r}(t) = \beta(t)$ for any transition $n_r = \{\tau_1\tau_2\ldots\tau_{N-1}1\} \to n'_r = \{\tau_1\tau_2\ldots\tau_{N-1}0\}$ so that $j_{n'_r n_r}(t) = \beta(t)P_{n_r}(t)$. Hence, the master equation for this model is given as

$$\begin{aligned}
\frac{\partial P_{n_l}(t)}{\partial t} &= \sum_{n'_l} \left[j_{n_l n'_l}(t) - j_{n'_l n_l}(t) \right], \\
\frac{\partial P_{n}(t)}{\partial t} &= \sum_{n'} \left[j_{nn'}(t) - j_{n'n}(t) \right], \\
\frac{\partial P_{n_r}(t)}{\partial t} &= \sum_{n'_r} \left[j_{n_r n'_r}(t) - j_{n'_r n_r}(t) \right].
\end{aligned} \tag{6.1.5}$$

The first and third equations govern the time evolution of the probabilities at the boundaries. And the middle equation governs the probabilities in the bulk.

As an example, consider the familiar case of the TASEP with one site discussed in Section 3.1. This simple model is depicted in Figure 3.1. The microscopic currents are

$$j_{21}(t) = \beta(t)P_1(t), \tag{6.1.6}$$

and

$$j_{12}(t) = \alpha(t)P_2(t). \tag{6.1.7}$$

Therefore, the master equations read

$$\frac{\partial P_1(t)}{\partial t} = j_{12}(t) - j_{21}(t), \tag{6.1.8}$$

and

$$\frac{\partial P_2(t)}{\partial t} = j_{21}(t) - j_{12}(t). \tag{6.1.9}$$

Furthermore, the current densities in term of the microscopic currents are given as follows:

$$J_{\text{in}}(t) = j_{12}(t), \tag{6.1.10}$$

and

$$J_{\text{out}}(t) = j_{21}(t). \tag{6.1.11}$$

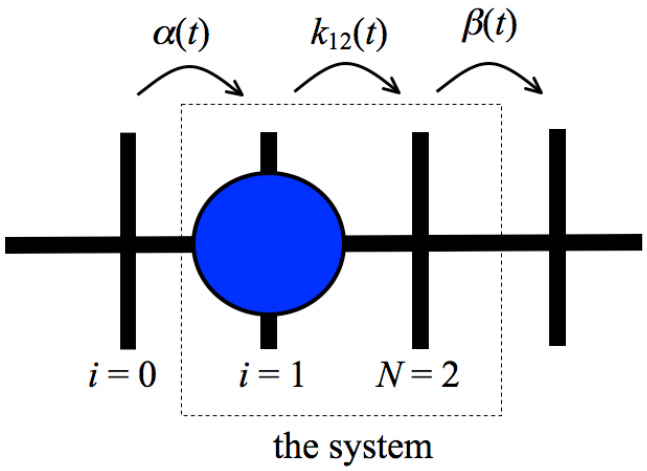

Figure 6.1: The TASEP which consists of two sites. The system is given inside the dashed box. The vertical (black) thick marks are the sites, while the filled blue circle is a hard core particle. A particle may enter the sites from site $i = 0$ with rate $\alpha(t)$ if there is no particle at site $i = 1$. If there is a particle at site $N = 2$ the particle may exit the sites with rate $\beta(t)$.

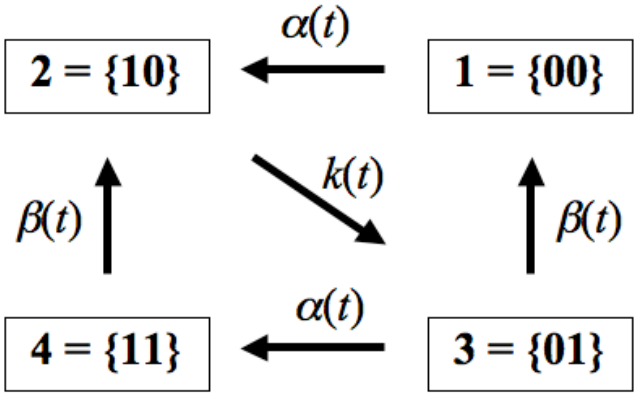

Figure 6.2: Microscopic transitions of the TASEP which consists of two sites. Each (possible) configurational state is given in the solid box. The arrows point to the direction of transitions corresponding to the appropriate transition rates.

Now, consider the TASEP with two sites, see Figure 6.1. As above, the possible microscopic states are $n = \{\tau_{i,n}\}_{i=1,2} = \{00\}, \{10\}, \{01\}, \{11\} \equiv 1, 2, 3, 4$. The non-zero transition rates are specified as follows, $w_{21}(t) = w_{43}(t) = \alpha(t)$, $w_{13}(t) = w_{24}(t) = \beta(t)$, and $w_{32}(t) = k_{12}(t)$, where $k_{12}(t)$ is the hopping rate of particles from site $i = 1$ to site $N = 2$. These non-zero transition rates give an indication of allowed microscopic transitions (see Fig. 6.2). Thus the microscopic currents are given as

$$\begin{aligned} j_{21}(t) &= w_{21}(t)P_1(t), \\ j_{43}(t) &= w_{43}(t)P_3(t), \\ j_{13}(t) &= w_{13}(t)P_3(t), \\ j_{32}(t) &= w_{32}(t)P_2(t), \\ j_{24}(t) &= w_{24}(t)P_4(t), \end{aligned} \tag{6.1.12}$$

where $P_1(t) = P(\{00\}, t)$, $P_2(t) = P(\{10\}, t)$, $P_3(t) = P(\{01\}, t)$, and $P_4(t) = P(\{11\}, t)$. Hence, the set of master equations is given as

$$\frac{\partial P_1(t)}{\partial t} = j_{13}(t) - j_{21}(t), \tag{6.1.13}$$

$$\frac{\partial P_2(t)}{\partial t} = j_{21}(t) + j_{24}(t) - j_{32}(t), \tag{6.1.14}$$

$$\frac{\partial P_3(t)}{\partial t} = j_{32}(t) - j_{43}(t) - j_{13}(t), \tag{6.1.15}$$

and

$$\frac{\partial P_4(t)}{\partial t} = j_{43}(t) - j_{24}(t). \tag{6.1.16}$$

One may obtain the current densities in term of the microscopic currents as

$$J_1(t) = j_{21}(t) + j_{43}(t), \tag{6.1.17}$$

$$J_2(t) = j_{13}(t) + j_{24}(t), \tag{6.1.18}$$

and

$$J_{12}(t) = j_{32}(t), \tag{6.1.19}$$

where $J_1(t)$ and $J_2(t)$ are the current densities coming into site $i = 1$ and going out from site $N = 2$, respectively, at time t. $J_{12}(t)$ is the current density from site $i = 1$ to site $N = 2$ at time t. Lastly, the continuity equations may be obtained by rearranging equations (6.1.13)-(6.1.19) such that

$$\frac{\partial \rho_1(t)}{\partial t} = J_1(t) - J_{12}(t), \tag{6.1.20}$$

and

$$\frac{\partial \rho_2(t)}{\partial t} = J_{12}(t) - J_2(t), \tag{6.1.21}$$

where the one-body density on the LHS of equations (6.1.20) and (6.1.21) are obtained following equation (2.2.9),

$$\rho_i(t) = \sum_{n=1}^{4} \tau_{i,n} P_n(t).$$

These are

$$\rho_1(t) = P_2(t) + P_4(t), \tag{6.1.22}$$

and

$$\rho_2(t) = P_3(t) + P_4(t). \tag{6.1.23}$$

A useful feature of equations (6.1.20) and (6.1.21) is that $\rho_1(t)$ and $\rho_2(t)$ depend on $J_1(t)$, $J_{12}(t)$ and $J_2(t)$. Thus, the one-body densities can be determined once the current densities are known.

6.2 Time-dependent non-equilibrium systems

Here, a formal argument for the variational framework of the current density functional using the time-dependent master equation is put forward. First, a functional of the (many-body) microscopic current is defined as follows

$$\mathcal{M}[\{\tilde{j}_{n'n}\}] = \int_0^\infty \mathrm{d}t \sum_{n',n} \tilde{j}_{n'n}(t) \left[\ln\left(\frac{\tilde{j}_{n'n}(t)}{w_{n'n}(t) P_n(t)} \right) - 1 \right], \tag{6.2.1}$$

where $P_n(t)$ satisfies equation (6.1.1). The minimum value of functional $\mathcal{M}[\{\tilde{j}_{n'n}\}]$ is obtained if $\tilde{j}_{n'n}(t)$ satisfies (6.1.2) via the Gibbs inequality. The proof is given in Appendix B. Thus, one ends up with an inequality attained via the Gibbs inequality

$$\mathcal{M}\left[\{\tilde{j}_{n'n}\}\right] \geq -\int_0^\infty \mathrm{d}t \sum_{n',n} w_{n'n}(t) P_n(t), \tag{6.2.2}$$

where again $P_n(t)$ satisfies equation (6.1.1). There is a reason as to why $P_n(t)$ in functional (6.2.1) satisfies equation (6.1.1), that is $P_n(t)$ can be thought of as an *explicit* functional of $j_{n'n}(t)$ rather than $w_{n'n}(t)$, i.e. $P_n\left([j_{n'n}];t\right)$. $P_n(t)$ is the true solution of the system that corresponds to the microscopic current $j_{n'n}(t)$.

The above formulation is still on the microscopic (many-body) level of the physical system. Hence, this requires solving the full many-body problem, that is calculating the microscopic current and hence the probabilities. However, as in classical DFT, in order to reduce the number of degrees of freedom, one relates the above framework to the averaged (macroscopic) quantities, i.e. the one-body and current densities. The one-body density follows from (2.2.9) and the continuity equation. The current density from site i to site k, i.e. $J_{ik}(t)$, can be determined by summing over all microscopic states n', n of the microscopic currents, $j_{n'n}(t)$, or [118]:

$$J_{ik}(t) = \sum_{n',n} \left(\hat{J}_{ik,n'n} \right) j_{n'n}(t) = \sum_{n',n} \tau_{i,n} \tau_{k,n'} [1 - \tau_{i,n'}][1 - \tau_{k,n}] j_{n'n}(t). \tag{6.2.3}$$

This formal argument proceeds via the constrained search method [1, 95]. This may be realized by defining a functional in the form of,

$$\mathcal{G}[\tilde{J}_{ik}] = \min_{\tilde{j}_{n'n}} \left\{ \int_0^\infty \mathrm{d}t \sum_{n',n} \tilde{j}_{n'n}(t) \left[\ln\left(\frac{\tilde{j}_{n'n}(t)}{w^{\mathrm{int}}_{n'n} P_n(t)} \right) - 1 \right] \right\}, \tag{6.2.4}$$

where $P_n(t)$ satisfies equation (6.1.1). It is essential to understand the meaning of functional (6.2.4). $\mathcal{G}[\tilde{J}_{ik}]$ searches all sets of $\left\{\tilde{j}_{n'n}(t)\right\}$ that yields a fixed trial density

current, $\tilde{J}_{ik}(t)$, where $\tilde{J}_{ik}(t)$ need not has the v-representability property. $\mathcal{G}[\tilde{J}_{ik}]$ then delivers a minimum value by choosing a particular set from all the sets of $\{\tilde{j}_{n'n}(t)\}$ that minimizes (6.2.4). Let the set of the configurational currents that minimizes (6.2.4) be $\{\tilde{j}^{\min}_{n'n}(t)\}$. Then, (6.2.4) becomes

$$\mathcal{G}[\tilde{J}_{ik}] = \int_0^\infty \mathrm{d}t \sum_{n',n} \tilde{j}^{\min}_{n'n}(t) \left[\ln \left(\frac{\tilde{j}^{\min}_{n'n}(t)}{w^{\mathrm{int}}_{n'n} P_n(t)} \right) - 1 \right]. \tag{6.2.5}$$

In order for $\mathcal{G}[\tilde{J}_{ik}]$ in (6.2.4) to be a valid (universal) functional of the current densities, it is necessary to argue the relations below,

$$\mathcal{G}[\tilde{J}_{ik}] - \int_0^\infty \mathrm{d}t \sum_{i,k} \tilde{J}_{ik}(t) V^{\mathrm{ext}}_{ik}(t) \geq \mathcal{M}_0 = - \int_0^\infty \mathrm{d}t \sum_{n',n} j_{n'n}(t), \tag{6.2.6}$$

and

$$\mathcal{G}[J_{ik}] - \int_0^\infty \mathrm{d}t \sum_{i,k} J_{ik}(t) V^{\mathrm{ext}}_{ik}(t) = \mathcal{M}_0. \tag{6.2.7}$$

Inequality (6.2.6) is clearly satisfied from the Gibbs inequality. In order to check equation (6.2.7) an additional notation is needed following (6.2.5), that is

$$\mathcal{G}\left[J_{ik}\right] = \int_0^\infty \mathrm{d}t \sum_{n',n} j^{\min}_{n'n}(t) \left[\ln \left(\frac{j^{\min}_{n'n}(t)}{w^{\mathrm{int}}_{n'n} P_n(t)} \right) - 1 \right]. \tag{6.2.8}$$

Furthermore, according to the variational principle, one has

$$\int_0^\infty \mathrm{d}t \sum_{n',n} j^{\min}_{n'n}(t) \left[\ln \left(\frac{j^{\min}_{n'n}(t)}{w_{n'n}(t) P_n(t)} \right) - 1 \right] \geq \mathcal{M}_0. \tag{6.2.9}$$

But it is clear that

$$\mathcal{M}_0 = \int_0^\infty \mathrm{d}t \sum_{n',n} j_{n'n}(t) \left[\ln \left(\frac{j_{n'n}(t)}{w_{n'n}(t) P_n(t)} \right) - 1 \right], \tag{6.2.10}$$

by inserting $\tilde{j}_{n'n}(t) = j_{n'n}(t)$ into (6.2.1). Combining (6.2.9) and (6.2.10) gives

$$\int_0^\infty \mathrm{d}t \sum_{n',n} j^{\min}_{n'n}(t) \left[\ln \left(\frac{j^{\min}_{n'n}(t)}{w_{n'n}(t) P_n(t)} \right) - 1 \right] \geq \int_0^\infty \mathrm{d}t \sum_{n',n} j_{n'n}(t) \left[\ln \left(\frac{j_{n'n}(t)}{w_{n'n}(t) P_n(t)} \right) - 1 \right]. \tag{6.2.11}$$

However, according to the constraint search method, $j_{n'n}(t)$ and $j^{\min}_{n'n}(t)$ yield the same density current, i.e. $J_{ik}(t)$. Hence,

$$\begin{aligned} &\int_0^\infty \mathrm{d}t \sum_{n',n} j^{\min}_{n'n}(t) \left[\left(\frac{j^{\min}_{n'n}(t)}{w^{\mathrm{int}}_{n'n} P_n(t)} \right) - 1 \right] - \int_0^\infty \mathrm{d}t \sum_{i,k} J_{ik}(t) V^{\mathrm{ext}}_{ik}(t) \\ &\geq \int_0^\infty \mathrm{d}t \sum_{n',n} j_{n'n}(t) \left[\left(\frac{j_{n'n}(t)}{w^{\mathrm{int}}_{n'n} P_n(t)} \right) - 1 \right] - \int_0^\infty \sum_{i,k} J_{ik}(t) V^{\mathrm{ext}}_{ik}(t), \end{aligned} \tag{6.2.12}$$

or

$$\int_0^\infty \mathrm{d}t \sum_{n',n} j_{n'n}^{\min}(t) \left[\left(\frac{j_{n'n}^{\min}(t)}{w_{n'n}^{\mathrm{int}} P_n(t)} \right) - 1 \right] \geq \int_0^\infty \mathrm{d}t \sum_{n',n} j_{n'n}(t) \left[\left(\frac{j_{n'n}(t)}{w_{n'n}^{\mathrm{int}} P_n(t)} \right) - 1 \right]. \tag{6.2.13}$$

By definition of $j_{n'n}^{\min}(t)$ the following inequality should also hold,

$$\int_0^\infty \mathrm{d}t \sum_{n',n} j_{n'n}^{\min}(t) \left[\left(\frac{j_{n'n}^{\min}(t)}{w_{n'n}^{\mathrm{int}} P_n(t)} \right) - 1 \right] \leq \int_0^\infty \mathrm{d}t \sum_{n',n} j_{n'n}(t) \left[\left(\frac{j_{n'n}(t)}{w_{n'n}^{\mathrm{int}} P_n(t)} \right) - 1 \right]. \tag{6.2.14}$$

The last two inequalities hold simultaneously if and only if

$$\int_0^\infty \mathrm{d}t \sum_{n',n} j_{n'n}^{\min}(t) \left[\left(\frac{j_{n'n}^{\min}(t)}{w_{n'n}^{\mathrm{int}} P_n(t)} \right) - 1 \right] = \int_0^\infty \mathrm{d}t \sum_{n',n} j_{n'n}(t) \left[\left(\frac{j_{n'n}(t)}{w_{n'n}^{\mathrm{int}} P_n(t)} \right) - 1 \right], \tag{6.2.15}$$

or

$$\int_0^\infty \mathrm{d}t \sum_{n',n} j_{n'n}(t) \left[\left(\frac{j_{n'n}(t)}{w_{n'n}^{\mathrm{int}} P_n(t)} \right) - 1 \right] = \mathcal{G}\left[J_{ik}\right], \tag{6.2.16}$$

using equation (6.2.8). Finally, using (6.2.10) and (6.2.16) yield equation (6.2.7). Inequality (6.2.6) may be written as a functional derivative, that is

$$\left. \frac{\delta \mathcal{M}[\tilde{J}_{ik}]}{\delta \tilde{J}_{ik}(t)} \right|_{J_{ik}} = 0, \tag{6.2.17}$$

where

$$\mathcal{M}[\tilde{J}_{ik}] = \mathcal{G}[\tilde{J}_{ik}] - \int_0^\infty \mathrm{d}t \sum_{i,k} \tilde{J}_{ik}(t) V_{ik}^{\mathrm{ext}}(t), \tag{6.2.18}$$

following the LHS of inequality (6.2.6), and

$$\mathcal{M}[J_{ik}] = \mathcal{M}_0, \tag{6.2.19}$$

which follows from equation (6.2.7).

Equation (6.2.18) is not strictly a splitting between the 'intrinsic' (free energy) functional, $\mathcal{G}$, and the external hopping rate contribution. This is due to the definition of $\mathcal{G}$ given in (6.2.4). The definition consists of $P_n(t)$, which depends on the external hopping rate through equation (6.1.1).

Moreover, this Section gives some insights into Chapter 5. Here, the variational principle is argued via the constrained search method giving (6.2.17) and (6.2.19) which is previously postulated in (5.1.6) and (5.1.9).

6.3 The equilibrium case

In the equilibrium case, we set

$$V_{ik}^{\text{ext}}(t) = 0, \tag{6.3.1}$$

and

$$\frac{\partial P_n(t)}{\partial t} = 0. \tag{6.3.2}$$

The former equation ensures that the external source of the driving force is turned off, i.e.: $w_{n'n}^{\text{ext}}(t) = 1$, such that

$$w_{n'n} = w_{n'n}^{\text{int}}. \tag{6.3.3}$$

Equation (6.3.3) means that, in equilibrium, the transition rates becomes time-independent and only depend on the internal transition rate from state n to state n'. Using equations (2.1.1), (6.1.2) and (6.3.2), the master equation in steady state reduces to

$$\sum_{n'} j_{nn'} = \sum_{n'} j_{n'n}. \tag{6.3.4}$$

But for the equilibrium case, a stronger requirement gives

$$j_{nn'} = j_{n'n}, \tag{6.3.5}$$

where $j_{n'n} = w_{n'n}P_n$. Equation (6.3.5) states that given any two microscopic states, say, n and n', the (microscopic) current going into state n from n' is equal to the current going out of state n' to state n. Hence, there is no net effect of the (microscopic) current between any two microscopic states. However, the values of the microscopic currents which are not directly related via equation (6.3.5), need not be equal. Thus, we obtain again the detailed balance condition of (2.1.5), viz.:

$$w_{nn'}P_{n'} = w_{n'n}P_n.$$

Next, a configurational functional is defined for the time-independent case. Based on functional (6.2.1), the configuration functional for the time-independent case is given as

$$\mathcal{M}[\{\tilde{j}_{n'n}\}] = \sum_{n,n'} \tilde{j}_{n'n} \left[\ln\left(\frac{\tilde{j}_{n'n}}{w_{n'n}P_n} \right) - 1 \right], \tag{6.3.6}$$

where there is no integration over time. Because the role of the configurational current is reduced to equation (6.3.5), therefore we constraint $\tilde{j}_{n'n}$ such that it satisfies

$$\tilde{j}_{n'n} = w_{n'n}\tilde{P}_n, \tag{6.3.7}$$

where $\tilde{P}_n$ is a trial probability of state n. So, now the main microscopic quantity is shifted from $\tilde{j}_{n'n}$ to $\tilde{P}_n$. Using the aforementioned constrained and (6.3.3), the functional (6.3.6) may be written as

$$\mathcal{M}^{\mathrm{eq}}[\tilde{P}_n] = \sum_n \left(\sum_{n'} w^{\mathrm{int}}_{n'n} \right) \tilde{P}_n \left[\ln \left(\frac{\tilde{P}_n}{P_n} \right) - 1 \right]. \tag{6.3.8}$$

Next, a normalization condition is applied, i.e. $\sum_{n'} w^{\mathrm{int}}_{n'n} = 1$. This constrains further the steady state condition (2.1.4) as

$$1 = \sum_{n'} \left(\frac{P_{n'}}{P_n} \right) w^{\mathrm{int}}_{nn'}. \tag{6.3.9}$$

Then (6.3.8) becomes,

$$\mathcal{M}^{\mathrm{eq}}[\tilde{P}_n] = \sum_n \tilde{P}_n \left[\ln \left(\frac{\tilde{P}_n}{P_n} \right) - 1 \right]. \tag{6.3.10}$$

For continuous set of configurational states n, the discrete sum is modified to an integral, viz. $\sum_n \to \int \mathrm{d}n$ such that (6.3.10) becomes,

$$\mathcal{M}^{\mathrm{eq}}[\tilde{P}] = \int \tilde{P}(n) \left[\ln \left(\frac{\tilde{P}(n)}{P(n)} \right) - 1 \right] \mathrm{d}n. \tag{6.3.11}$$

If $n = \{\mathbf{r}_m, \mathbf{p}_m\}_{m=1,\ldots,M}$, where $\mathbf{r}_m$ and $\mathbf{p}_m$ are the position and momentum of particle m, respectively, then $\int \mathrm{d}n \to \sum_{M=0}^{\infty} 1/(h^{3M} M!) \int \mathrm{d}\mathbf{r}_1 \ldots \mathbf{r}_M \int \mathrm{d}\mathbf{p}_1 \ldots \mathbf{p}_M \equiv \mathrm{Tr}_{\mathrm{cl}}$. Furthermore, recall the (continuous) probability density of (2.3.1), i.e.:

$$P = \Xi^{-1} \exp\left(-\mathcal{B}\left[H_M - \mu M\right]\right) = f_0,$$

where H_M is the Hamiltonian defined by equation (2.3.9), μ is a constant chemical potential, and Ξ is the grand canonical partition function given by (2.3.2). Using the phase space representation for state n and replacing $\tilde{P}$ by f as the trial probability density, the integral in functional (6.3.11) becomes,

$$\mathcal{B}^{-1}\mathcal{M}^{\mathrm{eq}}[f] = \mathcal{B}^{-1}\mathrm{Tr}_{\mathrm{cl}} f \left[\ln \left(\frac{f}{f_0} \right) - 1 \right]. \tag{6.3.12}$$

Inserting the expression for the equilibrium probability density (2.3.1) into the functional (6.3.12), gives

$$\begin{aligned} \mathcal{B}^{-1}\mathcal{M}^{\mathrm{eq}}[f] &= \mathcal{B}^{-1}\mathrm{Tr}_{\mathrm{cl}} f \left[\ln(f) - \ln\left(\Xi^{-1} \exp\left(-\mathcal{B}\left[H_M - \mu M\right]\right)\right) - 1 \right] \\ &= \mathrm{Tr}_{\mathrm{cl}} f \left[\mathcal{B}^{-1} \ln(f) + H_N - \mu M \right] + \mathcal{B}^{-1} \left(\ln \Xi - 1 \right). \end{aligned} \tag{6.3.13}$$

Add both sides of equation (6.3.13) by $-\mathcal{B}^{-1}(\ln \Xi - 1)$, produces

$$\mathcal{B}^{-1}\left(\mathcal{M}^{\mathrm{eq}}[f] - \ln \Xi + 1\right) = \mathrm{Tr}_{\mathrm{cl}} f\left[\mathcal{B}^{-1} \ln(f) + H_M - \mu M\right]. \tag{6.3.14}$$

By defining the LHS of equation (6.3.14) as

$$\mathcal{B}^{-1}\left(\mathcal{M}^{\mathrm{eq}}[f] - \ln \Xi + 1\right) \equiv \Omega^{\mathrm{eq}}[f], \tag{6.3.15}$$

the equilibrium Mermin functional of (2.3.4) is obtained from (6.3.14) and (6.3.15) as

$$\Omega^{\mathrm{eq}}[f] = \mathrm{Tr}_{\mathrm{cl}} f\left[\mathcal{B}^{-1} \ln(f) + H_M - \mu M\right].$$

Chapter 7

Discussion

A general aim of this project was to explore different methods of relating non-equilibrium and equilibrium systems. Then it may be possible to derive the properties of the non-equilibrium system through calculations carried out for the equilibrium one. Of course there are many different non-equilibrium systems, which can be studied via numerous methods suitable for each particular system. In this project, we restrict the non-equilibrium systems to special cases of the TASEP in 1D and 2D. Three main ideas have been put forward to achieve the above objective, i.e.:

i) Constructing a relationship between the TASEP and the lattice fluid mixtures in 2D. A simplification of the TASEP in 2D yielded the TASEP with a junction.

ii) Proposing an alternative mapping between the TASEP in 1D and the hard rod model, and

iii) Constructing a current density functional for non-equilibrium hopping models which is similar to that of the classical density functional theory. At the moment, a formal argument for the current density functional is given, where the current density is considered as the main quantity rather than the one-body density.

First some phenomenological results of the TASEP and its variants are highlighted. The one-body and current densities are the main physical quantities being determined. A motivation of conducting these exercises is to obtain some insights concerning the TASEP with time-dependent input and output rates and the TASEP in 2D.

We start with arguably the simplest possible case, that is the TASEP with a single site. Here, the master equation is formulated for the TASEP with time-dependent input

and output hopping rates. An important result from this calculation is that one may determine the current densities coming into and out of the site [equations (3.1.18) and (3.1.19)] that only depend on the boundary rates. Thus, one may consider the current densities as the main quantities and use them as the starting quantities. In turn, the one-body density may be determined by integrating the continuity equation. This is the basic concept used in the current density functional construction of the TASEP in 1D (Chapters 5 and 6).

The boundary rates of the TASEP with one site is also simplified to constant values. For this case, the current densities are time-dependent, but this dependency is exponentially decreasing. At a sufficiently long time, the current densities become equal. Hence, according to the continuity equation the one-body density becomes stationary. The latter condition means that the system reaches steady state. These steady state results are further applied in Chapter 4 where a correspondence between the TASEP and the continuous hard rod fluids are proposed.

Phenomenological results of the TASEP in 1D with N sites and time-dependent input and output hopping rates are shown in Section 3.2. In this model the hopping rates in the bulk are kept homogenous and constant. Section 3.2 is not intended to give a full account of this model, but rather to highlight some ideas concerning the effect of adding a periodic, time-dependent term into the boundary hopping rates. The parameters to be varied include the initial hopping rates, the oscillation strength, and the period of oscillation. The system consists of 100 sites. The types of dynamics applied are the sequential and parallel updating.

First, variation of the oscillation period is discussed. In all cases given for the sequential and updating dynamics, varying the oscillation period changes the one-body and current density profiles. Interesting results can be observed from each type of dynamics. In the case of sequential updating, a sequence of flat, coexistence phase (low and high density phases), and a maximal current phase for the one-body density profiles is observed as the period is increased. As for the parallel updating, a sequence of low density, coexistence, and a high density phases is observed. Only at period of 10^4 time steps does the two types of dynamics show a coexistence phase, although the detail profiles are different for each case.

As explained in Section 2.2, the one-body density of the TASEP with constant input and output rates have stationary profiles (Figs. 2.4-2.7). However, this is not the case

if the input and output rates are periodically time-dependent, both for the sequential and parallel dynamics. Instead, after a long time evolution, the one-body and current densities do change every period (from 0 to 2π-the period of cosine function). More interestingly, the one-body and current densities repeat every (multiple) period of the oscillation term producing a periodic steady state condition.

Furthermore, varying the oscillation strength may alter the one-body and current densities. This is clearly observed in Fig. 3.4(i)-(ii) for the sequential updating, where increasing the strength of oscillation changes the one-body and current density profiles. In fact there seems to be a phase transition from a maximal current to a coexistence phases as the strength of oscillation is increased. For the parallel updating in Fig. 3.7(i)-(ii), the overall one-body densities are of a coexistence phase. As the strength of oscillation is increased the densities change only at the details of the high and low phase regions.

We would also like to address the comparison between the mean-field and simulation results. Qualitative agreements between the mean-field and simulation results are better for sequential rather than parallel dynamics. For the current density profiles of the sequential updating the mean-field results agree quite well with simulations. However, this is not the case for the parallel updating. A good agreement between the mean-field and simulation results for the one-body and current density profiles are obtained for considerably low current, e.g. see Figs. 3.6(i)-(vi). In fact, the theory breaks down for high values of the initial input and output rates.

Another interesting extension of the TASEP is to consider a 2D square lattice $\mathcal{L}^2$ where particles may hop to the right or upper nearest neighbour with constant rates. The input and output hopping rates are constant as well. A relationship between the TASEP and the equilibrium lattice fluid mixture in 2D is exploited in order to derive the one-body and current density equations for the TASEP. Basically this correspondence relies upon the identification of particles defined in the equilibrium system with the hopping of particles in the TASEP. This method offers some flexibility to invent various particles (in the equilibrium system) corresponding to various jumps of particles (in the TASEP), thus proposing various (dynamic) variation of the TASEP.

In this thesis, two cases of the mean-field TASEP in 2D are given, which are shown in Figs. 3.10 and 3.11. Fig. 3.10 gives the one-body and current density profiles with input and output rates specified by $\alpha_1 = \beta_2 = 0.9$ and $\alpha_2 = \beta_1 = 0.1$. The one-body density

profile shows reminiscent of the TASEP in 1D, i.e. coexistence and maximal current phase regions. Interestingly, these phases are located around the boundary (ends) sites. Around the middle sites the one-body density seems to be suppressed by the competing rates such that the profile is flat with value 0.5. A similar situation occurs for the second case where $\alpha_1 = \alpha_2 = \beta_1 = \beta_2 = 0.1$. In this case the one-body density shows coexistence phases around the ends of the sites, whereas the middle sites is flat. Clearly this is a reminiscent of the TASEP in 1D as well. Furthermore, the current densities for both cases are flat and constant throughout the plane with value 0.1. This shows the systems reaches steady states.

One way to modify the TASEP in 2D into a more physical situation, e.g. a street with a junction, is to consider particular sites (middle sites at each axis) that form a junction (Fig. 3.12). Here, two models are considered based on the number of boundary rates, viz.: i) two input and two output rates, ii) one input and two output rates. For the first model two examples are considered, i.e.: i) $\alpha_2 = \beta_1 = 0.4$ and $\alpha_1 = \beta_2 = 0.1$, and ii) $\alpha_2 = \beta_2 = 0.5$ and $\alpha_1 = 0.1$; $\beta_1 = 0.2$. The second model are obtained by setting $\alpha_1 = 0.0$ for the aforementioned examples.

The one-body and current density profiles of the first model are given in Figs. 3.13 and 3.15. In Fig. 3.13 all paths (I-IV) are in coexistence phases (CP). Interestingly, the CPs on paths III and IV follows from the boundary rates, $\alpha_2 = \beta_1 = 0.4$, and $\alpha_1 = \beta_2 = 0.1$, respectively. Hence, adding path III to path IV or vice versa does not affect the one-body density profile of each path. According to the TASEP in 1D, paths I and II should be high (HD) and low (LD) density phases, respectively. Here, however the densities turned out to be in CP. Hence adding path II to path I or vice versa changes the one-body densities of each path. The current densities of paths I and II show a jump, whereas paths III and IV are flat with constant values except at the center.

Furthermore, in Fig. 3.15, adding path II to path I produces a coexistence between maximal current and low density phases, i.e. MC-LD. According to the given boundary rates, path III (without any additional path) should give a high density phase. Combining path IV to path III at the junction affect path III from the entrance to the junction site, i.e. it decreases the one-body density from a high density to a maximal current regimes. On the other hand, path IV without any additional path should give a flat low density phase. However, in the presence of path III, a jump at the junction occurs between two low density phases. The current densities of paths III and IV show jumps

at the junction.

Turning off the input rate of path II produces the second model in Figs. 3.14 and 3.16. In this model the existing paths reduces to paths V and VI. As this is a simplification of the previous examples, one may compare these results with the previous. Paths V and I are actually the same paths. When $\alpha_1 = 0$, path I becomes path V. One obvious difference between these paths is the dip of the one-body density profiles around the junction for path V. In path I of Fig. 3.13(i) the one-body density at the junction is 0.5 but in Fig. 3.14(i) the one-body density of path V dips to a value of 0.2. This is also the case for Fig. 3.15(i) and Fig. 3.16(i). Hence, turning off one of the input rate resulted in the decrease (a dip) of the one-body density at the junction. Moreover, one may compare path VI in Fig. 3.14(i) with path III of Fig. 3.13(i). Turning off α_1 causes the one-body density profile from the junction to the exit sites to collapse from a HD to an LD phase, such that a phase changes occurs from CP (path III) to an LD phase (path VI). One may also compare path VI of Fig. 3.16(i) and path III of Fig. 3.15(i). Again a collapse of the one-body density profile (from HD to LD regions) is observed from the junction to the exit sites, when α_1 is turned off.

It may be observed that for the first model with two input and two output rates, there is a sharp increase in the value of the current density at the junction site, i.e. $(51, 51)$, while this is not the case for the second model. Hence, this sharp increase should occur due to the existence of the two input rates in the first model. Hence, it appeared that adding a path (at the center of another path) increases the probability of particles going through the junction such that a sharp increase of the current density is develop at the junction. But, if one of the input rate is turned off (the second model), then the sharp profiles disappear. This is expected as there is only one way to enter the lattice sites.

We now discuss an alternative correspondence between the continuous hard rod model and the particle trajectories of the TASEP. As mentioned in Chapter 4, the objective here is to determine the one-body and current densities of the TASEP via the well-known hard rod model. The TASEP with one site is considered and then extended to the mean-field TASEP with N sites. The main idea of this correspondence (for the TASEP with a single site) is identifying some physical quantities of the continuous hard rod model with the quantities of the TASEP. So, to visually understand this relationship we compare the sketches of the hard rod model (Fig. 2.10) and the trajectories of the

TASEP with one site (Fig. 4.1). Fig. 2.10 shows a possible configuration of the equilibrium model where the x-axis is the continuous spatial coordinate with total length L. Hard rods occupy the 1D space and they cannot overlap with each other (due to infinite repulsive potential). Fig. 4.1 shows the trajectories of particles of the TASEP with one site. A particle may enter the site with constant rate α. The particle stays at the site with lifetime γ, and then exit the site with constant rate β. This process is repeated as time evolves. These trajectories may not overlap. The actual dynamics between the TASEP and its equilibrium counterpart is obviously different. For the hard rod model the total length of the system is given. As time evolves hard rods enter or exit the system (the x-coordinate) randomly according to the chemical potential μ. A hard rod may try to fill an empty space between two other hard rods as long as the diameter of the rod is equal or smaller than that empty space.

A crucial correspondence between the TASEP with one site and the hard rod model is that one full particle trajectory (a particle enters the site, stays at the site for some time, and finally exits the site) resembles a hard rod. Thus, the trajectories of the TASEP with a single site in Fig. 4.1 (last picture) is equivalent to the continuous hard rod fluid in Fig. 2.10. Consequently, the time parameter, t, is associated to the spatial coordinate, x. Hence, one may identify the quantities of the TASEP with the quantities of the 1D hard rod model. Here the life time of the particles in the site is identified as the length of the rod. The output rate corresponds to the number of particles per length occupied by the particles, and the input rate is associated to the total pressure of the hard rod fluid. Using this correspondence it was concluded that the one-body density of the TASEP with one site corresponds to the total packing fraction of the hard rods, whereas the current density corresponds to the total density of the hard rods.

We extend this correspondence for the TASEP with N sites. The objective here is to derive the equation for the mean-field current density at steady state. The particle trajectories are given in Fig. 4.2. In this case, instead of one site, we deal with N sites where each site has its own particle trajectories. If one takes into account the correlations between the sites (the dashed-arrow lines in Fig. 4.2) then the trajectories of particles resemble non-overlapping polymers. This of course complicates matter. Therefore, to simplify this problem these correlations are neglected such that each site becomes an independent 'time rod'. Following through a similar procedure as that of the TASEP with a single site yields equation (2.2.39), which is the current density for the mean-field

TASEP with N sites at steady state.

As presented in Section 3.1, the current densities of the TASEP with a single site may be written as functions of the input and output rates. The one-body density is then obtained with the help of the continuity equation. Hence, one may consider the current density as the main quantity to determine other quantities. This framework is utilized in Chapter 5 where functionals of the current density are constructed for the TASEP. We derive the exact functional for the TASEP with one site and proceed to the TASEP with N sites (within the mean-field approximation). The construction of the current density functional is done in a reverse manner where the solutions, i.e. the equation of motions of the TASEP, are assumed to exist. Then the functionals are constructed such that the equation of motions are retrieved. As in classical DFT, the functional contains a 'free energy' term that accounts for the interatomic interactions in the system. The free energy is further separated into two parts, i.e. the 'ideal' and 'excess' parts. In order to obtain the full functional, additional terms need to be added to the functional. These are constraints corresponding to the current densities. The constraints are then determined via a postulated variational principle. It turned out that these constraints are related to external hopping rates that act upon the current densities of the system. These functionals have to be accompanied by appropriate continuity equations to fully describe the system.

The derivation of the current density functional above is mainly conducted on the one-body density level, i.e. by exploiting the current densities of the TASEP. It is therefore worth the effort to give a formal argument for the current density functional similar to the proof given for the classical DFT in [69, 70]. It is this fundamental argument for the current density functional which is proposed in Chapter 6. The master equation (2.1.1) is the starting point. A new microscopic quantity, viz. the microscopic (configurational) current, is invented and incorporated into the master equation. This new quantity indicates the current of a transition from one (microscopic) state to another and gives rise to the current densities. Moreover, the transition rates are considered to be products of internal and external contributions. The internal hopping rate is a time-independent quantity that takes care of the type of dynamics in the system, while the external hopping rate is the time-dependent contribution to the transition rate that comes from an external potential (or an external one-body hopping rate). Finally, a functional of the microscopic currents is defined. An argument for its existence is given

using a similar methods in [1]. Hence, an argument for the variational principle of the current density functional can be proposed.

Chapter 8

Conclusion and Outlook

All the results obtained from this project have been presented, especially in Chapters 3, 4, 5, and 6. These results have been discussed in Chapter 7. Now, we come to some conclusions of the project.

1) The master equation has been applied to the simple case of the TASEP with one site and time-dependent input and output hopping rates. The probabilities were obtained explicitly which depend on the input and output rates. Further calculations yielded the one-body and current densities. These densities again depend only on the input and output hopping rates. The single site TASEP is simplified further to the case of time-independent input and output rates, and finally to the steady state condition.

2) Various phenomenological results were presented concerning variants of the TASEP in 1D and 2D. Two main quantities were determined, i.e. the one-body and current densities. These quantities are obtained from simulations and from (mean-field) theory calculations. Firstly, examples of the TASEP with open boundaries and time-dependent input and output rates were investigated. The main equation used was the time evolution of the one-body density (continuity equation) where the input and output hopping rates consist of a constant value (in the bulk) and a periodic (time-dependent) term at the boundaries. Different types of dynamics (in discrete time parameter) were considered, i.e. the sequential and parallel updating. Then a correspondence between the TASEP and the hard core lattice fluid in 2D is applied to discuss the TASEP with constant input and output hopping rates in 2D. Finally, the TASEP in 2D was simplified to the case of a junction.

3) An alternative correspondence was proposed between equilibrium and non-equilibrium systems, putting forward a relationship between the TASEP and the continuous 1D hard rod model via the DFT. We started from the one site and extended the relationship to the case of N sites. This correspondence highlights similarity between the trajectories of the TASEP with the allowed configuration of the 1D continuous hard rod model. Hence quantities of the TASEP are identified with quantities of the hard rod model. The lifetime of particle to occupy a site is identified as the length of a rod, the output hopping rate is associated to the number of particles per volume of the system, and the input rate is identified with the total pressure. Hence conducting calculations in the hard rod model via FMT, two other correspondence are obtained, i.e. the one-body density of the TASEP turns out to be the total packing fraction of the hard rod model, whereas the current density corresponds to the total density of the hard rod model.

4) A functional of the current density for the TASEP in 1D was constructed. Here, the current density becomes the main quantity. We consider the TASEP with one site and extend the functional to the TASEP with N sites. We started by assuming the current densities of the TASEP as the true equation of motions. Then a functional is constructed such that the Euler-Lagrange equations are the true equation of motions. The Lagrange multipliers method was used to obtain constraints of the functional. Hence the obtained functional, supported by the continuity equation, gives a full account of the dynamics of the TASEP.

5) A fundamental argument for the current density functional is proposed to elucidate its existence. Our starting point is the master equation. We rewrite the master equation in terms of the microscopic (configurational) current. The latter becomes a basic (microscopic) quantity. We define a functional of the microscopic current and argue the existence of the current density functional using the constrained search method.

Investigating the correspondence between equilibrium and non-equilibrium systems is certainly open-ended. Hence, there are many interesting open problems that can be investigated as future research projects. Some of these are stated in the following.

1) One could explore variants of the TASEP in 1D and 2D other than those given in Chapter 3. The correspondence between the hopping model and the hard core

lattice fluids is quite flexible and allows to construct various different movements in the hopping models. Hence, various types of (mean-field) hopping models may be generated from this correspondence. These hopping models include the TASEP with next nearest neighbour hopping, the TASEP with two (or more) species, and the partially asymmetric simple exclusion process (PASEP) where particles may enter or exit sites $i = 0$ and $i = N$. In fact one may extend the TASEP to 3D.

2) There are interesting follow-up questions that may be asked concerning the correspondence between the TASEP and the 1D continuous hard rod model. For example, in the case of the single site, one may ask of using the correspondence for time-dependent boundary rates. In this case, one may employ the full density functional of the 1D hard rod model. According to [106, 107] the Euler-Lagrange equations of the hard rods are of self-consistent nature, and hence are not closed. On the contrary, the one-body and current density solutions to the time-dependent TASEP with one site produce closed equations. What may possibly be done then is to compare the results of the TASEP and the (full) 1D hard rod model, or compare to simulation results.

   In Section 4.2 the correspondence between the TASEP with N sites and the hard rods was obtained but within the mean-field approximation. Here, the TASEP with N sites are thought of as disjoint 'time' rods. However, the exact one-body and current densities of the TASEP with N sites have yet to be obtained through this correspondence. Hence, in order to address the latter case, it might be interesting to consider the TASEP with N sites as an equilibrium system of non-overlapping polymers which behave in a certain way.

3) In Chapter 5 the exact current density functional of the TASEP with one site was derived. When this derivation was extended to N sites, the current density functional is of the mean-field type. The exact current density functional of the TASEP with N sites is still illusive.

4) A topic for future study may also be suggested concerning Chapter 6. At the moment the status of the current density functional foundation is still an argumentative level. It is yet to be a proper proof of the existence of the current density functional. Thus, it is certainly a challenge to investigate further the formal argument such that it may be elevated into a proper proof.

Moreover, one may attempt to derive a formal argument for the current density functional based upon the Mermin and Evans (chain) of arguments [70, 105]. This formal argument was not given in this thesis as the constrained search method is relatively easier to understand.

Bibliography

[1] M. Levy, *Proc. Natl. Acad. Sci.* **76**, 6062 (1979).

[2] C. M. V. Vliet, *Equilibrium and Non-Equilibrium Statistical Mechanics*, World Scientific, 2008.

[3] S. Ayik, *Phys. Lett.* **B63**, 22 (1976).

[4] E. B. Davies, *Commun. Math. Phys.* **39**, 91 (1974).

[5] B. Baretzky, M. D. Baró, G. P. Grabovetskaya, J. Gubicza, M. B. Ivanov, Y. R. Kolobov, T. G. Langdon, J. Lendvai, A. G. Lipnitskii, A. A. Mazilkin, A. A. Nazarov, J. Nogués, I. A. Ovidko, S. G. Protasova, G. I. Raab, A. Révész, N. V. Skiba, J. Sort, M. J. Starink, B. B. Straumal, S. Surinach, T. Ungár, and A. P. Zhilyaev, *Rev. Adv. Mater. Sci.* **9**, 45 (2005).

[6] V. S. Khrapai, S. Ludwig, J. P. Kotthaus, H. P. Tranitz, and W. Wegscheider, *Physica E* **40**, 995 (2008).

[7] R. Zwanzig, *Nonequilibrium Statistical Mechanics*, Oxford University Press, 2001.

[8] D. C. Mattis, *Statistical Mechanics made Simple: A Guide for Students and Researchers*, World Scientific, 2003.

[9] J. Keizer, *Statistical Thermodynamics of Nonequilibrium Processes*, Springer-Verlag, 1987.

[10] C. P. Royall, J. Dzubiella, M. Schmidt, and A. Blaaderen, *Phys. Rev. Lett.* **98**, 188304 (2007).

[11] M. Schmidt, C. P. Royall, A. van Blaaderen, and J. Dzubiella, *J. Phys.: Condens. Matter* **20**, 494222 (2008).

[12] L. Giomi, M. C. Marchetti, and T. B. Liverpool, *Phys. Rev. Lett.* **101**, 198101 (2008).

[13] A. Ahmadi, T. B. Liverpool, and M. C. Marchetti, *Phys. Rev. E* **72**, 060901 (2005).

[14] S. Dodelson and M. S. Turner, *Phys. Rev. D* **46**, 3372 (1992).

[15] D. Chowdhury, A. Schadschneider, and K. Nishinari, *Phys. Life Rev.* **2**, 319 (2005).

[16] A. Awazu, *Physica A* **373**, 425 (2007).

[17] A. Awazu, *J. Phys. Soc. Jpn.* **74**, 3127 (2005).

[18] M. C. Cross and P. C. Hohenberg, *Rev. Mod. Phys.* **65**, 851 (1993).

[19] D. Chowdhury, K. Nishinari, and A. Schadschneider, *Phase Transitions* **77**, 601 (2004).

[20] H. Hinrichsen, *Adv. Phys.* **49**, 815 (2000).

[21] P. Bak, K. Chen, and C. Tang, *Phys. Lett. A* **147**, 297 (1990).

[22] A. S. Sharma, A. Y. ukhorskiy, and M. I. Sitnov, *Nonequilibrium Phenomena in Plasmas* **321**, 117 (2005).

[23] L. V. Abdurakhomov, M. Y. Brazhnikov, G. V. Kolmakov, A. A. Levchenko, and L. P. Mezhov-Deglin, *J. Low Temp. Phys.* **148**, 245 (2007).

[24] T. N. Palmer, *Rep. Prog. Phys.* **63**, 71 (2000).

[25] D. Chowdhury, A. Schadschneider, and K. Nishinari, *Traffic and Granular Flow'05* , 223 (2007).

[26] M. Plischke and B. Bergersen, *Equilibrium Statistical Physics*, World Scientific, 2006.

[27] A. Chatterjee, B. K. Chakrabarti, and R. B. Stinchcombe, *Phys. Rev. E* **72**, 026162 (2005).

[28] D. S. Fisher, K. Dahmen, and S. Ramanathan, *Phys. Rev. Lett.* **78**, 4885 (1997).

[29] D. S. Fisher, *Phys. Rep.* **301**, 113 (1998).

[30] Y. Sugiyama, M. Fukui, M. Kikuchi, K. Hasebe, A. Nakayama, K. Nishinari, S. Tadaki, and S. Yukawa, *New J. Phys.* **10**, 033001 (2008).

[31] D. Helbing and M. Treiber, *Phys. Rev. Lett.* **81**, 3042 (1998).

[32] T. Kriecherbauer and J. Krug, *J. Phys. A: Math. Theor.* **43**, 403001 (2010).

[33] G. M. Schutz, *J. Stat. Phys.* **88**, 427 (1997).

[34] B. Derrida and M. R. Evans, *The Asymmetric Exclusion Model: Exact Results Through a Matrix Approach (Nonequilibrium Statistical Mechanics in One Dimension)*, chapter V, pp. 277–302, Cambridge University Press, 1997.

[35] W. S. B. Dwandaru, Theory of Dynamics in Driven Lattice Fluids, Master's thesis, Bristol University, Bristol, 2006.

[36] B. Derrida, E. Domany, and D. Mukamel, *J. Stat. Phys.* **69**, 667 (1992).

[37] J. G. Brankov, V. V. Papoyan, V. S. Poghosyan, and V. B. Priezzhev, *Physica A* **368**, 471 (2006).

[38] H. Hinsch and E. Frey, *Phys. Rev. Lett.* **97**, 095701 (2006).

[39] C. MacDonald, J. Gibbs, and A. Pipkin, *Biopolymers* **6**, 1 (1968).

[40] A. Pipkin and J. Gibbs, *Biopolymers* **4**, 3 (1966).

[41] A. Parmeggiani, T. Franosch, and E. Frey, *Phys. Rev. E* **70**, 046101 (2004).

[42] E. Frey, A. Parmeggiani, and T. Franosch, *Genome Informatics* **15**, 46 (2004).

[43] S. Srinivasa and M. Haenggi, The TASEP: A Statistical Mechanics Tool to Study the Performance of Wireless Line Networks, in *Proceedings of 19th IEEE International Conference on Computer Communications and Networks (ICCCN'10)*, Zurich, Switzerland, 2010.

[44] B. Derrida, M. R. Evans, V. Hakim, and V. Pasquier, *J. Phys. A* **26**, 1493 (1993).

[45] W. S. B. Dwandaru and M. Schmidt, *J. Phys. A: Math. Theor.* **40**, 13209 (2007).

[46] J.-P. Hansen and I. R. MacDonald, *Theory of Simple Liquids, 3rd Edition*, Academic Press (Elsevier), 2006.

[47] D. Chowdhury and D. Stauffer, *Principles of Equilibrium Statistical Mechanics*, Wiley-VCH, 2000.

[48] J. Lebowitz and E. W. Montroll, *Studies in Statistical Mechanics: Non-Equilibrium Phenomena* 1 *The Boltzmann Equation*, North-Holland Publishing Company, 1983.

[49] S. P. Heims, *Phys. Rev.* **138**, A587 (1965).

[50] J. Keizer, *J. Stat. Phys.* **6**, 67 (1971).

[51] G. Nicolis and M. M. Mansour, *Phys. Rev. A* **29**, 2845 (1997).

[52] B. J. Alder and T. E. Wainwright, *J. Chem. Phys.* **31**, 459 (1959).

[53] J.-P. Hansen, *Phys. Rev. A* **8**, 3096 (1973).

[54] W. A. Curtin and N. W. Ashcroft, *Phys. Rev. A* **32**, 2909 (1985).

[55] M. N. Rosenbluth and A. Rosenbluth, *J. Chem. Phys.* **22**, 881 (1954).

[56] W. W. Wood and J. D. Jacobson, *J. Chem. Phys.* **27**, 1207 (1957).

[57] B. J. Alder and T. E. Wainwright, *J. Chem. Phys.* **27**, 1208 (1957).

[58] R. J. Baxter, *J. Chem. Phys.* **49**, 2770 (1968).

[59] A. A. Brian, H. L. Frisch, and L. S. Lerman, *Biopolymers* **20**, 1305 (1981).

[60] H. C. Longuet-Higgins and B. Widom, *Molecular Physics* **8**, 549 (1964).

[61] P. N. Pusey, E. Zaccarelli, C. Valeriani, E. Sanz, W. C. K. Poon, and M. E. Cates, *Phil. Trans. R. Soc. A* **367**, 4993 (2009).

[62] G. Parisi and F. Zamponi, *Rev. Mod. Phys.* **82**, 789 (2010).

[63] D. M. Burley, *Proc. Phys. Soc.* **75**, 262 (1960).

[64] D. M. Burley, *Proc. Phys. Soc.* **77**, 451 (1961).

[65] D. S. Gaunt, *J. Chem. Phys.* **46**, 3237 (1985).

[66] D. Nicholson and N. G. Parsonage, *Computer Simulation and the Statistical Mechanics of Absorption*, Academic Press, 1982.

[67] M. T. M. Koper, J. J. Lukkien, A. P. J. Jansen, and R. A. van Santen, *J. Phys. Chem. B* **103**, 5522 (1999).

[68] M. Ausloos, I. Mroz, A. Pekalski, and N. Vandewalle, *Physica A* **248**, 155 (1998).

[69] R. Evans, *Fundamentals of Inhomogeneous Fluids* (ed. D. Henderson), pp. 85–175, Dodrecht: Kluwer, 1997.

[70] R. Evans, *Adv. Phys.* **28**, 143 (1979).

[71] R. Evans, *Les Houches Session XL VIII: Liquids At Interfaces*, pp. 30–66, North-Holland, 1988.

[72] J. K. Percus, *Int. J. Quantum Chem.* **110**, 2996 (2010).

[73] M. Schmidt, *J. Phys.: Condens. Matter* **14**, 12119 (2002).

[74] M. Schmidt, L. Lafuente, and J. A. Cuesta, *J. Phys.: Condens. Matter* **15**, 4695 (2003).

[75] M. Schmidt, *J. Phys. Condens. Matter* **15**, S101 (2003).

[76] J. A. Cuesta, L. Lafuente, and M. Schmidt, *Phys. Rev. E* **72**, 031405 (2005).

[77] T. Munakata, *J. Phys. Soc. Jpn.* **58**, 2434 (1989).

[78] W. Dieterich, H. L. Frisch, and A. Majhofer, *Z. Phys. B-Condensed Matter* **78**, 317 (1990).

[79] U. M. B. Marconi and P. Tarazona, *J. Chem. Phys.* **110**, 8032 (1999).

[80] H. Löwen, *J. Phys.: Condens. Matter* **15**, V1 (2003).

[81] A. J. Archer and R. Evans, *J. Chem. Phys.* **121**, 4246 (2004).

[82] G. K. Chan and R. Finken, *Phys. Rev. Lett.* **94**, 183001 (2005).

[83] A. J. Archer, *J. Phys.: Condens. Matter* **18**, 5617 (2006).

[84] U. M. B. Marconi and P. Tarazona, *J. Phys.: Condens. Matter* **12**, A413 (2000).

[85] A. Yoshimori, T. J. F. Day, and G. N. Patey, *J. Chem. Phys.* **108**, 6378 (1998).

[86] A. J. Archer and M. Rauscher, *J. Phys. A: Math. Gen.* **37**, 9325 (2004).

[87] T. R. Kirkpatrick and D. Thirumalai, *J. Phys. A: Math. Gen.* **22**, L149 (1989).

[88] J. Dzubiella and C. N. Likos, *J. Phys.: Condens. Matter* **15**, L147 (2003).

[89] M. Bier and R. van Roij, *Phys. Rev. E* **76**, 021405 (2007).

[90] T. R. Kirkpatrick, *Phys. Rev. A* **31**, 939 (1985).

[91] B. Bagchi, *Physica A* **145A**, 273 (1987).

[92] D. S. Dean, *J. Phys. A: Math. Gen.* **29**, L613 (1996).

[93] R. L. Jack and P. Sollich, *Prog. Theor. Phys. Supp.* **184**, 304 (2010).

[94] J. P. Garrahan, R. L. Jack, V. Lecomte, E. Pitard, K. van Duijvendijk, and F. van Wijland, *J. Phys. A* **42**, 075007 (2009).

[95] M. Levy, *Int. J. Quantum Chem.* **110**, 3140 (2010).

[96] J. Tailleur, J. Kurchan, and V. Lecomte, *J. Phys. A: Math. Theor.* **41**, 505001 (2008).

[97] H. J. Kreuzer, *Monographs on the Physics and Chemistry of Materials: Non-equilibrium Thermodynamics and its Stastistical Foundations*, Oxford Science Publications, 1981.

[98] M. L. Bellac, Non Equilibrium Statistical Mechanics, in *Lectures Given at Les Houches Predoctoral School*, France, 2007.

[99] A. Prados, J. J. Brey, and B. Sánchez-Rey, *J. Stat. Phys.* **89**, 709 (1997).

[100] M. L. Bellac, F. Mortessagne, and G. G. Batrouni, *Equilibrium and Non-Equilibrium Thermodynamics*, Cambridge University Press, 2004.

[101] D. Chowdhury, *Physica Scripta* **T106**, 13 (2003).

[102] P. Hohenberg and W. Kohn, *Phys. Rev.* **136**, B 864 (1964).

[103] M. Levy and J. P. Perdew, *Int. J. Quantum Chem. Symp.* **21**, 511 (1982).

[104] W. Kohn, Electronic Structure of Matter-Wave Functions and Density Functionals, in *Nobel Lecture*, 1999.

[105] N. D. Mermin, *Phys. Rev.* **137**, A1441 (1965).

[106] J. K. Percus, *J. Stat. Phys.* **15**, 505 (1976).

[107] J. K. Percus, *J. Chem. Phys.* **75**, 1316 (1981).

[108] L. Lafuente and J. A. Cuesta, *J. Phys.: Condens. Matter* **14**, 12079 (2002).

[109] L. Lafuente and J. A. Cuesta, *Phys. Rev. Lett.* **93**, 130603 (2004).

[110] L. Lafuente and J. A. Cuesta, *J. Phys. A: Math. Gen.* **38**, 7461 (2005).

[111] T. Donnellan, *Lattice Theory*, Pergamon Press, 1968.

[112] B. A. Davey and H. A. Priestley, *Introduction to Lattices and Order*, Cambridge University Press, 1990.

[113] Y. Rosenfeld, *Phys. Rev. Lett.* **63**, 980 (1989).

[114] H. Löwen, 3rd Warsaw School of Statistical Physics Kazimierz Dolny Poland, 2009.

[115] C. P. Amann, T. Schmiedl, and U. Seifert, *J. Chem. Phys.* **132**, 041102 (2010).

[116] J. Bisquert, *Am. J. Phys.* **73**, 735 (2005).

[117] V. Popkov, M. Salerno, and G. M. Schütz, *Phys. Rev. E* **78**, 011122 (2008).

[118] R. K. P. Zia and B. Schmittmann, *J. Stat. Mech.* **07**, P07012 (2007).

[119] L. Lafuente and J. A. Cuesta, *J. Phys.: Condens. Matter* **14**, 12079 (2002).

Appendix A

One-Body Density Functional Calculations for the Lattice Fluid Mixture in 2D

Here a thorough derivation of the one-body densities for the lattice fluid mixture in 2D is provided via the LFMT. As we treat a static equilibrium mixture, there is no dependence on time t.

A.1 The variational principle

Recall from Section 3.2 that there are three different species of particles which are considered. The grand potential of the lattice fluids with three species can be expressed as

$$\Omega([\rho_1,\rho_2,\rho_3],\mu_1,\mu_2,\mu_3,\mathcal{T},A)=\mathcal{F}([\rho_1,\rho_2,\rho_3],\mathcal{T},A)-\sum_{p=1}^{3}\sum_{\mathbf{i}\in\mathcal{L}^2}\left(\mu_p-V_p^{\text{ext}}(\mathbf{i})\right)\rho_p(\mathbf{r}), \tag{A.1.1}$$

where $\mathcal{F}([\rho_1,\rho_2,\rho_3],\mathcal{T},A)$ is the (Helmholtz) free energy functional, μ_p is the chemical potential of species p, $\rho_p(\mathbf{i})$ is the average (one-body) density of species p, $\mathcal{T}$ is the temperature, and A is the size of the lattice $\mathcal{L}^2$. The equilibrium density distributions are those that fulfill the Euler-Lagrange equations, i.e.:

$$\frac{\delta\Omega([\rho_p],\mu_p,\mathcal{T},A)}{\delta\rho_p(\mathbf{i}')}=0,\quad p=1,2,3. \tag{A.1.2}$$

The free energy functional is conveniently split into the free energy functional of an ideal gas, $\mathcal{F}_{\rm id}$, and an excess part, $\mathcal{F}_{\rm exc}$, due to interactions between species, that is

$$\mathcal{BF}([\rho_p],\mathcal{T},A)=\sum_{p=1}^{3}\sum_{\mathbf{i}\in\mathcal{L}^2}\rho_p(\mathbf{i})[\ln(\rho_p(\mathbf{i}))-1]+\mathcal{BF}_{\rm exc}([\rho_p],\mathcal{T},A). \tag{A.1.3}$$

Hence, inserting equation (A.1.3) into (A.1.1), and conducting the functional derivative of (A.1.2) gives,

$$\begin{aligned}\frac{\delta\mathcal{B}\Omega}{\delta\rho_m(\mathbf{i}')} &= \frac{\delta\mathcal{BF}_{\rm exc}}{\delta\rho_p(\mathbf{i}')}+\frac{\delta}{\delta\rho_p(\mathbf{i}')}\left(\sum_{p=1}^{3}\sum_{\mathbf{i}\in\mathcal{L}^2}\rho_p(\mathbf{i})[\ln(\rho_p(\mathbf{i}))-1]\right)\\ &\quad -\frac{\delta}{\delta\rho_p(\mathbf{i}')}\left(\mathcal{B}\sum_{p=1}^{3}\sum_{\mathbf{i}\in\mathcal{L}^2}(\mu_p-V_p^{\rm ext}(\mathbf{i}))\right),\end{aligned} \tag{A.1.4}$$

where $\mathcal{B}=1/(k_{\rm B}\mathcal{T})$ is the Boltzmann constant. The first term on the RHS of equation (A.1.4) is a functional derivative of the excess free energy functional with respect to the one-body density, which is the (negative) one-body direct correlation function, i.e. $c^{(1)}_{\rho_p}$. The second term is the functional derivative of the ideal free energy functional, i.e.:

$$\begin{aligned}\frac{\delta\mathcal{BF}_{\rm id}}{\delta\rho_p(\mathbf{i}')} &= \frac{\delta}{\delta\rho_p(\mathbf{i}')}\left(\sum_{p=1}^{3}\sum_{\mathbf{i}\in\mathcal{L}^2}\rho_p(\mathbf{i})[\ln(\rho_p(\mathbf{i}))-1]\right)\\ &= \sum_{\mathbf{i}\in\mathcal{L}^2}\frac{\delta}{\delta\rho_p(\mathbf{i}')}\left(\rho_p(\mathbf{i})[\ln(\rho_p(\mathbf{i}))-1]\right)\\ &= \sum_{\mathbf{i}\in\mathcal{L}^2}\left(\frac{\delta\rho_p(\mathbf{i})}{\delta\rho_p(\mathbf{i}')}\ln(\rho_p(\mathbf{i}))+1-\frac{\delta\rho_p(\mathbf{i})}{\delta\rho_p(\mathbf{i}')}\right)\\ &= \sum_{\mathbf{i}\in\mathcal{L}^2}\delta_{\mathbf{ii}'}\ln(\rho_p(\mathbf{i}))+1-\sum_{\mathbf{i}\in\mathcal{L}^2}\delta_{\mathbf{ii}'}\\ &= \ln(\rho_p(\mathbf{i}'))+1-1=\ln(\rho_p(\mathbf{i}')).\end{aligned} \tag{A.1.5}$$

Thus substituting back the direct correlation function and equation (A.1.5) into equation (A.1.4), gives

$$\frac{\delta\mathcal{B}\Omega([\rho_p],\mu_p,\mathcal{T},A)}{\delta\rho_p(\mathbf{i}')}=-c^{(1)}_{\rho_p}+\ln(\rho_p(\mathbf{i}'))-\mathcal{B}(\mu_p-V_p^{\rm ext}(\mathbf{i}'))=0, \tag{A.1.6}$$

or by rearranging the above equation and dropping the prime signs yields the needed quantity,

$$\rho_p(\mathbf{i}')=e^{\mathcal{B}(\mu_p-V_p^{\rm ext}(\mathbf{i}))}e^{c^{(1)}_{\rho_p}}, \tag{A.1.7}$$

which is similar to its continuous counterpart of equation (2.3.42). In order to obtain the one-body density of equation (A.1.7), one must determine first $c^{(1)}_{\rho_p}$ from the excess free energy functional. The calculation of the latter equation is shown below.

A.2 Excess free energy functional via the LFMT

An approximation for the excess free energy functional for this model is obtained via the lattice fundamental measure theory (LFMT) [109, 110, 119]. A non-standard concept which is used here is the maximal cavity. A maximal 0D cavity is a 0D cavity that stops being a 0D cavity if one site is added to it. It is the largest 0D cavity of the system such that any 0D cavity is a subset of it. Hence, we start by determining the maximal cavities of the model. For species 1, 2, and 3 these are given as

$$\mathcal{W}_{\max,1} = (\{\mathbf{i}, \mathbf{i}+\hat{\mathbf{e}}_x\}_1) = (\{(i_x,i_y),(i_x+1,i_y)\}_1)\,, \tag{A.2.1}$$

$$\mathcal{W}_{\max,2} = (\{\mathbf{i}, \mathbf{i}+\hat{\mathbf{e}}_y\}_2) = (\{(i_x,i_y),(i_x,i_y+1)\}_2)\,, \tag{A.2.2}$$

$$\mathcal{W}_{\max,3} = (\{\mathbf{i}\}_3) = (\{i_x,i_y\}_3)\,,\,, \tag{A.2.3}$$

respectively. $\hat{\mathbf{e}}_x$ and $\hat{\mathbf{e}}_y$ are the unit vectors to the x and y-directions, respectively. Hence the maximal cavity of the mixture is

$$\begin{aligned}\mathcal{W}_{\max,\text{mix}} &= \mathcal{W}_{\max,1}+\mathcal{W}_{\max,2}+\mathcal{W}_{\max,3}\\ &= (\{(i_x,i_y),(i_x+1,i_y)\}_1)+(\{(i_x+1,i_y-1),(i_x+1,i_y)\}_2)+(\{i_x+1,i_y\}_3)\\ &= (\{(i_x,i_y),(i_x+1,i_y)\}_1,\{(i_x+1,i_y-1),(i_x+1,i_y)\}_2,\{(i_x+1,i_y)\}_3),\\ &.\end{aligned} \tag{A.2.4}$$

for $i_x, i_y \in \mathcal{L}^2$. Because the maximal cavity corresponds to its weighted densities, thus one obtains,

$$\begin{aligned}\mathcal{W}_{\max,\text{mix}} &= (\{(i_x,i_y),(i_x+1,i_y)\}_1,\{(i_x+1,i_y-1),(i_x+1,i_y)\}_2,\{(i_x+1,i_y)\}_3)\\ &= \sum_{p=1}^{3}\sum_{\mathbf{i}\in\mathcal{C}_p}\rho_{\mathcal{C}_p}(\mathbf{i}) = \sum_{\mathbf{i}\in\mathcal{C}_1}\rho_{\mathcal{C}_1}(\mathbf{i})+\sum_{\mathbf{i}\in\mathcal{C}_2}\rho_{\mathcal{C}_2}(\mathbf{i})+\sum_{\mathbf{i}\in\mathcal{C}_3}\rho_{\mathcal{C}_3}(\mathbf{i})\\ &= \rho_1(i_x,i_y)+\rho_1(i_x,i_y)+\rho_2(i_x+1,i_y-1)+\rho_2(i_x+1,i_y)+\rho_3(i_x+1,i_y).\end{aligned} \tag{A.2.5}$$

Using the weighted density (A.2.5) the first ansatz for the excess free energy functional is obtained from equation (2.3.48) as

$$\begin{aligned}&\mathcal{BF}_{\text{exc}}^{\text{FM1}}[\rho_1,\rho_2,\rho_3]\\ &= \sum_{\mathbf{i}\in\mathcal{L}^2}\Phi_0\left(\rho_1(i_x,i_y)+\rho_1(i_x+1,i_y)+\rho_2(i_x+1,i_y-1)+\rho_2(i_x+1,i_y)+\rho_3(i_x+1,i_y)\right).\end{aligned} \tag{A.2.6}$$

Next, the ansatz (A.2.6) is evaluated to test whether (A.2.6) produces the correct 0D limit of the density profile. Therefore, $\rho_{\mathcal{C}_{\text{test}}}$ is chosen as a test case for a 0D density profile with

$$\mathcal{C}_{\text{test}} = (\rho_1(i'_x, i'_y) + \rho_1(i'_x + 1, i'_y) + \rho_2(i'_x + 1, i'_y - 1) + \rho_2(i'_x + 1, i'_y) + \rho_3(i'_x + 1, i'_y)),$$

such that

$$\rho_{\text{test},1}(i_x, i_y) = \begin{cases} \rho_1(i'_x, i'_y); & \text{if} \quad i_x = i'_x; i_y = i'_y, \\ \rho_1(i'_x + 1, i'_y); & \text{if} \quad i_x = i'_x + 1; i_y = i'_y, \\ 0; & \text{otherwise}, \end{cases} \tag{A.2.7}$$

$$\rho_{\text{test},2}(i_x, i_y) = \begin{cases} \rho_2(i'_x + 1, i'_y - 1); & \text{if} \quad i_x = i'_x + 1; i_y = i'_y - 1, \\ \rho_2(i'_x + 1, i'_y); & \text{if} \quad i_x = i'_x + 1; i_y = i'_y, \\ 0; & \text{otherwise}, \end{cases} \tag{A.2.8}$$

and

$$\rho_{\text{test},3} = \begin{cases} \rho_3(i'_x + 1, i'_y); & \text{if} \quad i_x = i'_x + 1; i_y = i'_y, \\ 0; & \text{otherwise}. \end{cases} \tag{A.2.9}$$

Hence, evaluating the excess free energy functional against the test weighted density gives

$$\begin{aligned} &\mathcal{BF}^{\text{FM1}}_{\text{exc}}[\mathcal{C}_{\text{test}}] = \\ &\Phi_0(\rho_1(i'_x - 1, i'_y) + \rho_1(i'_x, i'_y) + \rho_2(i'_x, i'_y - 1) + \rho_2(i'_x, i'_y) + \rho_3(i'_x, i'_y)) \\ &+\Phi_0(\rho_1(i'_x, i'_y) + \rho_1(i'_x + 1, i'_y) + \rho_2(i'_x + 1, i'_y - 1) + \rho_2(i'_x + 1, i'_y) + \rho_3(i'_x + 1, i'_y)) \\ &+\Phi_0(\rho_1(i'_x + 1, i'_y) + \rho_1(i'_x + 2, i'_y) + \rho_2(i'_x + 2, i'_y - 1) + \rho_2(i'_x + 2, i'_y) + \rho_3(i'_x + 2, i'_y)) \\ &+\Phi_0(\rho_1(i'_x, i'_y + 1) + \rho_1(i'_x + 1, i'_y + 1) + \rho_2(i'_x + 1, i'_y) + \rho_2(i'_x, i'_y + 1) + \rho_3(i'_x, i'_y + 1)) \\ &+\Phi_0(\rho_1(i'_x, i'_y - 1) + \rho_1(i'_x + 1, i'_y - 1) + \rho_2(i'_x + 1, i'_y - 2) + \rho_2(i'_x + 1, i'_y - 1) \\ &+\rho_3(i'_x + 1, i'_y - 1)). \end{aligned} \tag{A.2.10}$$

However, the contributions from the RHS of (A.2.10) could only come from the test weighted density of equations (A.2.7)-(A.2.9), therefore equation (A.2.10) reduces to

$$\begin{aligned} &\mathcal{BF}^{FM1}_{\text{exc}}[\mathcal{C}_{\text{test}}] = \\ &\Phi_0(\rho_1(i'_x, i'_y)) \\ &+\Phi_0(\rho_1(i'_x, i'_y) + \rho_1(i'_x + 1, i'_y) + \rho_2(i'_x + 1, i'_y - 1) + \rho_2(i'_x + 1, i'_y) + \rho_3(i'_x + 1, i'_y)) \\ &+\Phi_0(\rho_1(i'_x + 1, i'_y)) + \Phi_0(\rho_2(i'_x, i'_y)) + \Phi_0(\rho_2(i'_x + 1, i'_y - 1)). \end{aligned} \tag{A.2.11}$$

We only need the second term on the RHS of equation (A.2.11) in order to yield the correct 0D limit of the (test) density profile. Thus, other terms in equation (A.2.11) are considered as spurious terms and have to be eliminated. In order to remove these spurious terms (one by one), a second ansatz of the excess free energy functional is constructed, i.e.:

$$\begin{aligned}\mathcal{BF}_{\rm exc}^{\rm FM2} &= \sum_{\mathbf{i}\in\mathcal{L}^2}\{\Phi_0(\rho_1(i_x,i_y+\rho_1(i_x+1,i_y)+\rho_2(i_x+1,i_y-1)+\rho_2(i_x+1,y)\\ &\qquad +\rho_3(i_x+1,y))+a(\rho_1(i_x,i_y))\Phi_0(\rho_1(i_x,i_y))\}\,. \end{aligned}\tag{A.2.12}$$

The previous procedure is then repeated by setting $a(\rho_1(i_x,i_y))=-1$, giving

$$\begin{aligned}\mathcal{BF}_{\rm exc}^{\rm FM2} &= \sum_{\mathbf{i}\in\mathcal{L}^2}\{\Phi_0(\rho_1(i_x,i_y+\rho_1(i_x+1,i_y)+\rho_2(i_x+1,i_y-1)+\rho_2(i_x+1,i_y)\\ &\qquad +\rho_3(i_x+1,i_y))-\Phi_0(\rho_1(i_x,i_y))\}\,. \end{aligned}\tag{A.2.13}$$

The same $\rho_{\mathcal{C}_{\rm test}}$ is applied to test equation (A.2.13). But the first term of equation (A.2.13) is already evaluated [in $\mathcal{F}^{\rm FM1}$], hence only the second term needs to be evaluated, i.e.:

$$\begin{aligned}&\mathcal{BF}_{\rm exc}^{\rm FM2}=\Phi_0(\rho_1(i'_x,i'_y))\\ +\;&\Phi_0(\rho_1(i'_x,i'_y)+\rho_1(i'_x+1,i'_y)+\rho_2(i'_x+1,i'_y-1)+\rho_2(i'_x+1,i'_y)+\rho_3(i'_x+1,i'_y))\\ +\;&\Phi_0(\rho_1(i'_x+1,i'_y))+\Phi_0(\rho_2(i'_x,i'_y))+\Phi_0(\rho_2(i'_x+1,i'_y))\\ -\;&\Phi_0(\rho_1(i'_x,i'_y))-\Phi_0(\rho_1(i'_x+1,i'_y)),\end{aligned}\tag{A.2.14}$$

or

$$\begin{aligned}\mathcal{BF}_{\rm exc}^{\rm FM2}[\rho_{\mathcal{C}_{\rm test}}] &= \Phi_0(\rho_1(i'_x,i'_y)+\rho_1(i'_x+1,i'_y)+\rho_2(i'_x+1,i'_y-1)+\rho_2(i'_x+1,i'_y)\\ &\qquad +\rho_3(i'_x+1,i'_y))+\Phi_0(\rho_2(i'_x+1,i'_y))+\Phi_0(\rho_2(i'_x+1,i'_y-1)).\end{aligned}\tag{A.2.15}$$

Two spurious terms are eliminated in equation (A.2.15). However, there are still two other spurious terms left. In order to remove the remaining terms the excess free energy functional is modified once more, yielding,

$$\begin{aligned}&\mathcal{BF}_{\rm exc}^{\rm FM3}=\\ &\sum_{\mathbf{i}\in\mathcal{L}^2}\{\Phi_0(\rho_1(i_x,i_y)+\rho_1(i_x+1,i_y)+\rho_2(i_x+1,i_y-1)+\rho_2(i_x+1,i_y)+\rho_3(i_x+1,i_y))\\ &\qquad -\Phi_0(\rho_1(i_x,i_y))+a(\rho_2(i_x+1,i_y-1))\Phi_0(\rho_2(i_x+1,i_y-1))\}\,.\end{aligned}\tag{A.2.16}$$

Setting $a(\rho_2(i_x+1, i_y-1)) = -1$, one obtains from (A.2.16)

$$\begin{aligned}
&\mathcal{B}\mathcal{F}_{\text{exc}}^{\text{FM3}} = \\
&\sum_{\mathbf{i}\in\mathcal{L}^2} \{\Phi_0(\rho_1(i_x,i_y)+\rho_1(i_x+1,i_y)+\rho_2(i_x+1,i_y-1)+\rho_2(i_x+1,i_y)+\rho_3(i_x+1,i_y)) \\
&\qquad -\Phi_0(\rho_1(i_x,i_y)) - \Phi_0(\rho_2(i_x+1,i_y-1))\}\,. \qquad \text{(A.2.17)}
\end{aligned}$$

$\rho_{\mathcal{C}_{\text{test}}}$ is used once more and evaluate the additional weighted density against the test density profile, such that

$$\begin{aligned}
&\mathcal{F}_{\text{exc}}^{\text{FM3}}[\rho_{\mathcal{C}_{\text{test}}}] = \\
&\Phi_0(\rho_1(i'_x,i'_y)+\rho_1(i'_x+1,i'_y)+\rho_2(i'_x+1,i'_y-1)+\rho_2(i'_x+1,i'_y)+\rho_3(i'_x+1,i'_y)) \\
&+\Phi_0(\rho_2(i'_x+1,i'_y-1)) + \Phi_0(\rho_2(i'_x+1,i'_y)) \\
&-[\Phi_0(\rho_2(i'_x+1,i'_y-1)) + \Phi_0(\rho_2(i'_x+1,i'_y))], \qquad \text{(A.2.18)}
\end{aligned}$$

or

$$\mathcal{B}\mathcal{F}_{\text{exc}}^{\text{FM3}}[\rho_{\mathcal{C}_{\text{test}}}] = \Phi_0(\rho_1(i'_x,i'_y)+\rho_1(i'_x+1,i'_y)+\rho_2(i'_x+1,i'_y-1)+\rho_2(i'_x+1,i'_y)+\rho_3(i'_x+1,i'_y)), \qquad \text{(A.2.19)}$$

which is the correct 0D limit for the density profile test. Hence the final excess free energy functional is given by $\mathcal{B}\mathcal{F}_{\text{exc}}^{\text{FM3}}$, i.e.:

$$\begin{aligned}
&\mathcal{B}F_{\text{exc}}([\rho_1,\rho_2,\rho_3],\mathcal{T},A) = \\
&\sum_{\mathbf{i}\in\mathcal{L}^2} \{\Phi_0(\rho_1(\mathbf{i}+\hat{\mathbf{e}}_x)+\rho_1(\mathbf{i})+\rho_2(\mathbf{i}+\hat{\mathbf{e}}_x-\hat{\mathbf{e}}_y)+\rho_2(\mathbf{i}+\hat{\mathbf{e}}_x)+\rho_3(\mathbf{i}+\hat{\mathbf{e}}_x)) \\
&\qquad -\Phi_0(\rho_1(\mathbf{i})) - \Phi_0(\rho_2(\mathbf{i}+\hat{\mathbf{e}}_x-\hat{\mathbf{e}}_y))\}\,, \qquad \text{(A.2.20)}
\end{aligned}$$

where $\Phi_0(\cdot)$ is given by $\Phi_0(\eta) = (1-\eta)\ln(1-\eta)+\eta$ representing the excess free energy density of a 0D system, i.e. that of an isolated site with mean occupancy number η. Applying the aforementioned 0D cavity excess free energy, $\Phi_0(\eta)$, in each term on the RHS of equation (A.2.20), gives

$$\begin{aligned}
&\mathcal{B}\mathcal{F}_{\text{exc}} = \\
&\sum_{\mathbf{i}\in\mathcal{L}^2} \{(1-\rho_1(\mathbf{i})-\rho_1(\mathbf{i}+\hat{\mathbf{e}}_x)-\rho_2(\mathbf{i}+\hat{\mathbf{e}}_x-\hat{\mathbf{e}}_y)-\rho_2(\mathbf{i}+\hat{\mathbf{e}}_x)-\rho_3(\mathbf{i}+\hat{\mathbf{e}}_x)) \\
&\qquad \times\ln(1-\rho_1(\mathbf{i})-\rho_1(\mathbf{i}+\hat{\mathbf{e}}_x)-\rho_2(\mathbf{i}+\hat{\mathbf{e}}_x-\hat{\mathbf{e}}_y)-\rho_2(\mathbf{i}+\hat{\mathbf{e}}_x)-\rho_3(\mathbf{i}+\hat{\mathbf{e}}_x)) \\
&\qquad +(\rho_1(\mathbf{i})+\rho_1(\mathbf{i}+\hat{\mathbf{e}}_x)+\rho_2(\mathbf{i}+\hat{\mathbf{e}}_x-\hat{\mathbf{e}}_y)+\rho_2(\mathbf{i}+\hat{\mathbf{e}}_x)+\rho_3(\mathbf{i}+\hat{\mathbf{e}}_x)) \\
&\qquad -(1-\rho_1(\mathbf{i}))\ln(1-\rho_1(\mathbf{i})) - \rho_1(\mathbf{i}) \\
&\qquad -(1-\rho_2(\mathbf{i}-\hat{\mathbf{e}}_x-\hat{\mathbf{e}}_y))\ln(1-\rho_2(\mathbf{i}-\hat{\mathbf{e}}_x-\hat{\mathbf{e}}_y)) - \rho_2(\mathbf{i}+\hat{\mathbf{e}}_x-\hat{\mathbf{e}}_y). \qquad \text{(A.2.21)}
\end{aligned}$$

A.3 The one-body densities

The direct correlation function of each species may now be calculated using equation (A.2.21), that is

$$\begin{aligned} c_{\rho_1}^{(1)} &= -\frac{\delta\mathcal{B}\mathcal{F}_{\text{exc}}}{\delta\rho_1(\mathbf{i}')} \\ &= \ln(1-\rho_1(\mathbf{i}')-\rho_1(\mathbf{i}'+\hat{\mathbf{e}}_x)-\rho_2(\mathbf{i}'+\hat{\mathbf{e}}_x-\hat{\mathbf{e}}_y)-\rho_2(\mathbf{i}'+\hat{\mathbf{e}}_x)-\rho_3(\mathbf{i}'+\hat{\mathbf{e}}_x)) \\ &\quad +\ln(1-\rho_1(\mathbf{i}'-\hat{\mathbf{e}}_x)-\rho_1(\mathbf{i}')-\rho_2(\mathbf{i}'-\hat{\mathbf{e}}_y)-\rho_2(\mathbf{i}')-\rho_3(\mathbf{i}'))-\ln(1-\rho_1(\mathbf{i}')). \end{aligned} \tag{A.3.1}$$

$$\begin{aligned} c_{\rho_2}^{(1)} &= -\frac{\delta\mathcal{B}\mathcal{F}_{\text{exc}}}{\delta\rho_2(\mathbf{i}')} \\ &= \ln(1-\rho_1(\mathbf{i}-\hat{\mathbf{e}}_x+\hat{\mathbf{e}}_y)-\rho_1(\mathbf{i}')-\rho_2(\mathbf{i}+\hat{\mathbf{e}}_y)-\rho_3(\mathbf{i}+\hat{\mathbf{3}}_y)) \\ &\quad +\ln(1-\rho_1(\mathbf{i}-\hat{\mathbf{e}}_x)-\rho_1(\mathbf{i})-\rho_2(\mathbf{i}-\hat{\mathbf{e}}_y)-\rho_2(\mathbf{i})) \\ &\quad -\ln(1-\rho_2(\mathbf{i}-\hat{\mathbf{e}}_x+\hat{\mathbf{e}}_y)), \end{aligned} \tag{A.3.2}$$

and finally,

$$\begin{aligned} c_{\rho_3}^{(1)} &= -\frac{\delta\mathcal{B}\mathcal{F}_{\text{exc}}}{\delta\rho_3(\mathbf{i}')} \\ &= \ln(1-\rho_1(\mathbf{i}-\hat{\mathbf{e}}_x)-\rho_1(\mathbf{i})-\rho_2(\mathbf{i}-\hat{\mathbf{e}}_y)-\rho_2(\mathbf{i})-\rho_3(\mathbf{i})) \end{aligned} \tag{A.3.3}$$

In order to establish a correspondence to the TASEP equations (A.3.1)-(A.3.3) are linearized by considering low densities of ρ_1 and ρ_2, i.e.: $\rho_1, \rho_2 \to 0$, such that

$$c_{\rho_1}^{(1)} = \ln\left[(1-\rho_3(\mathbf{i}+\hat{\mathbf{e}}_x))(1-\rho_3(\mathbf{i}))\right], \tag{A.3.4}$$

$$c_{\rho_2}^{(1)} = \ln\left[(1-\rho_3(\mathbf{i}+\hat{\mathbf{e}}_y))(1-\rho_3(\mathbf{i}))\right], \tag{A.3.5}$$

and also,

$$c_{\rho_3}^{(1)} = \ln\left[1-\rho_3(\mathbf{i})\right]. \tag{A.3.6}$$

Hence, inserting the correlation functions (A.3.4)-(A.3.6) into equation (A.1.7), yields the one-body density of each species as

$$\begin{aligned} \rho_1(\mathbf{i}) &= e^{\mathcal{B}(\mu_1-V_1^{\text{ext}}(\mathbf{i}))}e^{\ln[(1-\rho_3(\mathbf{i}+\hat{\mathbf{e}}_x))(1-\rho_3(\mathbf{i}))]} \\ &= e^{\mathcal{B}(\mu_1-V_1^{\text{ext}}(\mathbf{i}))}\left[(1-\rho_3(\mathbf{i}+\hat{\mathbf{e}}_x))(1-\rho_3(\mathbf{i}))\right], \end{aligned} \tag{A.3.7}$$

$$\begin{aligned} \rho_2(\mathbf{i}) &= e^{\mathcal{B}(\mu_2-V_2^{\text{ext}}(\mathbf{i}))}e^{\ln[(1-\rho_3(\mathbf{i}+\hat{\mathbf{e}}_y))(1-\rho_3(\mathbf{i}))]} \\ &= e^{\mathcal{B}(\mu_2-V_2^{\text{ext}}(\mathbf{i}))}\left[(1-\rho_3(\mathbf{i}+\hat{\mathbf{e}}_y))(1-\rho_3(\mathbf{i}))\right], \end{aligned} \tag{A.3.8}$$

and

$$\begin{aligned} \rho_3(\mathbf{i}) &= e^{\mathcal{B}(\mu_3 - V_3^{\text{ext}}(\mathbf{i}))} e^{\ln[1-\rho_3(\mathbf{i})]} \\ &= e^{\mathcal{B}(\mu_3 - V_3^{\text{ext}}(\mathbf{i}))} \left[1 - \rho_3(\mathbf{i})\right], \end{aligned} \tag{A.3.9}$$

or

$$[1 - \rho_3(\mathbf{i})] = \frac{\rho_3(\mathbf{i})}{e^{\mathcal{B}(\mu_3 - V_3^{\text{ext}}(\mathbf{i}))}}. \tag{A.3.10}$$

Furthermore, inserting equation (A.3.10) into (A.3.8) and (A.3.9) gives

$$\rho_1(\mathbf{i}) = \frac{e^{\mathcal{B}(\mu_1 - V_1^{\text{ext}}(\mathbf{i}))}}{e^{\mathcal{B}(\mu_3 - V_3^{\text{ext}}(\mathbf{i}))}} \rho_3(\mathbf{i})(1 - \rho_3(\mathbf{i} + \hat{\mathbf{e}}_x)), \tag{A.3.11}$$

and

$$\rho_2(\mathbf{i}) = \frac{e^{\mathcal{B}(\mu_2 - V_2^{\text{ext}}(\mathbf{i}))}}{e^{\mathcal{B}(\mu_3 - V_3^{\text{ext}}(\mathbf{i}))}} \rho_3(\mathbf{i})(1 - \rho_3(\mathbf{i} + \hat{\mathbf{e}}_y)). \tag{A.3.12}$$

Appendix B

A Proof of the Minimum Value of the Microscopic Functional (6.2.1)

In this Appendix, a detail account of the proof for the minimum value of $\mathcal{M}[\{\tilde{j}_{n'n}\}]$ is given. First the ingredients needed for this proof are provided. Therefore, consider the proposed functional of equation (6.2.1),

$$\mathcal{M}[\{\tilde{j}_{n'n}\}] = \int_0^\infty \mathrm{d}t \sum_{n',n} \tilde{j}_{n'n}(t) \left[\ln\left(\frac{\tilde{j}_{n'n}(t)}{w_{n'n}(t)P_n(t)} \right) - 1 \right],$$

where $P_n(t)$ satisfies

$$P_n(t) = P_n(t=0) + \int_0^t \mathrm{d}t' \sum_{n'} \left\{ j_{nn'}(t') - j_{n'n}(t') \right\},$$

of equation (6.1.1), and

$$j_{n'n}(t) = w_{n'n}(t)P_n(t).$$

We wish to proof that the minimum value of $\mathcal{M}[\tilde{j}_{n'n}]$ is

$$\mathcal{M}_0 = -\int_0^\infty \sum_{n',n} w_{n'n}(t)P_n(t)\mathrm{d}t.$$

$\mathcal{M}_0$ is obtained if and only if $\tilde{j}_{n'n}(t) = w_{n'n}(t)P_n(t) \equiv j_{n'n}(t)$, $\forall n' \neq n$. In order to proof the aforementioned statement, we apply a logarithm property that $\ln z \leq (z-1)$. In this case we take,

$$z = \frac{w_{n'n}(t)P_n(t)}{\tilde{j}_{n'n}(t)}. \tag{B.1}$$

Equation (B.1) measures (how far) the difference is between the trial configurational current, $\tilde{j}_{n'n}(t)$, to the true solution, $j_{n'n}(t)$. Thus, using the aforementioned logarithm property (Gibbs inequality) we have

$$\begin{aligned}
& \ln\left(\frac{w_{n'n}(t)P_n(t)}{\tilde{j}_{n'n}(t)}\right) \leq \frac{w_{n'n}(t)P_n(t)}{\tilde{j}_{n'n}(t)} - 1 \\
\Rightarrow \quad & -\ln\left(\frac{\tilde{j}_{n'n}(t)}{w_{n'n}(t)P_n(t)}\right) \leq \frac{w_{n'n}(t)P_n(t)}{\tilde{j}_{n'n}(t)} - 1 \\
\Rightarrow \quad & \tilde{j}_{n'n}(t)\ln\left(\frac{\tilde{j}_{n'n}(t)}{w_{n'n}(t)P_n(t)}\right) \geq -\tilde{j}_{n'n}(t)\left[\frac{w_{n'n}(t)P_n(t)}{\tilde{j}_{n'n}(t)} - 1\right] \\
\Rightarrow \quad & \tilde{j}_{n'n}(t)\ln\left(\frac{\tilde{j}_{n'n}(t)}{w_{n'n}(t)P_n(t)}\right) \geq -w_{n'n}(t)P_n(t) + \tilde{j}_{n'n}(t). \qquad \text{(B.2)}
\end{aligned}$$

Inequality (B.2) applies for any pair of microscopic states, n' and n. We then sum over all the microscopic states with $n' \neq n$, to obtain

$$\begin{aligned}
& \sum_{n',n} \tilde{j}_{n'n}(t)\ln\left(\frac{w_{n'n}(t)P_n(t)}{\tilde{j}_{n'n}(t)}\right) \geq -\sum_{n',n} \tilde{j}_{n'n}(t)\left(\frac{w_{n'n}(t)P_n(t)}{\tilde{j}_{n'n}(t)} - 1\right) \\
\Rightarrow \quad & \sum_{n',n} \tilde{j}_{n'n}(t)\left[\ln\left(\frac{\tilde{j}_{n'n}(t)}{w_{n'n}(t)P_n(t)}\right) - 1\right] \geq -\sum_{n',n} w_{n'n}(t)P_n(t)\mathrm{d}t. \qquad \text{(B.3)}
\end{aligned}$$

And finally integrating inequality (B.3) with respect to the time parameter, yields

$$\int_0^\infty \mathrm{d}t \sum_{m,n} \tilde{j}_{mn}(t)\left[\ln\left(\frac{\tilde{j}_{mn}(t)}{w_{mn}(t)P_n(t)}\right) - 1\right] \geq -\int_0^\infty \mathrm{d}t \sum_{m,n} w_{mn}(t)P_n(t), \qquad \text{(B.4)}$$

or using equation (6.2.1) for the LHS of equation (B.4), gives

$$\mathcal{M}[\{\tilde{j}_{n'n}\}] \geq -\int_0^\infty \mathrm{d}t \sum_{n',n} w_{n'n}(t)P_n(t). \qquad \text{(B.5)}$$

Hence, the inequality (B.5) shows that the microscopic functional $\mathcal{M}[\tilde{j}_{n'n}]$ possesses a minimum value. Furthermore, the equality (for the minimum value) is obtained if

$$\ln\left[\frac{w_{n'n}(t)P_n(t)}{\tilde{j}_{n'n}(t)}\right] = \frac{w_{n'n}(t)P_n(t)}{\tilde{j}_{n'n}(t)} - 1. \qquad \text{(B.6)}$$

Equation (B.6) is taken from the first line of inequality (B.2). The former equation is satisfied if and only if $\tilde{j}_{n'n}(t)$ is replaced by $j_{n'n}(t) = w_{n'n}(t)P_n(t)$, which is the true solution of (6.1.2). This completes the proof.